Structural behaviour of cold-formed stainless steel channel lipped sections with edge-stiffened holes, un-stiffened holes, and plain webs subjected to axial compression

Gagan Sengundham Dinesh

A thesis submitted in fulfilment of the requirements
for the degree of Master of Engineering

Supervised by

Dr Zhiyuan (Arthur) Fang, Dr Krishanu Roy and Prof James Lim

School of Engineering

The University of Waikato

New Zealand

THE UNIVERSITY OF
WAIKATO
Te Whare Wānanga o Waikato

2024

ABSTRACT

In recent years, stainless steel has seen increased use in construction due to its exceptional corrosion resistance and mechanical strength, especially in structural elements like channel sections, hollow pipes, and angles. Cold-formed stainless steel (CFSS) channel sections with edge-stiffened web holes have emerged as a significant development in the construction industry, with a focus on streamlining the installation of plumbing and electrical services. Previous research indicated that these edge stiffened web holes offer comparable axial capacity to plain webs in cold-formed steel (CFS) channel columns. In building industry, stiffening of the web hole is very common, which results in increase of the load carrying capacity of the stainless-steel column. However, no comprehensive study has been reported in the literature for such stainless-steel column subjected to compression. This paper investigates the axial capacity of the stainless-steel column with unstiffened and edge-stiffened web holes. A non-linear finite element (FE) model is developed and validated against the experimental results available in the literature. An extensive parametric study is conducted based on 2016 validated FE models. EN 1.4509 (Ferritic), EN 1.4462 (Duplex) and EN 1.4301 (Austenitic) grades of stainless steel are considered for the current study. Subsequently, parametric study results are compared with guidelines available for stainless steel in the standards, namely AS/NZS 4600: 2018, ASCE: 08, AISI. Finally, a modified EWM and DSM equations are proposed for the CFSS section with edge-stiffened web holes. Finally, a reliability analysis was conducted to ensure that the proposed equation could be reliable.

Keywords: Cold-formed stainless-steel channel, channel sections, axial compression, edge-stiffened web hole, finite element model, effective width method, direct Strength method

PREFACE

This thesis is submitted to the University of Waikato, New Zealand, in fulfilment of the requirement for the master's degree in civil engineering. The work contained in this thesis has not been previously submitted for a degree or diploma at any other higher educational institution. To the best of my knowledge and belief, the thesis contains no material previously published or written by another person except where due reference is made.

ACKNOWLEDGEMENTS

Firstly, my sincere thanks to my main supervisor, Dr. Zhiyuan (Arthur) Fang, co-supervisors Dr. Krishanu Roy, and Professor James B.P. Lim, for their unwavering support throughout my research, whose constant guidance and contributions were integral to the successful submission of my journal papers, making me an independent researcher.

Heartfelt gratitude goes to Shubam Tiwari and Dinesh Lakshmanan Chandramohan for their continuous support. I extend my sincere thanks to my well-wishers in New Zealand for shaping my thesis with invaluable encouragement.

I express my appreciation to my best friends in New Zealand, Vivekanandan Shivaji, Harsh Birwadkar and Gowrava Mohanswamy for their year-round support. Special thanks to the University of Waikato, School of Engineering, for providing computing machines and research assistance.

Finally, I want to express my gratitude to my family, my father Dinesh S K, my mother Lilly S D, my Brother Deepak Dinesh and sister in law Bhavana for their unwavering support to pursue my masters.

TABLE OF CONTENTS

LIST OF FIGURES

LIST OF TABLES

CHAPTER 1. Introduction

1.1 General

Cold-formed stainless steel (CFSS) channels are increasingly favoured as structural elements due to their appealing aesthetics and advantageous material properties, including heat and corrosion resistance. These sections commonly feature web perforations, facilitating the convenient installation of various services. The austenitic, ferritic, and duplex grades stand out as the most prevalent among all stainless steel material grades. Its widely acknowledged that the stress-strain behaviour of stainless steel deviates from that of carbon steel, where the latter typically exhibits an approximately linear relationship up to the point of yield stress.

The utilization of CFSS has appeared as a good corrosion protection and compelling material choice in structural engineering, merging the cost-effectiveness and adaptability of cold-formed steel with the exceptional characteristics of stainless steel. This combination presents a distinct array of benefits, including corrosion resistance, durability, and visual appeal, considering CFSS as a promising candidate for diverse structural process.

This research investigates the compression characteristics of CFSS channel profiles featuring plain webs, unstiffened web holes, and web holes with edge stiffened. The study utilizes material property data sourced from literature for stainless-steel types EN 1.4509 (ferritic), EN 1.4462 (duplex), and EN 1.4301 (austenitic) [1, 2-4]. Two specific channel profiles, C200 and C300, are analysed [3]. The web holes have designated nominal diameters (a) relative to the web depth, set at ratios of 0.2, 0.4, and 0.6, positioned centrally within the sections. Meanwhile, the nominal length of the edge stiffener (q) is standardized at 10 mm and 15 mm. Notably, existing literature lacks studies on determining the axial capacity of CFSS channel profiles. Additionally, guidelines provided by the American Society of Civil Engineers

(ASCE) [5] which not offer any guidelines for determining axial capacity of CFSS channel sections with edge stiffened holes.

The study accounted for the impact of column length and opening spacing. Material properties were sourced from existing literature, and initial imperfections were assessed via laser scanning. The results of load-axial displacement, load-lateral displacement, load-strain relationship, and failure modes were reported.

1.2 Manufacturing process

Cold-formed stainless-steel components are typically manufactured through the process of cold forming or cold rolling. Cold forming is the process of shaping metal at temperatures lower than its recrystallization point, often carried out at room temperature. This method is commonly employed in the fabrication of diverse stainless-steel profiles, including channels, angles, tubes, and other structural configurations, distinguishing it from Hot Rolled Steel (HRS) members. In the case of CFSS channel sections, web holes are punched at predetermined positions to facilitate service installation, thus simplifying the assembly process. Illustrated in Figures 1–1, the manufacturing procedure involves shaping the material via press-braking or cold-roll forming to achieve required shape [2].

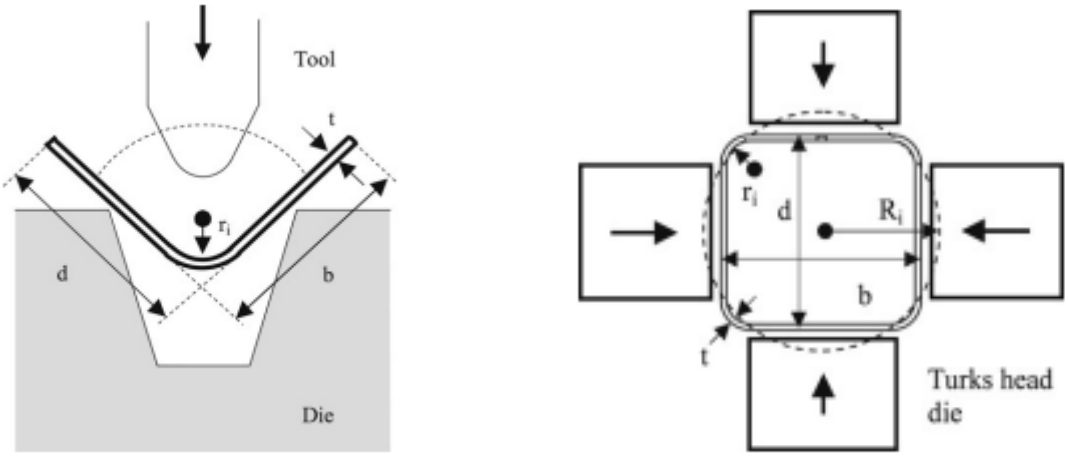

Press breaking for an angle Cold rolling of a box section

Figure 1-1: CFSS manufacturing process [6]

1.3 Application of CFSS channel sections in building industry

The utilisation of edge-stiffened holes in the webs of cold-formed steel channels (CFS) has become widely adapted in New Zealand, primarily aimed at simplifying the installation of plumbing and electrical services. CFSS channel sections find extensive utilization across various industries and construction ventures owing to their distinct advantages. In building construction, CFS serve as essential components for floor framing, roof systems, and wall studs, notable for their exceptional strength, resistance to corrosion, and adaptability to diverse structural requirements. Beyond building construction, CFSS channel members are deployed in numerous industries, including infrastructure projects such as bridges, walkways, and support structures for various installations like solar panel frames, equipment mounts, and platforms. Additionally, they are utilized in architectural applications to craft aesthetically pleasing and structurally robust elements like handrails, facades, and decorative terms. In transportation, CFSS channel sections find application in constructing trailer frames, truck bodies, and railcar components. Moreover, they play a crucial role in the energy sector, supporting components in power plants, and contributing to the construction of wind turbine towers and solar panel structures. Notably, their corrosion resistance makes CFSS channel sections indispensable in marine and offshore structures, including shipbuilding, offshore platforms, and port facilities, where exposure to saltwater is a prevalent challenge. With their versatility, strength, and corrosion resistance, CFSS channel sections have emerged as a preferred choice across several industries, making them popular choice in diverse array of applications.

Two recent examples of structures prominently utilizing cold-formed stainless steel tubular elements include the Regents Place Pavilion in London [7] and Cala galdana Bridge in

Europe [8]. The Regents Place Pavilion, shown in Figure 1–2 and opened to the public in 2009, is entirely constructed from stainless steel. It contains 258 cold-formed rectangular hollow section columns, each measuring 7.8 meters in length, supporting a roof plane. The hollow sections, sized at 50 × 50 × 4, are fabricated from austenitic stainless steel grade EN 1.4404. Figure 1–3 showcases the Cala Galdana bridge crosses the Algenda river in Menorca. The main structure of this bridge is completely stainless steel eventually considered the duplex grade 1.4462 and having two parallel arches, two longitudinal beams and traverse beams which supports the deck. Reinforced concrete holds up the abutments at every end, which lays on pile foundations. The bridge, inaugurated in 2005, and it was the first stainless steel road bridge in Europe.

Figure: 1-2 The Regents Place Pavilion [7]

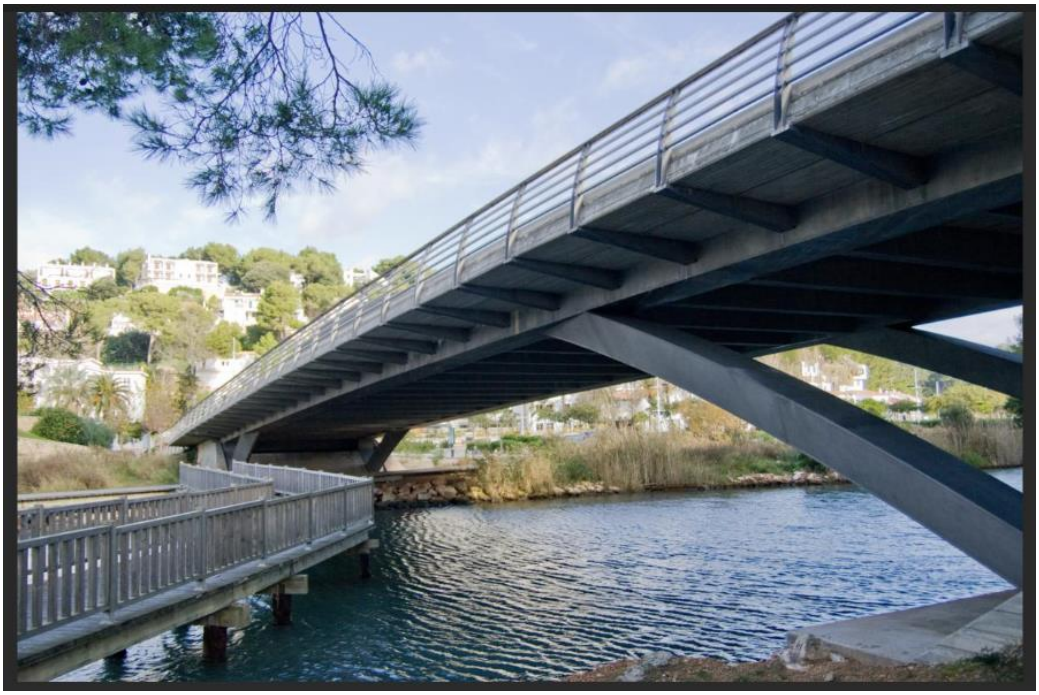

Figure: 1-3 The Cala Galdana bridge [8]

Figure 1-4: Photo of CFS channel beams having edge-stiffened web holes in CFS concrete flooring system [9].

CHAPTER 2. Literature review

2.1 Introductory remarks

This chapter offers an in-depth review of literature concerning the behaviour of cold formed steel and CFSS section, focusing on the effects of edge stiffened hole, unstiffened hole, and plain webs, under various loading conditions like compression, shear and web crippling. The literature review encompasses two main components. Notably, there is no current research literature regarding the investigation on axial capacity of CFSS channel sections with edge-stiffened web holes.

2.2 Research on CFSS channel sections

The literature review on the structural behaviours of CFSS channel section offers a comprehensive overview of key studies carried out by various researchers. Cold formed stainless steel is gaining favour as structural material due to its enhanced resistance to corrosion and longer lifespan when compared to carbon steel. The investigation conducted by Roy et al. [10] focuses on the buckling behaviour of face-to-face built-up cold-formed stainless steel channel sections under axial compression. The use of face-to-face built-up CFSS channel sections as compression members are becoming more popular. Three different grades of stainless steel i.e. duplex EN1.4462, ferritic EN1.4003 and austenitic EN1.4404 have been considered. In total, 160 Finite Element models were analysed. Analysis of the parametric study results reveals that AISI and AS/NZS standards exhibit a conservative estimation by approximately 15% for all stainless steel face-to-face built-up columns that fail due to global buckling. Conversely, these standards demonstrate an unconservative trend by approximately 5% for face-to-face built-up stainless steel columns that fail due to local buckling. Another research focused on back-to-back cold-formed stainless steel lipped channel section under axial compression conducted by Roy et al. [11] A thorough parametric investigation was conducted,

covering a wide range of slenderness ratios and various cross-sections, aiming to evaluate the strength of current design standards outlined by AISI and AS/NZS. A total of 647 finite element models were developed. The findings from this study revealed that both AISI and AS/NZS guidelines tend to be conservative, with an approximate margin of 10 to 20%, for cold-formed stainless steel built-up lipped channels failing due to overall buckling, regardless of the stainless steel grades employed. However, these standards may exhibit slight minimization, by approximately 6%, for all three grades of stainless steel built-up channels that fail due to local buckling.

The investigation conducted by Yousefi et al. [12] focus into the phenomenon of web crippling failure in specific cold formed ferritic stainless steel (CFSS) sections featuring offset web holes and fastened flanges, providing a unified set of design equations. A total of 18 test experimental tests and a parametric study including a total of 576 finite element models were reported. The experimental and FE results were compared against strength predicted in accordance with American Iron and Steel Institute (AISI) [13] and Australia and New Zealand standard (AS/NZS) [14] Upon evaluating cold-formed carbon steel plain-lipped channel sections and equations proposed by previous researchers for stainless steel plain-lipped channel sections, it was discovered that the design equations exhibit an unreliability and lack conservatism by 22% for cold-formed ferritic stainless steel unlipped channel sections. Consequently, in light of the study's findings, two reliable and dependable web crippling strength reduction factor equations were proposed.

Yousefi et al. [15] conducted a combined experimental and Finite Element Analysis (FEA) approach to examine the web crippling strength of cold-formed ferritic stainless steel unlipped channel sections featuring fastened flanges under the end-two-flange loading condition. The study comprised a total of 27 web crippling tests: 9 tests were conducted on channel sections with plain webs, while 18 tests were performed on channel sections with web

holes. In tests involving web holes, the holes were positioned either centrally or offset from the load and reaction plates. A parametric investigation was carried out utilizing quasi-static finite element analysis. The strengths derived from reduction factor equations were initially compared to those computed from equations recently proposed for cold-formed stainless steel, which were unconservative by 10%, and the experimental investigation also shows that, for the case of unlipped channels without web holes, the European Standard (EN 1993-1-4) [16] and ASCE [5] are too conservative by 43% and 28%, respectively. So, based on the experimental and FE results, web crippling design equations are proposed for both sections, with and without web holes.

Fang et al. [3] conducted a finite element analysis on the web crippling strength of cold-formed stainless steel channel sections featuring circular web holes, subjected to end-one-flange loading conditions. The study encompassed three grades of stainless steel: EN 1.4509 (ferritic), EN 1.4462 (duplex), and EN 1.4301 (austenitic). A total of 1728 Finite Element (FE) models were executed. The investigation involved varying parameters, including: the depth of the web (b_w) ranging from 100 mm to 300 mm; the ratio of flange width to web height (b_f/b_w) ranging from 0.2 to 0.5; the ratio of lip width to flange width (b_l/b_f) ranging from 0.4 to 0.6; the ratio of hole diameter to web flat depth (a/h) ranging from 0.2 to 0.8; the ratio of hole distance to web flat depth (x/h) ranging from 0.04 to 0.98; and the ratio of bearing length to web flat depth (N/h) ranging from 0.17 to 1.14. The outcomes of the parametric study led to the proposal of new web crippling strength equations and strength reduction factor equations, which surpassed the equations provided by ASCE [5], AISI [13], and AS/NZS [14].

Yousefi et al. [2] investigated the shear behaviour of cold-formed ferritic stainless-steel channel sections featuring circular web holes, through both experimental and numerical approaches. Their study involved conducting 21 shear tests on paired channel sections, subjected to loading at mid-length with a span aspect ratio of 1.0. The positioning of web holes

varied, including centre, mid-span, or offset from the applied load. They developed finite element (FE) models, validated against experimental results, and utilized them for a parametric investigation across different web thicknesses (t) ranging from 1.5 to 2.0 mm and channel clear height to thickness ratios (h/t) spanning from 86.05 to 167.63. These investigations encompassed three distinct cross-section heights: C175, C200, and C250. Notably, existing guidelines lack regarding specific shear strength reduction factors for stainless steel; the commonly referenced North American specifications for carbon steel members, AISI [13] and AS/NZS [14], are considered unreliable and unconservative, particularly for ferritic stainless steel channel sections, exhibiting a difference of 20%. Drawing upon their experimental and numerical findings, the authors propose new, dependable design equations in the form of shear strength reduction factors.

2.3 Research on CFS channel sections

Cold-formed steel (CFS) channel sections are increasingly favoured as load-bearing elements in building structures, often featuring web openings to facilitate the installation of various services. A new generation of CFS channel sections with edge-stiffened web openings have been developed, offering more strength compared to sections with unstiffened holes. These sections are widely used in New Zealand. Chen et al. [18] conducted a comprehensive study, presenting a total of 75 results comprising 26 axial compression tests and 49 Finite Element Analysis (FEA) outcomes on the compression resistance of CFS channel sections with edge-stiffened, unstiffened web openings, and plain webs. A parametric investigation, utilizing a validated FE model, explored the influences of column length, hole diameter, stiffener length, number of holes, and fillet radius. Findings indicate that, for channel sections featuring seven edge-stiffened web openings, compression resistance increased by up to 22% compared to plain channel sections. Sections with unstiffened web openings experienced a 20% reduction in compression resistance compared to plain sections. Comparison between compression

resistance derived from FE analysis and design strengths computed through the Direct Strength Method revealed DSM's conservatism of approximately 34.5% for plain channel sections with plain web, which failed either due to global buckling or a combination of local and global buckling.

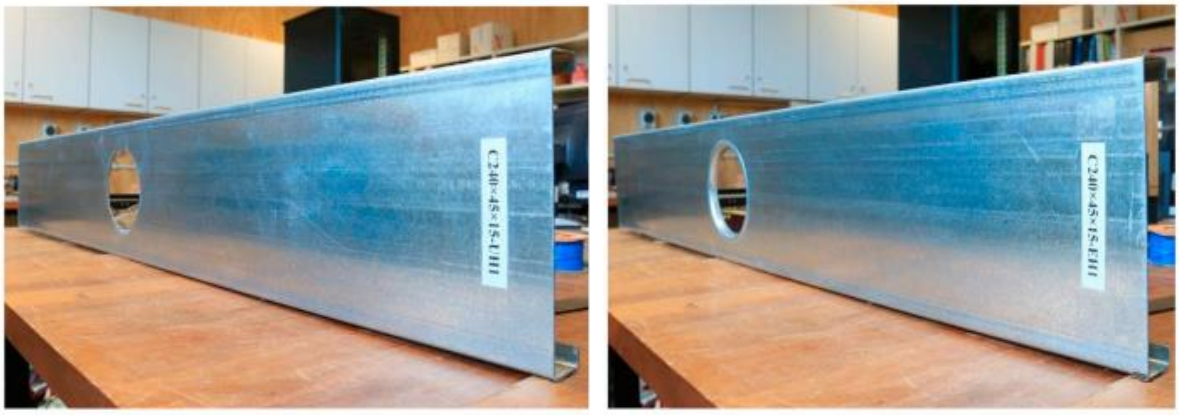

(a) Section with unstiffened web hole (b) Section with edge stiffened web hole

Figure 2-1: Cold formed steel channel sections by Chen et al. [18]

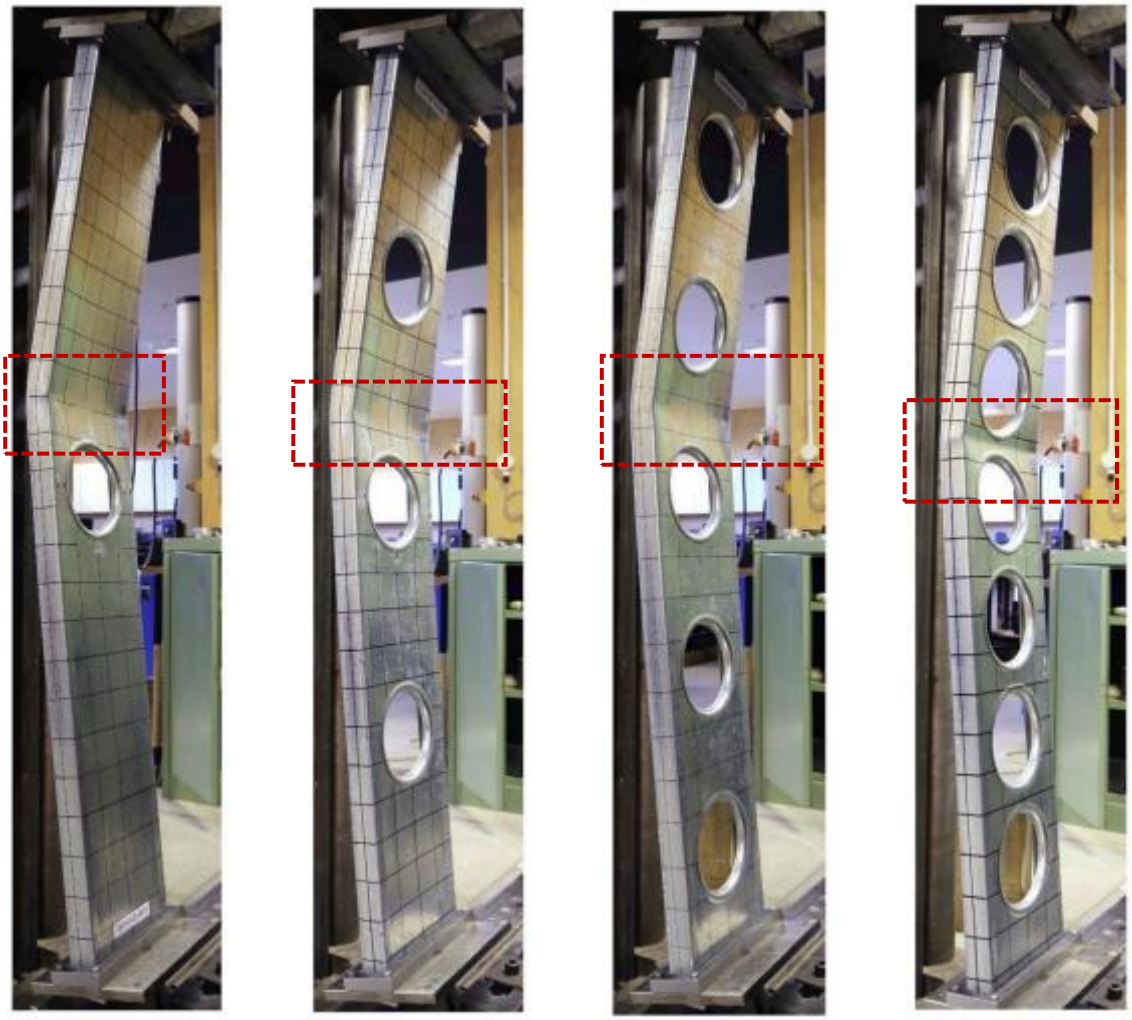

(a) EH-1 (b) EH-3 (c) EH-5 (d) EH-7

Figure 2-2: Failure modes of CFS with Edge stiffened holes under axial compression.

2.4 Aim and scope of the research.

The main objective of this study is to investigate the capacity of Cold formed stainless steel channel sections with edge-stiffened web holes subjected to axial compression. The study will be analysed and conducted based on finite element analysis. Specific objectives of the work are listed below:

1. To develop nonlinear finite-element (FE) models to simulate the structural behaviour of CFSS channel sections subjected to axial compression. The measured cross-sectional dimensions, material properties obtained from the literature and geometric

imperfections were included in the finite-element models and then the model is validated against the result obtained from the test conducted by Chen et al [18] in terms of deformed shapes, stress strain curves and axial capacity.

2. The validated FE models will be utilised for a parametric investigation, involving 2016 finite-element models, to investigate the effects of various parameters on the load bearing capacity of CFSS channel sections featuring edge-stiffened web holes subjected to axial compression.
3. To assess the accuracy of existing design guidelines in predicting the load-bearing capacity of CFS channel sections with edge-stiffened web holes, finite element analysis (FEA) results will be compared with the design strengths predicted by current design guidelines such as AISI (2016) and AS/NZS (2018).
4. Following the findings of the parametric study, we will propose appropriate equations for design reduction factors to determine the load-bearing capacity of CFSS channel sections featuring edge-stiffened web holes. Additionally, a reliability analysis will be conducted to assess the accuracy and dependability of these proposed reduction factor equations.

2.5 Outline of the thesis

This thesis is focused on the capacity of CFSS channel sections with edge-stiffened web holes subjected to compression. The thesis is structured into the following six chapters:

Chapter 1 Briefly introduces the background, problem statement, and outline of the thesis.

Chapter 2 Summaries the literature review on the behaviour and design of both CFSS and CFS channel sections including the case channel sections with edge-stiffened web holes, un-stiffened web holes, and plain webs subjected to compression, web crippling, and shear.

Chapter 3 Describes the finite element modelling.

Chapter 4 Describes the numerical analysis work conducted in this study to assess the axial capacity of CFSS channel sections with edge-stiffened web holes, un-stiffened web holes, and plain webs.

Chapter 5 Provides Design recommendations in accordance with the American Iron and Steel Institute (AISI) [13] and Australia and New Zealand Standard (AZ/NZS) [14].

Chapter 6 Describes the proposed design reduction factor equation and the reliability of the proposed reduction factor equations for CFSS channel sections with edge-stiffened web holes.

Chapter 7 Provides conclusions including the limitations of the current study and recommendations for future researchers and practicing engineers.

CHAPTER 3. Description of finite element modelling

3.1 General

Nonlinear elasto-plastic finite element (FE) models were developed using ABAQUS [19] software to simulate the behaviour of CFSS channel sections experiencing axial compression, specifically for sections having unstiffened hole and edge-stiffened hole. The FE modelling considered centreline and initial geometric imperfections and cross section dimensions for the CFSS channel sections. The subsequent sections furnish a detailed exposition of the modelling methodologies employed.

3.2 Summary of experimental test done by Chen et al [18]

Chen et al. [18] conducted experiment tests and calculated the axial capacity of CFS channel section with plain webs, unstiffened hole and edge-stiffened web holes, which were adapted for validation on this study. The data extracted from test specimens [18], enclosing section dimensions, geometrical imperfections, and boundary conditions was utilised to validate the developed Finite Element (FE) model against the experiment results. This study

drew upon the test results of Chen et al. [18] to validate the FE models for cold formed stainless steel channel sections with plain webs, unstiffened and edge stiffened circular web holes.

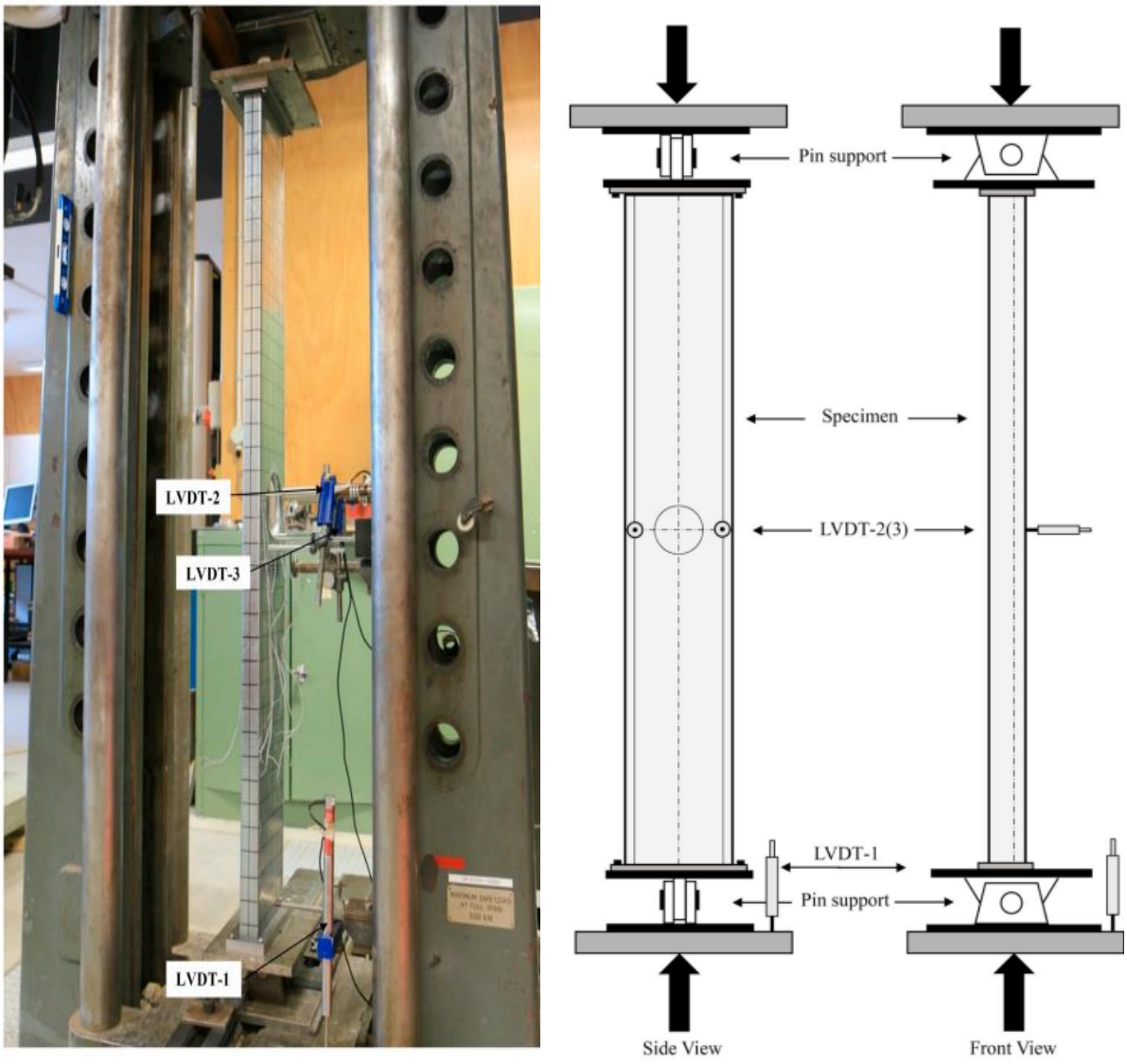

(a) Experiment test set up (b) Schematic drawing

Figure 3-1: Experimental test conducted by Chen et al. [18] to determine the axial capacity of cold formed steel channel sections.

3.3 Material properties

An elastic-plastic model was used for modelling the overall geometry of the channel sections with web openings (edge-stiffened and unstiffened) and without web holes. The geometrical dimensions and material properties for the CFSS sections for this study were taken from Yousefi et al. [18]. Refer Table 1 for material properties used in this study.

As per the ABAQUS [19], the engineering material curve was converted into a true material curve by following the equations below:

$$\sigma_{true} = \sigma(1+\varepsilon) \tag{1}$$

$$\varepsilon_{true(pl)} = \ln(1+\varepsilon) - \frac{\sigma_{true}}{E} \tag{2}$$

Where E is the Young's modulus, σ true is the true stress, σ_u is the ultimate tensile strength, σ and ε are the engineering stress and strain respectively in ABAQUS [19].

Table 1 Summary of material properties used in this study [20, 2-3]

Stainless Steel Material	**Yield Stress, f_y**	**Ultimate Stress, f_u**	**Modulus of Elasticity, E**
	MPa	MPa	MPa
Austenitic 304	205.62	825	193000
Duplex S32205	451.91	860	200000
Ferritic G430	205.62	597	200000

3.4 FE Meshing

The CFSS channel sections were simulated using S4R shell elements, each contains six degrees of freedom per node. Following a mesh sensitivity analysis, it was determined that a mesh size of 5 mm × 5 mm adequately suited both the length and width of the channel sections. However, finer mesh sizes were employed in specific regions: (a) the corner area between the flange and web of the section; (b) the corner area between the lip and flange of the section; (c)

the corner area between the web and edge-stiffener of the section; and (d) the length region of the stiffener (as illustrated in Fig. 3-2).

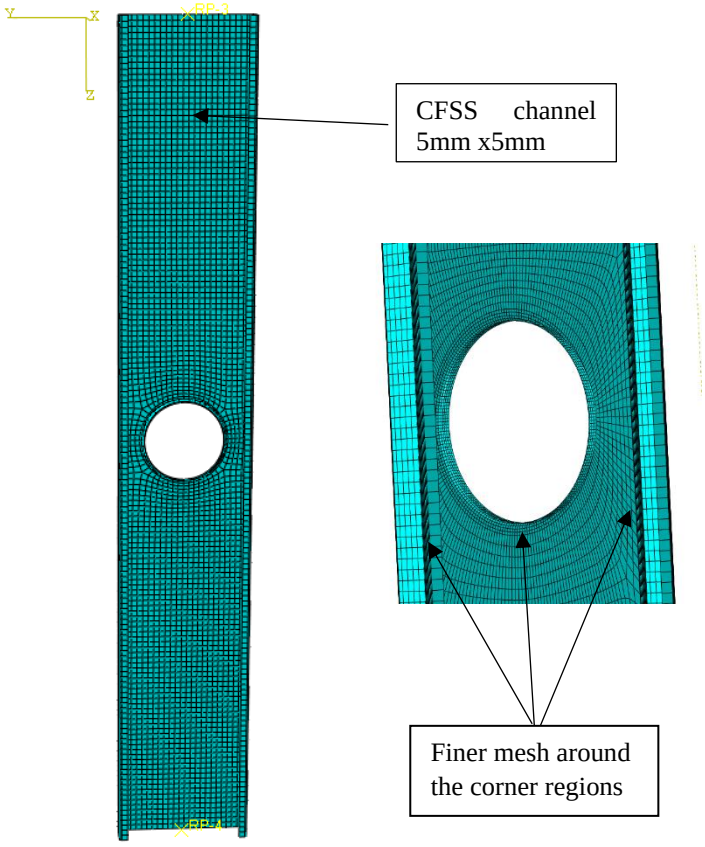

Figure 3-2: FE meshing of CFSS channel with EH1

3.5 Boundary and loading conditions.

In this study, pin-pin boundary conditions were applied to all finite element (FE) models. Two reference points, labelled R1 and R2, were designated at the top and bottom of the CFSS channel sections. To copy the experimental boundary conditions, a multipoint point constraint (MPC) was employed. These reference points were strategically located at the centre of gravity of the column cross-section.

Experimental setups might involve boundary conditions that cannot be directly modelled using standard constraints available in FEA software. MPCs provide a way to represent such

conditions by specifying relationships between different points or degrees of freedom. The use of MPCs ensures that the simulated model closely matches the experimental setup, allowing for good comparison and accurate predictions of system behaviour.

To replicate the pin-pin boundary condition, translational movements, expect those in the z-direction, were constrained at the top reference point. The axial compression load in the z-direction was applied via a reference point using the displacement-controlled method. The bottom reference point remained unrestrained. Notably, both reference points were permitted to rotate along the minor axis. Figure 3-3 depicts the boundary conditions of a CFSS channel column with EH.

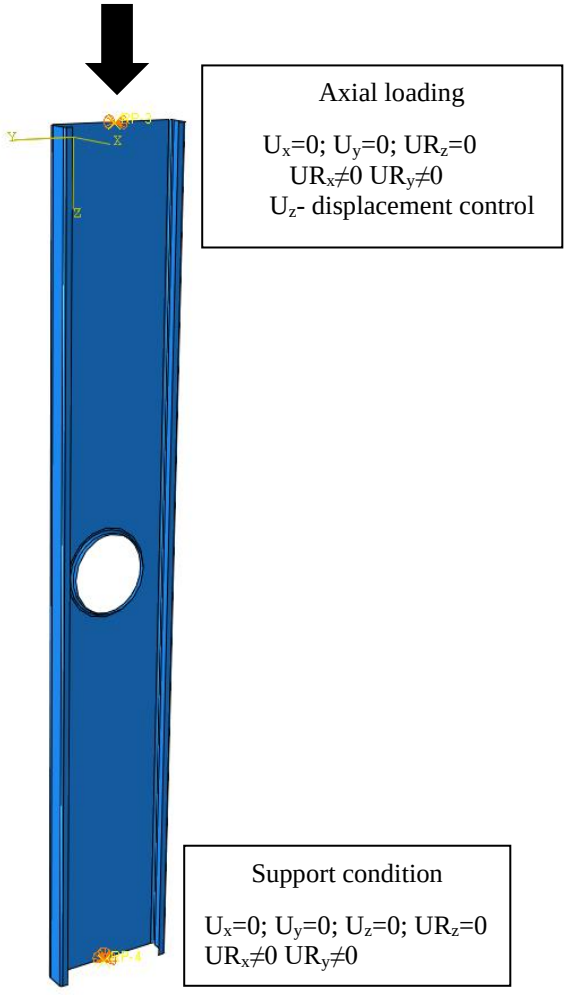

Figure 3-3: Applied boundary conditions for CFSS EH1 channel

3.6 Geometrical imperfections

During the finite element (FE) modelling process, initial geometric imperfections were considered. For CFS channels with a thickness (t) less than 3mm, the magnitude of the buckled shape was scaled to 0.34t and 0.94t for local and distortional buckling, respectively. For samples with a thickness (t) exceeding 3 mm, the imperfection magnitude was determined using the equation proposed by Walker [26]

$$\omega_d = 0.3t\sqrt{\frac{\sigma_{0.2\%}}{\sigma_{cr}}} = 0.3t\lambda_s$$

where $\sigma 0.2\%$ and σcr are 0.2% proof stress of the material and elastic critical local/distortional buckling stress of the cross-section, and λs is the cross-sectional slenderness, given by:

$$\lambda_s = \sqrt{f_y}/\sigma_{cr}$$

The overall buckling imperfection magnitude also accounted for the length of the member. It's important to note that in the FE models of short elements, either a local or distortional imperfection was integrated, depending on which mode had the lower critical buckling stress. However, for medium and long-length sections, a combination of three buckling modes local, distortional, and global was introduced. This approach was adopted to effectively incorporate the magnitudes of imperfections into the model [18].

3.7 Validation of the FE models

Table 2 provide a comparison of the test results from Chen et al. [18] with the FEA results. For UH, EH and plain sections the mean and coefficient of variation (COV) values for the ratio of test and FEA results were 0.97 and 0.03, respectively. Figs. 3-4 and 3-6 depict the failure modes of both the tests and the FEA. The failure modes of the developed FE model were good correlation to the test results for both UH and edge-stiffened circular web holes. The

load-displacement curves in Figs. 3-5 and 3-7 showed a reasonable agreement between the FEA and test results. In conclusion, the developed FE model in this study exhibited a good match with the test results.

Table 2 comparison of test results and FEA [18] for CFSS channel sections with plain, unstiffened and edge-stiffened circular web holes.

Section dimensions								Axial capacity		
Web depth d (mm)	Thickness of section t (mm)	Flange width b_f (mm)	Lip depth b_l (mm)	Length of column L (mm)	Hole depth d_w (mm)	Number of holes	Stiffener length q (mm)	Test P_{EXP} (kN)	FEA P_{FEA} (kN)	P_{EXP}/P_{FEA}
Plain section										
239	1.75	44.6	15.5	1505.8	-	-	-	62.3	61.74	0.99
240.5	1.74	44.2	14.8	1502.5	-	-	-	59.5	60.73	0.97
238.5	1.79	44.9	14.7	1500.1	-	-	-	60.8	64.37	0.95
Unstiffened web holes										
239.5	1.7	44.2	15.6	1502	145.2	1	-	52.1	50.76	1.02
238.2	1.71	44.8	15.2	1502.1	127.2	3	-	49.37	52.13	0.95
240.7	1.7	44.7	15.6	1501.2	130.2	5	-	48.22	50.16	0.96
239.7	1.73	44.6	14.8	1500	130.5	7	-	47.31	48.82	0.97
Edge-stiffened web holes										
238	1.75	45.7	15	1502	143.70	1	13	63.9	68.32	0.94
239.5	1.72	44.9	14.7	1502.5	142.70	3	13	66	67.07	0.98
238.5	1.73	44.7	14.5	1501.5	143.50	5	13	68	71.85	0.95
239.5	1.7	43.5	15.4	1501.8	140.5	7	13	73.2	72.01	1.02
									Mean	0.97
									COV	0.03

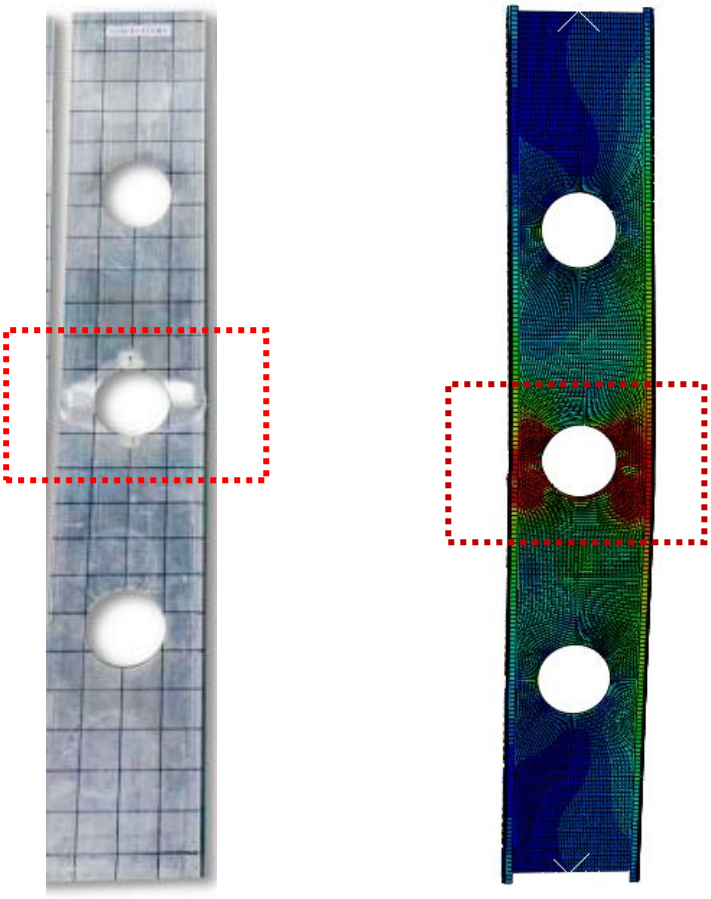

Figure 3-4: Failure modes of test [18] and FEA for UH3 CFSS section

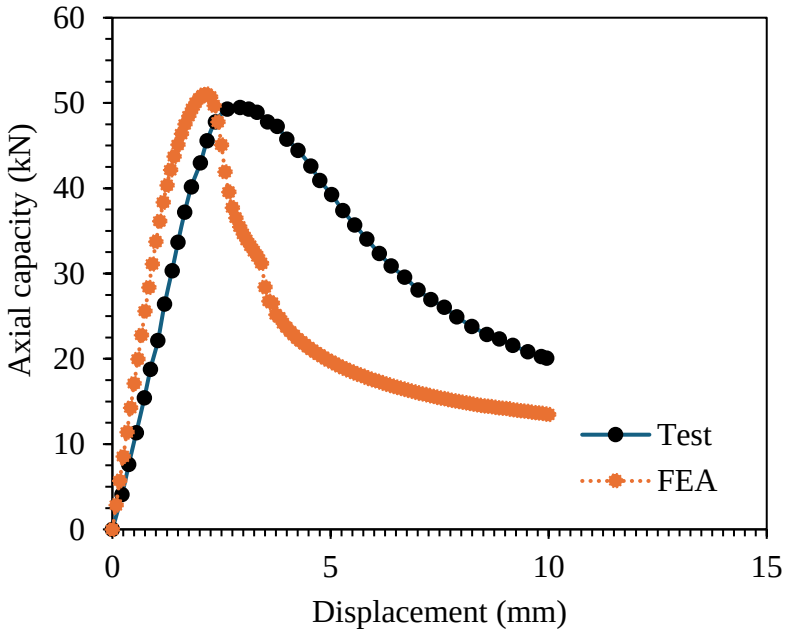

Figure 3-5: Load-displacement curves of FEA and test [18] of UH3 section

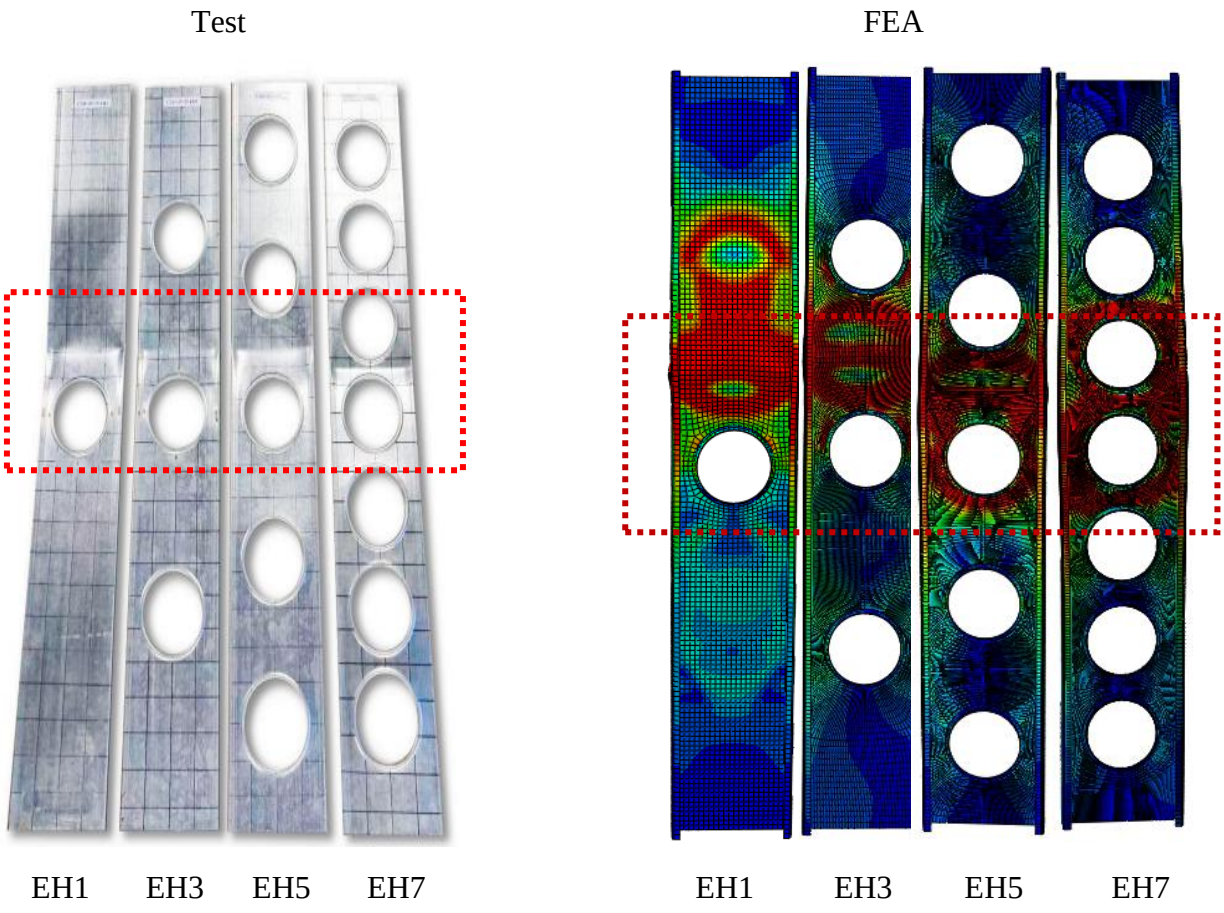

Figure 3-6: Failure modes of FEA and test [18] for sections with edge-stiffened holes

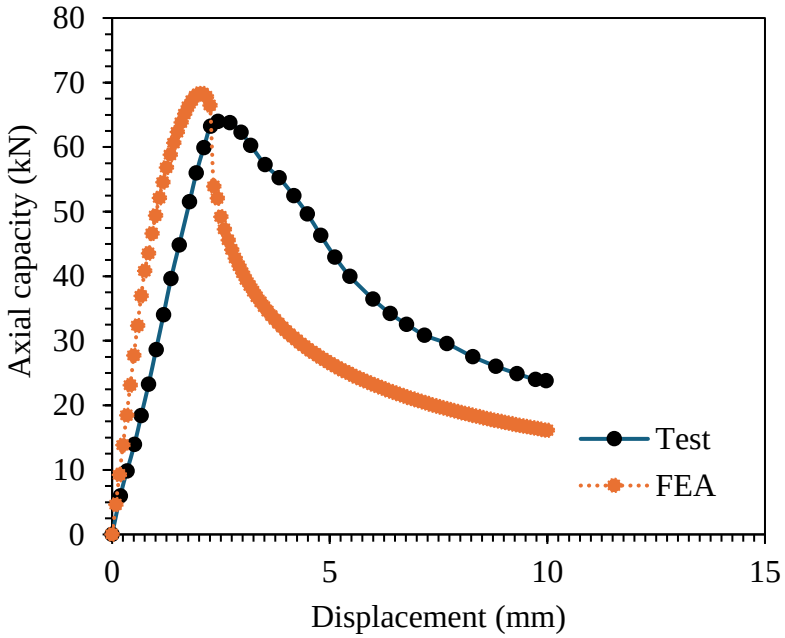

Figure 3-7: Load-displacement curves of FEA and test [18] for section (C240-L1500-EH1) with edge-stiffened web holes

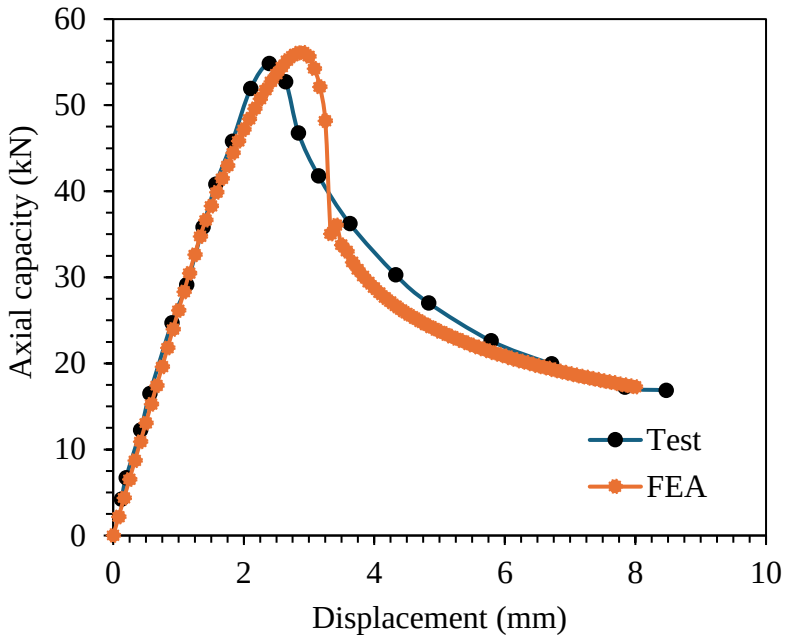

Figure 3-8: Load-displacement curves of FEA and test [18] for section (C240-L1500-NH) with no web holes

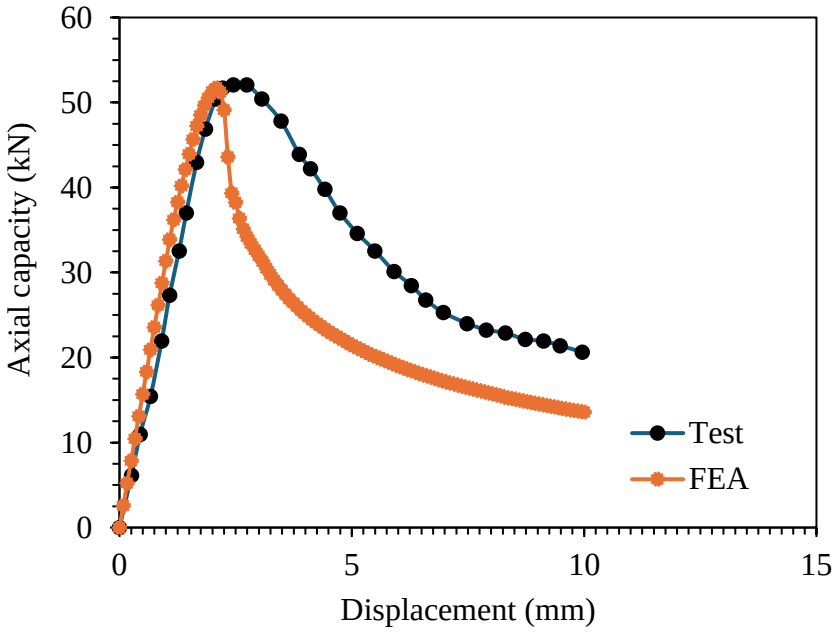

Figure 3-9: Load-displacement curves of FEA and test [18] for section (C240-L1500-UH1) with unstiffened web holes.

CHAPTER 4. Parametric study

4.1 General

A parametric study was conducted using validated FE models. The parametric study considered the C200x65x15 and C300x80x20 channel sections with a total number of 2016

finite element models having an opening diameter ratio a/h = 0.2,0.4 and 0.6 mm (for both the edge-stiffened and unstiffened web openings), covering columns length from 1000, 1500 and 2000 mm having thickness about 1.5, 2, 2.5 and 3 mm. The slenderness of column (λ_c) ranged from 0.45 to 1.41. considering 1, 3 and 5 holes with equal spacing, the parametric study also considered channel sections having edge-stiffened web openings, unstiffened web openings and no web openings (i.e. plain channel sections). The results are presented in Table 3.

The specimens were used for the parametric study and labelled based on thickness of channel, channels web depth, width, and lip, number of holes, length of stiffener around the web, ratio of web hole to depth and length of channel.

For example, the label "C200x65x15-T1.5-EH5-D0.2-Q10-L1500" is elaborated below.

- "C200x65x15" indicates Channel "depth x width x lip" that is d=200mm, b=65mm and l=15mm.
- "T1.5" defines as channel thickness, i.e., t=1.5mm.
- "EH5" represents the number of holes in the web and whether they are unstiffened (UH) or edge stiffened (EH) web holes.
- "D0.2" refers to the hole depth to web depth ratio, i.e., a/h = 0.2.
- "Q10" defines as the stiffener length around the web hole, i.e., q=10mm.
- "L1500" represents as the whole length of the channel. That is L=1500mm.

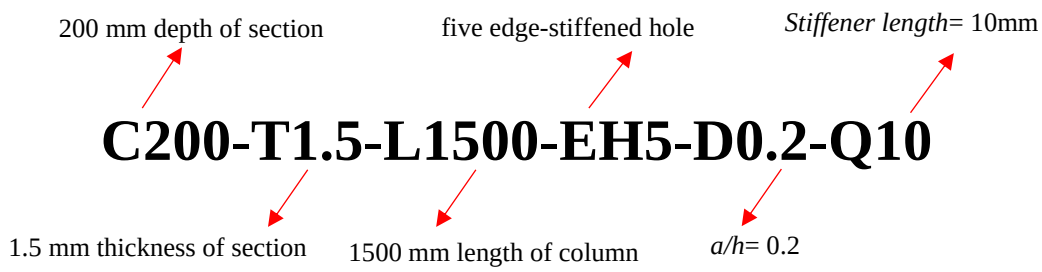

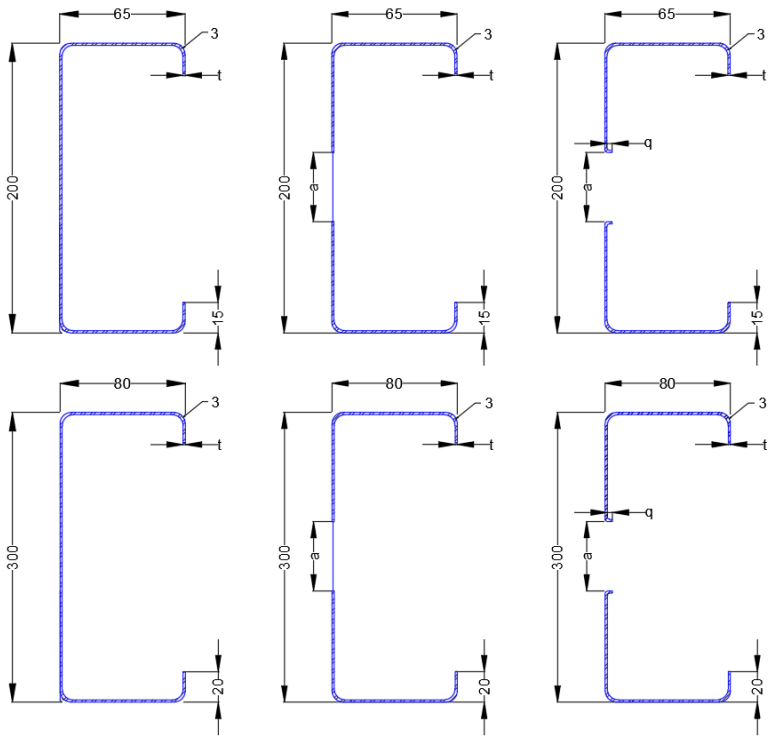

Figure 4-1: Cross sectional details (All dimensions are in mm)

4.2 CFSS channel sections with plain webs.

4.2.1 Effects of different grades of CFSS channel sections

Fig. 4-2 represents the effects of 3 different grade of cold-formed stainless-steel sections on average axial capacity. As its seen from Fig 4-2 the average increase in axial capacity was 48.56% when the grades of CFSS channel changed from austenitic to duplex. Similarly, an increment of 47.13% in axial capacity can be seen when the grades of steel changes from ferritic to duplex. Notably, despite having the same yield stress for austenitic and ferritic materials, the axial capacity decreases by 0.97% due to differences in Young's modulus, ultimate stress, and ultimate strain.

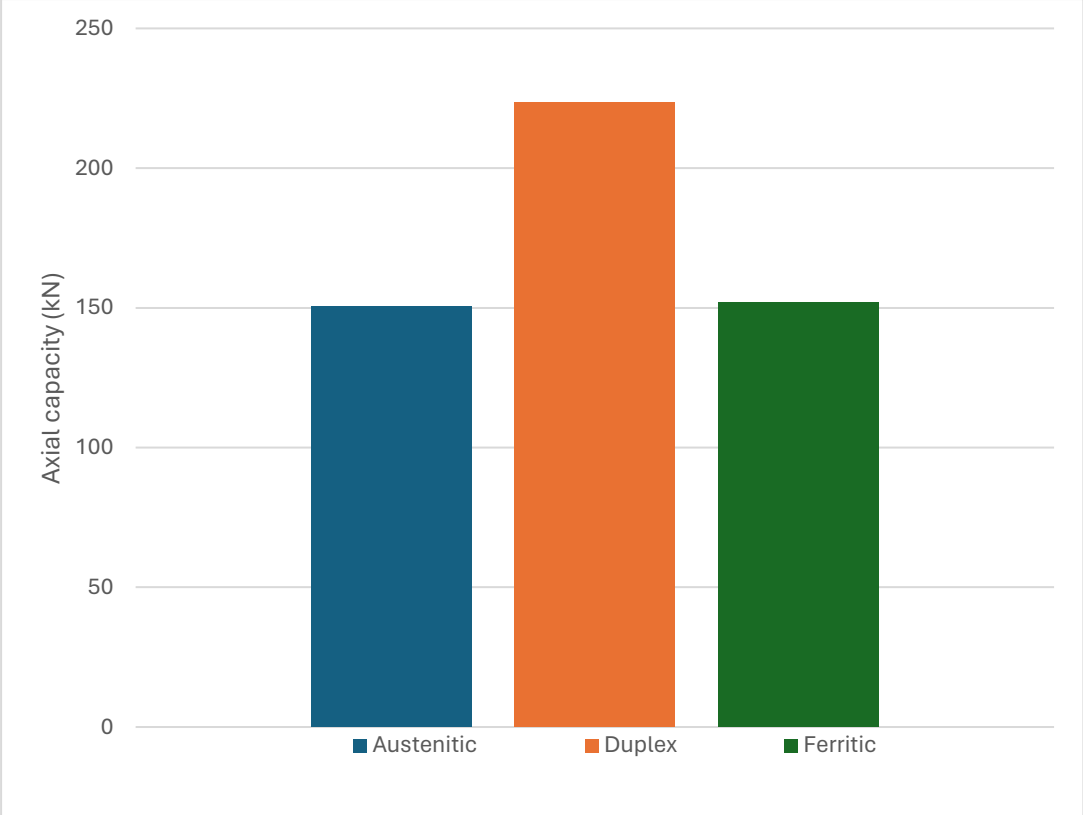

Figure 4-2: Effects of different grades of CFSS channel section

Table 3 Parametric study results for C200x65x15 and C300x80x20 channel sections with plain webs, unstiffened and edge-stiffened web holes

Austenitic stainless steel C200

Specimen	Plain web (kN)	Axial capacity results of plain, UH and EH from FEA, P_{FEA} (kN)								
		UH1	EH1		UH3	EH3		UH5	EH5	
			Q10	Q15		Q10	Q15		Q10	Q15
For L1000										
C200-T1.5-D0.2	56.28	56.772	58.351	59.125	54.903	57.221	57.314	54.22	57.099	58.891
C200-T1.5-D0.4	56.28	52.995	57.691	57.993	52.665	56.205	58.373	50.69	53.146	55.55
C200-T1.5-D0.6	56.28	49.792	50.22	50.778	48.228	49.263	51.228	43.773	48.88	51
C200-T2-D0.2	86.85	84.694	89.932	90.709	83.105	89.26	89.396	82.223	89.115	90.926
C200-T2-D0.4	86.85	82.114	89.248	90.018	81.95	88.614	90.675	80.223	84.67	86.11
C200-T2-D0.6	86.85	70.889	80.64	82.56	64.417	70.22	71.75	69.541	69.78	76.11
C200-T2.5-D0.2	121.71	118.24	128.4	129.96	117.44	127.96	128.32	116.98	126.56	128.73
C200-T2.5-D0.4	121.71	115.46	115.26	116.63	115.11	114.08	115.99	112.98	113.73	115.99
C200-T2.5-D0.6	121.71	87.378	98.266	99.774	83.011	95.745	96.707	80.23	92.333	99.15
C200-T3-D0.2	160.74	155.14	168.54	169.49	154.08	167.55	168.84	151.04	165.05	166.65
C200-T3-D0.4	160.74	133.83	137.31	140.51	132.67	136.21	139.37	130.04	134.36	135.78
C200-T3-D0.6	160.74	101.63	119.32	120.83	99.265	118.57	119.96	96.05	116.74	119.85
For L1500										
C200-T1.5-D0.2	51.77	53.961	57.39	58.43	52.428	54.48	55.505	51.22	52.618	52.685
C200-T1.5-D0.4	51.77	47.91	55.67	56.72	47.021	53.076	53.927	45.319	52.76	57.05
C200-T1.5-D0.6	51.77	40.785	48.56	49.5	39.996	46.88	47.995	36.16	44.8	47.17
C200-T2-D0.2	79.81	78.616	81.932	82.694	78.132	82.091	82.221	77.899	82.786	82.806
C200-T2-D0.4	79.81	72.866	81.428	81.692	70.84	76.248	77.996	68.115	80.27	80.758

C200-T2-D0.6	79.81	62.5	74.45	75.14	60.057	64.223	65.14	59.547	65.25	66.058
C200-T2.5-D0.2	113.49	112.96	122.44	124.5	112.11	120.35	122.73	111.42	118.16	119.25
C200-T2.5-D0.4	113.49	100.5	108.71	109.14	99.54	107.1	110.5	98.334	102.11	102.55
C200-T2.5-D0.6	113.49	80.572	91.5	90.69	79.707	89.43	90.133	78.582	88.102	89.16
C200-T3-D0.2	150.4	147.92	155.05	156.09	146.53	154.75	155.8	144.98	154.5	155.58
C200-T3-D0.4	150.4	126.93	128.79	131.83	125.82	125.96	126.3	120.56	121.58	122.9
C200-T3-D0.6	150.4	106.17	118.82	120.59	104.3	112.98	115.77	100.38	105.71	109.89
For L2000										
C200-T1.5-D0.2	46.05	49.926	52.923	53.638	48.627	52.615	54.651	48.067	50.976	52.158
C200-T1.5-D0.4	46.05	47.993	53.665	55.12	45.068	52.75	53.5	44.116	50.95	53.115
C200-T1.5-D0.6	46.05	43.408	50.62	51.74	37.125	47.193	48.93	36.36	46.12	46.75
C200-T2-D0.2	71.28	71.237	74.975	75.65	70.96	73.86	74.202	70.67	73.385	73.409
C200-T2-D0.4	71.28	67.794	71.408	71.714	66.471	71.22	71.65	66.005	70.311	72.27
C200-T2-D0.6	71.28	57.934	62.96	63.41	55.528	60.99	61.71	53.402	58.45	59.114
C200-T2.5-D0.2	95.7	100.81	114.49	114.95	99.991	110.19	112.08	99.161	105.22	105.96
C200-T2.5-D0.4	95.7	92.898	95.495	97.127	90.656	94.311	94.99	88.78	93.23	95.112
C200-T2.5-D0.6	95.7	74.75	81.77	82.408	70.395	74.22	75	66.605	71.46	72.99
C200-T3-D0.2	133.89	132.41	139.31	139.84	130.51	138.6	139.17	129.28	137.51	138.83
C200-T3-D0.4	133.89	115.52	117.27	118.65	111.84	116.59	117.15	108.18	110.75	111.15
C200-T3-D0.6	133.89	89.212	91.32	91.77	83.852	90.45	91.984	79.795	89.88	95.556

Austenitic stainless steel C300

Specimen	Plain web (kN)	Axial capacity results of plain, UH and EH from FEA, P_{FEA} (kN)								
		UH1	EH1		UH3	EH3		UH5	EH5	
			Q10	Q15		Q10	Q15		Q10	Q15
For L1000										
C300-T1.5-D0.2	62.26	62.451	65.95	66.54	62.107	65.58	66.18	60.333	63.71	64.29
C300-T1.5-D0.4	62.26	60.407	63.79	64.36	59.98	63.34	63.91	59.372	62.70	63.26
C300-T1.5-D0.6	62.26	56.559	59.73	60.26	51.06	53.92	54.40	45.391	47.93	48.36
C300-T2-D0.2	98.39	101.11	106.77	107.73	97.857	103.34	104.27	96.785	102.20	103.12
C300-T2-D0.4	98.39	90.791	95.88	96.74	89.887	94.92	95.77	89.518	94.53	95.38
C300-T2-D0.6	98.39	76.553	80.84	81.57	74.24	78.40	79.10	71.886	75.91	76.59
C300-T2.5-D0.2	134.06	134.61	142.15	143.43	133.15	140.61	141.87	132.23	139.63	140.89
C300-T2.5-D0.4	134.06	133.53	141.01	142.28	124.95	131.95	133.13	122.88	129.76	130.93
C300-T2.5-D0.6	134.06	117.23	123.79	124.91	104.79	110.66	111.65	101.84	107.54	108.51
C300-T3-D0.2	179.65	178.27	188.25	189.95	177.53	187.47	189.16	174.93	184.73	186.39
C300-T3-D0.4	179.65	162.09	171.17	172.71	161.55	170.60	172.13	159.83	168.78	170.30
C300-T3-D0.6	179.65	145.26	153.39	154.78	140.07	147.91	149.25	139.84	147.67	149.00
For L1500										
C300-T1.5-D0.2	58.173	62.628	66.14	66.73	57.046	60.24	60.78	56.579	59.75	60.29
C300-T1.5-D0.4	58.173	54.235	57.27	57.79	53.856	56.87	57.38	52.266	55.19	55.69
C300-T1.5-D0.6	58.173	49.897	52.69	53.17	47.733	50.41	50.86	46.686	49.30	49.74
C300-T2-D0.2	92.96	91.254	96.36	97.23	90.864	95.95	96.82	89.897	94.93	95.79
C300-T2-D0.4	92.96	89.479	94.49	95.34	85.196	89.97	90.78	84.252	88.97	89.77

C300-T2-D0.6	92.96	71.983	76.01	76.70	69.807	73.72	74.38	67.103	70.86	71.50
C300-T2.5-D0.2	130.91	128.87	136.09	137.31	128.85	136.07	137.29	128.22	135.40	136.62
C300-T2.5-D0.4	130.91	119.46	126.15	127.29	119.04	125.71	126.84	116.08	122.58	123.68
C300-T2.5-D0.6	130.91	100.55	106.18	107.14	99.134	104.69	105.63	95.951	101.32	102.24
C300-T3-D0.2	172.14	172.13	181.77	183.41	170.73	180.29	181.91	170.53	180.08	181.70
C300-T3-D0.4	172.14	161.5	170.54	172.08	159.88	168.83	170.35	156.96	165.75	167.24
C300-T3-D0.6	172.14	140.4	148.26	149.60	133.76	141.25	142.52	125.55	132.58	133.77
For L2000										
C300-T1.5-D0.2	54.32	54.329	57.37	57.89	54.268	57.31	57.82	54.134	57.17	57.68
C300-T1.5-D0.4	54.32	54.282	57.32	57.84	54.065	57.09	57.61	53.59	56.59	57.10
C300-T1.5-D0.6	54.32	45.566	48.12	48.55	43.801	46.25	46.67	40.392	42.65	43.04
C300-T2-D0.2	86.32	87.144	92.02	92.85	87.048	91.92	92.75	86.574	91.42	92.24
C300-T2-D0.4	86.32	80.456	84.96	85.73	77.99	82.36	83.10	76.812	81.11	81.84
C300-T2-D0.6	86.32	68.645	72.49	73.14	65.039	68.68	69.30	62.972	66.50	67.10
C300-T2.5-D0.2	125.66	125.27	132.29	133.48	124.94	131.94	133.12	122.12	128.96	130.12
C300-T2.5-D0.4	125.66	112.94	119.26	120.34	112.13	118.41	119.47	112.05	118.32	119.39
C300-T2.5-D0.6	125.66	95.698	101.06	101.97	93.509	98.75	99.63	92.696	97.89	98.77
C300-T3-D0.2	159.02	161.27	170.30	171.83	160.98	169.99	171.52	160.73	169.73	171.26
C300-T3-D0.4	159.02	150.79	159.23	160.67	148.88	157.22	158.63	144.43	152.52	153.89
C300-T3-D0.6	159.02	120.64	127.40	128.54	118.36	124.99	126.11	116.04	122.54	123.64

Duplex stainless steel C200

Specimen	Plain web (kN)	Axial capacity results of plain, UH and EH from FEA, P_{FEA} (kN)									
		UH1	EH1		UH3	EH3		UH5	EH5		
			Q10	Q15		Q10	Q15		Q10	Q15	
For L1000											
C200-T1.5-D0.2	91.22	90.127	93.039	94.825	89.998	92.833	92.91	89.65	92.55	95.308	
C200-T1.5-D0.4	91.22	86.661	99.012	100.84	85.998	93.914	94.708	84.287	90.64	91.66	
C200-T1.5-D0.6	91.22	76.214	98.85	99.1	75.554	86.027	86.75	74.058	78.331	79.165	
C200-T2-D0.2	145.33	144.86	154.56	155.55	143.3	147.47	147.87	142.66	146.14	148.27	
C200-T2-D0.4	145.33	141.69	155.42	155.91	141.11	150.15	150.5	140.29	144.22	144.62	
C200-T2-D0.6	145.33	118.3	125.24	127.12	115.36	120.99	126.55	112.96	118.56	119.54	
C200-T2.5-D0.2	203.82	200.42	219.64	220.02	200.25	216.11	222.67	199.43	209.71	209.89	
C200-T2.5-D0.4	203.82	198.55	226.52	228.08	197.54	214.49	214.96	195.43	200.12	200.51	
C200-T2.5-D0.6	203.82	158.01	168.96	169.14	155.96	166.6	167.33	156.04	158.05	158.85	
C200-T3-D0.2	267.96	263.11	281.64	284.36	262.32	278.66	278.92	260.4	276.78	282.45	
C200-T3-D0.4	267.96	258.62	269.05	273.87	255.77	268.49	275.63	250.4	255.63	255.75	
C200-T3-D0.6	267.96	202.5	224.11	225.53	195.23	212.11	213.30	193.28	211.82	213.56	
For L1500											
C200-T1.5-D0.2	77.71	84.276	84.042	85.577	83.896	83.949	84.969	77.303	78.81	78.836	
C200-T1.5-D0.4	77.71	76.481	83.459	83.76	75.295	82.007	91.336	74.514	81.99	83.112	
C200-T1.5-D0.6	77.71	68.902	70.98	71.15	65.084	68.32	69.17	64.939	64.223	69.887	
C200-T2-D0.2	121.53	132.54	140.4	141.11	130.08	136.82	141.44	124.96	125.4	126.44	
C200-T2-D0.4	121.53	115.74	160.68	164.82	114.57	144.67	150.16	112.94	120.90	121.96	

C200-T2-D0.6	121.53	100.71	118.65	119.25	96.894	114.22	115.66	92.559	101.11	101.82
C200-T2.5-D0.2	170.11	169.67	193.04	195.49	169.02	192.23	194.78	165.57	184.03	185.35
C200-T2.5-D0.4	170.11	164.02	197.3	200.69	160.5	167.23	169.98	158.62	165.44	168.25
C200-T2.5-D0.6	170.11	141.59	155.23	156.74	134.73	144.89	145.56	131.58	142.12	144.99
C200-T3-D0.2	223.44	243.25	255.51	256.76	236.78	240.46	241.88	235.1	237.71	239.91
C200-T3-D0.4	223.44	213.92	221.51	223.87	208.05	214.18	216.1	203.22	215.31	216.16
C200-T3-D0.6	223.44	180.62	199.25	199.89	167.01	178.66	179.9	159.3	166.99	170.15
For L2000										
C200-T1.5-D0.2	61.91	67.599	79.194	80.505	61.648	77.873	78.105	60.654	72.264	74.268
C200-T1.5-D0.4	61.91	65.183	69.97	73.073	60.421	69.477	72.96	58.77	68.8	70.85
C200-T1.5-D0.6	61.91	55.709	66.75	67.21	54.656	66.125	67.58	51.968	60.25	60.82
C200-T2-D0.2	93.4	93.994	115.18	118.12	92.77	110.34	110.84	91.69	95.459	96.53
C200-T2-D0.4	93.4	90.886	100.56	116.22	89.821	96.33	95.15	87.846	95.12	100.66
C200-T2-D0.6	93.4	84.456	88.36	89.25	82.053	86.472	91.22	78.915	85.22	87.46
C200-T2.5-D0.2	128.61	128.51	131.21	131.53	128.08	135.28	136.46	127.81	131.88	131.97
C200-T2.5-D0.4	128.61	128.48	128.88	129.24	126.28	134.65	136.66	124.27	136.56	136.76
C200-T2.5-D0.6	128.61	116.77	122.94	123.09	110.57	118.56	119.65	109.88	115.96	116.78
C200-T3-D0.2	165.64	165.69	176.88	177.61	164.6	175.25	176.05	162.55	171.03	171.35
C200-T3-D0.4	165.64	160.47	172.22	173.52	158.22	169.04	182.44	157.37	167.6	168.99
C200-T3-D0.6	165.64	147.09	155.99	156.81	135.17	145.58	146.65	125.45	136.55	137.11

Duplex stainless steel C300

Specimen	Plain web (kN)	Axial capacity results of plain, UH and EH from FEA, P_{FEA} (kN)								
		UH1	EH1		UH3	EH3		UH5	EH5	
			Q10	Q15		Q10	Q15		Q10	Q15
For L1000										
C300-T1.5-D0.2	100.18	100.11	105.72	106.67	99.683	105.27	106.21	97.605	103.07	104.00
C300-T1.5-D0.4	100.18	98.492	104.01	104.94	96.92	102.35	103.27	96.12	101.50	102.42
C300-T1.5-D0.6	100.18	86.855	91.72	92.54	84.865	89.62	90.42	62.611	66.12	66.71
C300-T2-D0.2	163.11	163.53	172.69	174.24	162.4	171.49	173.04	161.63	170.68	172.22
C300-T2-D0.4	163.11	162.08	171.16	172.70	157.05	165.84	167.34	156.01	164.75	166.23
C300-T2-D0.6	163.11	137.24	144.93	146.23	136.76	144.42	145.72	120.88	127.65	128.80
C300-T2.5-D0.2	232.07	233.05	246.10	248.32	231.24	244.19	246.39	230.28	243.18	245.36
C300-T2.5-D0.4	232.07	222.49	234.95	237.06	220.55	232.90	235.00	220.18	232.52	234.61
C300-T2.5-D0.6	232.07	197.72	208.79	210.67	186.63	197.08	198.86	180.09	190.18	191.89
C300-T3-D0.2	305.84	305.84	322.97	325.87	303.19	320.17	323.05	300.13	316.94	319.79
C300-T3-D0.4	305.84	289.43	305.64	308.39	288.1	304.23	306.97	278.32	293.91	296.55
C300-T3-D0.6	305.84	240.65	254.13	256.41	235.89	249.10	251.34	233.06	246.11	248.33
For L1500										
C300-T1.5-D0.2	89.07	93.83	99.08	99.98	89.357	94.36	95.21	88.116	93.05	93.89
C300-T1.5-D0.4	89.07	89.664	94.69	95.54	85.7	90.50	91.31	83.965	88.67	89.47
C300-T1.5-D0.6	89.07	80.486	84.99	85.76	77.134	81.45	82.19	74.972	79.17	79.88
C300-T2-D0.2	144.77	142.5	150.48	151.83	141.93	149.88	151.23	141.3	149.21	150.56
C300-T2-D0.4	144.77	138.79	146.56	147.88	136.18	143.81	145.10	134.64	142.18	143.46

C300-T2-D0.6	144.77	122.78	129.66	130.82	121.33	128.12	129.28	118.49	125.13	126.25
C300-T2.5-D0.2	212.58	213.81	225.78	227.82	207.66	219.29	221.26	204	215.42	217.36
C300-T2.5-D0.4	212.58	200.59	211.82	213.73	198.55	209.67	211.56	195	205.92	207.77
C300-T2.5-D0.6	212.58	187.67	198.18	199.96	172.78	182.46	184.10	165.27	174.53	176.10
C300-T3-D0.2	282.16	281.58	297.35	300.02	273.82	289.15	291.76	272.57	287.83	290.42
C300-T3-D0.4	282.16	259.74	274.29	276.75	256.89	271.28	273.72	254.3	268.54	270.96
C300-T3-D0.6	282.16	222.69	235.16	237.28	214.36	226.36	228.40	212.75	224.66	226.69
For L2000										
C300-T1.5-D0.2	78.22	83.766	88.46	89.25	78.085	82.46	83.20	77.091	81.41	82.14
C300-T1.5-D0.4	78.22	77.645	81.99	82.73	76.108	80.37	81.09	75.99	80.25	80.97
C300-T1.5-D0.6	78.22	73.072	77.16	77.86	72.04	76.07	76.76	71.061	75.04	75.72
C300-T2-D0.2	126.8	125.75	132.79	133.99	124.8	131.79	132.97	124.3	131.26	132.44
C300-T2-D0.4	126.8	132.75	140.18	141.45	130.88	138.21	139.46	128.36	135.56	136.78
C300-T2-D0.6	126.8	111.54	117.79	118.85	108.88	114.98	116.01	106.39	112.35	113.36
C300-T2.5-D0.2	181.93	183.02	193.27	195.01	177.68	187.63	189.32	177.14	187.06	188.74
C300-T2.5-D0.4	181.93	177.3	187.23	188.91	176.28	186.15	187.83	172.75	182.42	184.07
C300-T2.5-D0.6	181.93	153.3	161.88	163.34	149	157.34	158.76	146.01	154.19	155.57
C300-T3-D0.2	232.25	255.98	270.31	272.75	250.29	264.31	266.68	233.53	246.61	248.83
C300-T3-D0.4	232.25	230.78	243.70	245.90	225.17	237.78	239.92	223.34	235.85	237.97
C300-T3-D0.6	232.25	198.56	209.68	211.57	192.6	203.39	205.22	188.05	198.58	200.37

Ferritic stainless steel C200

Specimen	Plain web (kN)	Axial capacity results of plain, UH and EH from FEA, P_{FEA} (kN)									
		UH1	EH1		UH3	EH3		UH5	EH5		
			Q10	Q15		Q10	Q15		Q10	Q15	
For L1000											
C200-T1.5-D0.2	57.13	55.806	58.934	59.733	54.023	58.669	59.992	54	57.89	57.996	
C200-T1.5-D0.4	57.13	53.739	57.756	58.338	52.023	57.22	58.988	50.11	56.997	60.15	
C200-T1.5-D0.6	57.13	44.965	57.43	58.486	43.75	55.1	55.994	41.269	50.7	51.894	
C200-T2-D0.2	87.78	85.148	90.427	90.792	84.649	89.556	91.4	84.123	89.114	91.67	
C200-T2-D0.4	87.78	79.819	89.358	94.435	79.115	88.33	91.378	77.45	87.64	89.969	
C200-T2-D0.6	87.78	66.743	79.99	81.179	64.974	76.98	77.011	60.829	74.22	77.984	
C200-T2.5-D0.2	122.87	119.57	128.12	128.75	119.13	129.14	130.92	118.07	129.88	129.98	
C200-T2.5-D0.4	122.87	116.25	114.15	117.03	115.99	113.55	116.4	112.07	112.79	113.15	
C200-T2.5-D0.6	122.87	84.203	90.222	91.16	83.308	90.1	90.974	80.824	99.1	99.75	
C200-T3-D0.2	162.54	156.72	169.53	169.98	155.56	168.98	170.12	152.66	165.68	167.34	
C200-T3-D0.4	162.54	150.64	150.44	152.86	149.26	146.58	149.71	146.66	144.44	151.89	
C200-T3-D0.6	162.54	101.86	118.56	118.96	99.6	116.25	117.11	98.332	115.95	116.55	
For L1500											
C200-T1.5-D0.2	52.52	55.272	57.056	58.172	51.781	53.236	53.27	51.601	53.24	53.455	
C200-T1.5-D0.4	52.52	50.99	60.553	60.94	49.55	58.856	59.499	49.005	57.85	58.136	
C200-T1.5-D0.6	52.52	42.39	50.11	51.39	40.646	49.77	56.265	40.699	44.38	45.54	
C200-T2-D0.2	81.11	79.653	83.914	84.092	79.338	83.433	83.855	78.983	83.211	84.013	
C200-T2-D0.4	81.11	75.992	82.288	82.624	74.502	78.523	79.6	74.115	78.005	79.16	

C200-T2-D0.6	81.11	69.194	78.899	79.66	61.227	67.55	68.417	60.66	65.889	68.03
C200-T2.5-D0.2	115.08	114.36	119.61	119.99	113.81	119.34	120.36	112.79	118.84	119.83
C200-T2.5-D0.4	115.08	101.81	114.47	116.93	100.19	112.22	113.56	98.942	102.84	103.11
C200-T2.5-D0.6	115.08	81.027	90.75	91.73	80.7	90.5	91.75	76.497	89.55	91.01
C200-T3-D0.2	151.86	149.19	156.57	157.54	148.05	155.78	157.34	146.61	155.67	156.92
C200-T3-D0.4	151.86	126.33	129.44	132.44	123.68	125.66	125.98	121.27	126.32	126.95
C200-T3-D0.6	151.86	105.29	120.34	121.11	92.331	119.98	120.14	88.75	118.22	123.09
For L2000										
C200-T1.5-D0.2	46.95	51.546	55.554	56.48	46.813	53.67	52.73	46.11	52.18	55.825
C200-T1.5-D0.4	46.95	48.088	55.098	55.261	47.051	54.236	56.19	46.893	54.19	55.46
C200-T1.5-D0.6	46.95	38.263	48.569	50.15	37.586	47.663	50.12	36.935	44.64	45.12
C200-T2-D0.2	72.70	72.551	75.343	76.522	72.326	74.479	74.61	71.854	73.872	74.94
C200-T2-D0.4	72.70	68.865	72.704	73.003	67.892	70.22	70.922	67.056	69.31	71.16
C200-T2-D0.6	72.70	58.647	68.77	69.85	56.286	66.96	67.69	54.098	60.55	61.88
C200-T2.5-D0.2	102.63	108.66	116.59	117.02	106.92	114.12	115.1	99.801	107.08	107.46
C200-T2.5-D0.4	102.63	94.102	96.579	98.294	91.808	95.14	96.99	89.906	94.321	95.114
C200-T2.5-D0.6	102.63	75.235	80.66	80.936	71.03	75.75	76.56	68.821	72.24	75.55
C200-T3-D0.2	136	134.88	141.35	142.13	133.07	140.09	141.47	131.41	139.79	140.82
C200-T3-D0.4	136	116.61	120.39	120.74	112.91	118.74	119.45	109.3	111.89	112.88
C200-T3-D0.6	136	89.81	92.314	93.17	84.472	90.339	91.651	80.796	88.646	90.89

Ferritic stainless steel C300

Specimen	Plain web (kN)	Axial capacity results of plain, UH and EH from FEA, P_{FEA} (kN)								
		UH1	EH1		UH3	EH3		UH5	EH5	
			Q10	Q15		Q10	Q15		Q10	Q15
For L1000										
C300-T1.5-D0.2	63.12	63.241	66.78	67.38	62.996	66.52	67.12	61.123	64.55	65.13
C300-T1.5-D0.4	63.12	60.972	64.39	64.97	59.007	62.31	62.87	58.954	62.26	62.82
C300-T1.5-D0.6	63.12	57.303	60.51	61.06	51.515	54.40	54.89	48.858	51.59	52.06
C300-T2-D0.2	98.1	97.737	103.21	104.14	98.76	104.29	105.23	96.448	101.85	102.77
C300-T2-D0.4	98.1	91.583	96.71	97.58	90.74	95.82	96.68	89.27	94.27	95.12
C300-T2-D0.6	98.1	82.409	87.02	87.81	77.486	81.83	82.56	73.389	77.50	78.20
C300-T2.5-D0.2	135.74	136.38	144.02	145.31	135.81	143.42	144.71	132.86	140.30	141.56
C300-T2.5-D0.4	135.74	126.85	133.95	135.16	125.8	132.84	134.04	123.08	129.97	131.14
C300-T2.5-D0.6	135.74	118.59	125.23	126.36	105.84	111.77	112.77	102.74	108.49	109.47
C300-T3-D0.2	181.53	180.41	190.51	192.23	180.33	190.43	192.14	176.88	186.79	188.47
C300-T3-D0.4	181.53	178.97	188.99	190.69	162.34	171.43	172.97	161.5	170.54	172.08
C300-T3-D0.6	181.53	150.96	159.41	160.85	146.81	155.03	156.43	130.89	138.22	139.46
For L1500										
C300-T1.5-D0.2	59.11	57.92	61.16	61.71	57.115	60.31	60.86	56.455	59.62	60.15
C300-T1.5-D0.4	59.11	55.531	58.64	59.17	54.539	57.59	58.11	52.064	54.98	55.47
C300-T1.5-D0.6	59.11	51.404	54.28	54.77	48.238	50.94	51.40	46.071	48.65	49.09
C300-T2-D0.2	94.27	92.212	97.38	98.25	91.686	96.82	97.69	91.459	96.58	97.45
C300-T2-D0.4	94.27	89.375	94.38	95.23	88.827	93.80	94.65	86.642	91.49	92.32

C300-T2-D0.6	94.27	77.216	81.54	82.27	76.706	81.00	81.73	72.389	76.44	77.13
C300-T2.5-D0.2	132.6	130.4	137.70	138.94	130.44	137.74	138.98	130.49	137.80	139.04
C300-T2.5-D0.4	132.6	124.19	131.14	132.32	123.96	130.90	132.08	120.32	127.06	128.20
C300-T2.5-D0.6	132.6	117.56	124.14	125.26	103.59	109.39	110.38	100	105.60	106.55
C300-T3-D0.2	174.27	173.11	182.80	184.45	172.93	182.61	184.26	172.51	182.17	183.81
C300-T3-D0.4	174.27	165.11	174.36	175.93	160.73	169.73	171.26	159.47	168.40	169.92
C300-T3-D0.6	174.27	140.34	148.20	149.53	135.23	142.80	144.09	126.77	133.87	135.08
For L2000										
C300-T1.5-D0.2	55.3	55.226	58.32	58.84	54.218	57.25	57.77	54.05	57.08	57.59
C300-T1.5-D0.4	55.3	55.112	58.20	58.72	54.99	58.07	58.59	50.75	53.59	54.07
C300-T1.5-D0.6	55.3	46.059	48.64	49.08	45.213	47.74	48.17	42.957	45.36	45.77
C300-T2-D0.2	87.79	88.413	93.36	94.20	88.38	93.33	94.17	87.798	92.71	93.55
C300-T2-D0.4	87.79	85.831	90.64	91.45	84.04	88.75	89.54	80.441	84.95	85.71
C300-T2-D0.6	87.79	73.496	77.61	78.31	69.552	73.45	74.11	68.926	72.79	73.44
C300-T2.5-D0.2	128.3	123.96	130.90	132.08	122.11	128.95	130.11	121.37	128.17	129.32
C300-T2.5-D0.4	128.3	119.61	126.31	127.44	116.51	123.03	124.14	113.51	119.87	120.95
C300-T2.5-D0.6	128.3	114.37	120.77	121.86	94.409	99.70	100.59	92.105	97.26	98.14
C300-T3-D0.2	161.62	163.39	172.54	174.09	162.89	172.01	173.56	160.13	169.10	170.62
C300-T3-D0.4	161.62	147.45	155.71	157.11	143.61	151.65	153.02	140.08	147.92	149.26
C300-T3-D0.6	161.62	127.45	134.59	135.80	121.22	128.01	129.16	116.92	123.47	124.58

4.2.2 Effect of thickness and length on axial capacity for CFSS plain channel section

Fig. 4-3(a) and 4-3(b) shows the impact of thickness on the axial capacity of cold-formed austenitic stainless steel (CFSS) plain channel sections. When increasing in thickness from 1.5 mm to 2 mm the average axial capacity increased by 54.39%. likewise for the thicknesses of 2mm to 2.5mm and 2.5mm to 3mm, the axial capacity is increased by 41.22% and 32.42% respectively. similarly, for duplex stainless-steel channel sections, thickness variations from 1.5 mm to 2 `mm and 30.74% for 2.5 mm to 3 mm. Ferritic stainless-steel channel sections presented axial capacity increases of 54.25%, 40.96%, and 32.24% for these respective thickness variations.

An overall length of CFSS channel plays a significant role on axial capacity. It's determined that the longer the length, there is a reduction on axial capacity. For austenitic stainless steel the axial capacity is decreased by 20.87% from the length 1000mm to 2000mm. Similarly, percentage decrease in the grade duplex was 57.35% from 1000mm to 2000mm and 20.10% for cold-formed ferritic stainless steel.

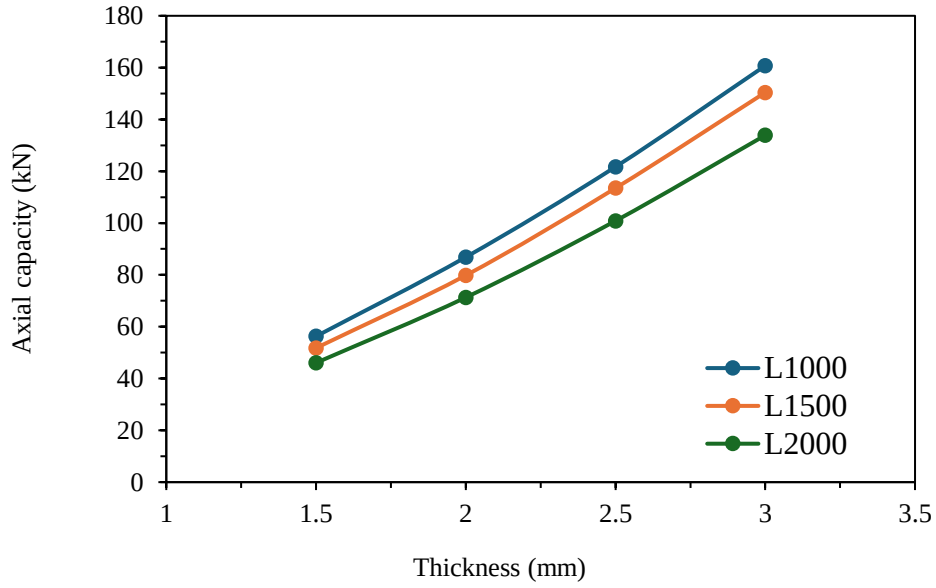

(a) Austenitic

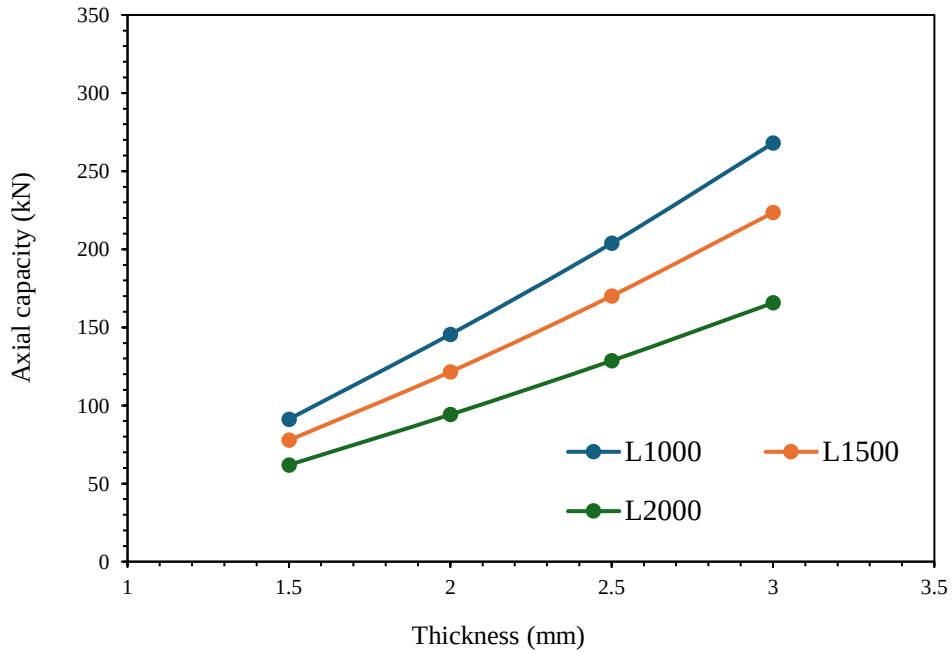

(b) Duplex

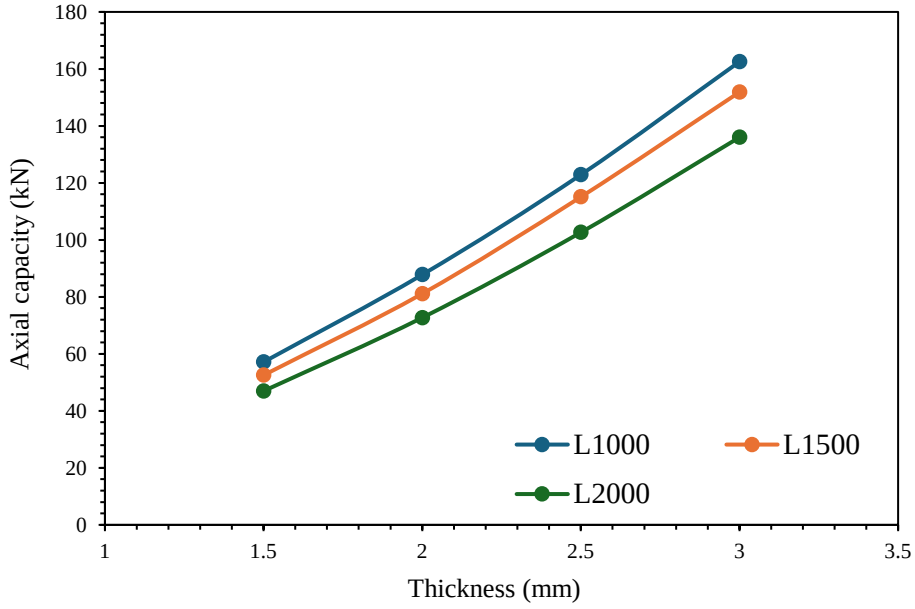

(c)Ferritic

Figure 4-3(a): Effect of thickness and length for CFSS plain channel section for C200x65x15

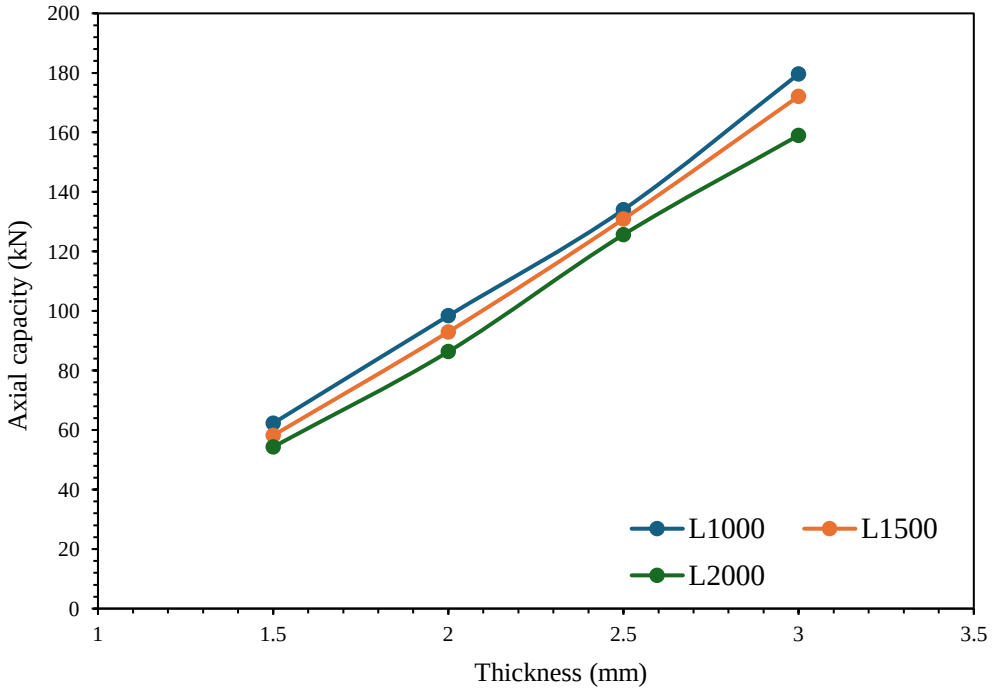

(a) Austenitic

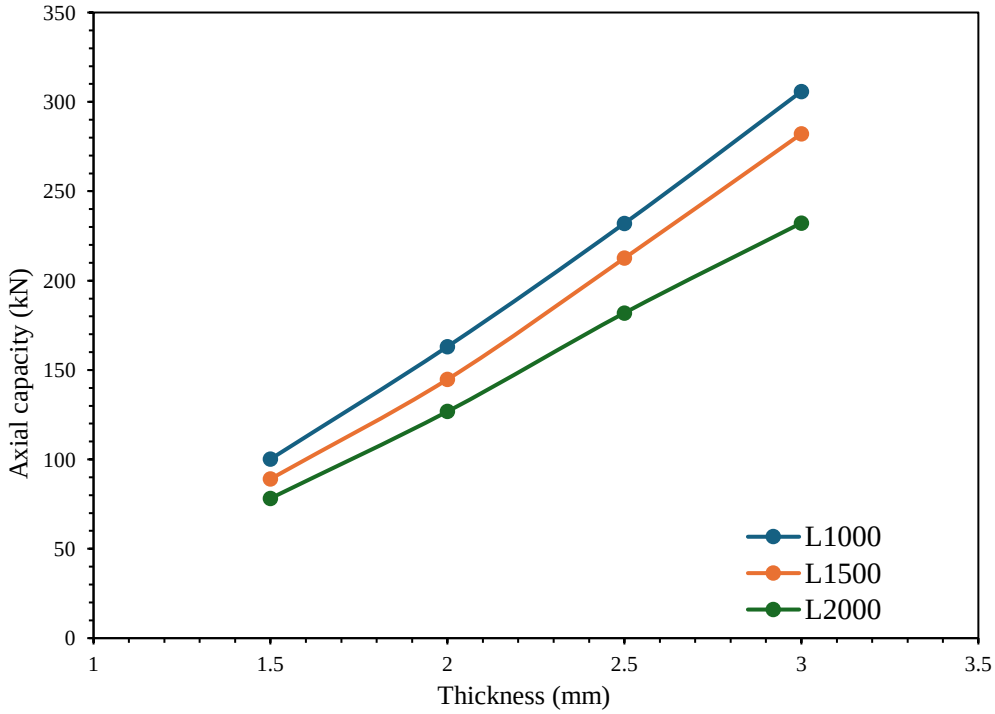

(b) Duplex

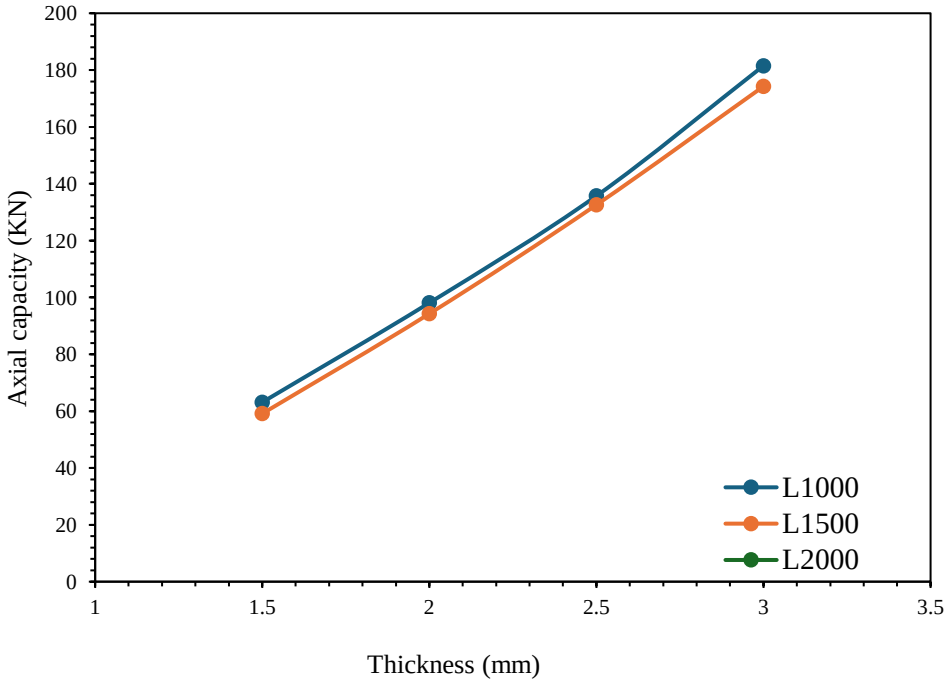

(c) Ferritic

Figure 4-3(b): Effect of thickness and length for CFSS plain channel section for C300x80x20

4.3 CFSS channel sections with unstiffened web holes

4.3.1 Effect of a/h ratio on axial capacity for CFSS channel section

The effects of a/h ratio on the axial capacity of the CFSS channel section with unstiffened web holes keeping the length constant i.e., L=1500mm are shown in Fig. 4-4(a) and 4-4(b). there is a noticeable decrease in axial capacity as the a/h ratio increases from 0.2 to 0.6. in the parametric analysis, it is observed that increasing the a/h ratio from 0.2 to 0.4 resulted in a 8.79% reduction in axial capacity for austenitic CFSS channel section. A similar trend was observed for duplex and ferritic CFSS channel sections, with axial capacities decreasing by 3.4% and 7.18% respectively. Comparatively, when comparing a/h ratios from 0.2 to 0.6, axial capacity decreased by 22.06%, 17.82% and 20.59% for austenitic, duplex and ferritic stainless steel, respectively. Similarly, comparing a/h ratios from 0.4 to 0.6 showed a decrease in axial

capacity of 14.65%, 10.99% and 14.51% for austenitic, duplex, and ferritic stainless steel, respectively. These findings underscore the significant influence of the a/h ratio on moment capacity.

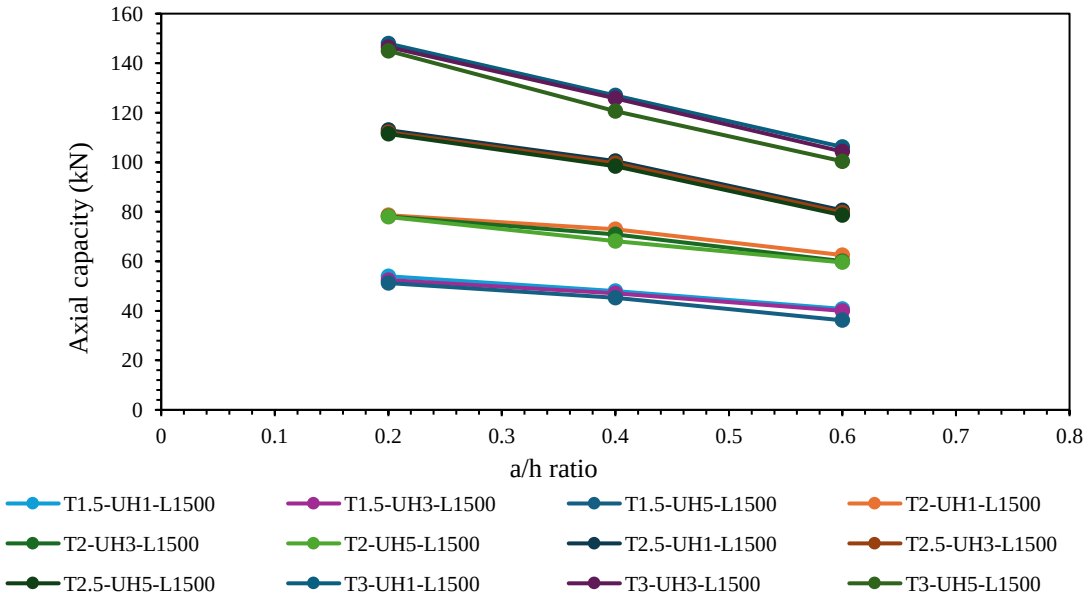

(a) Austenitic

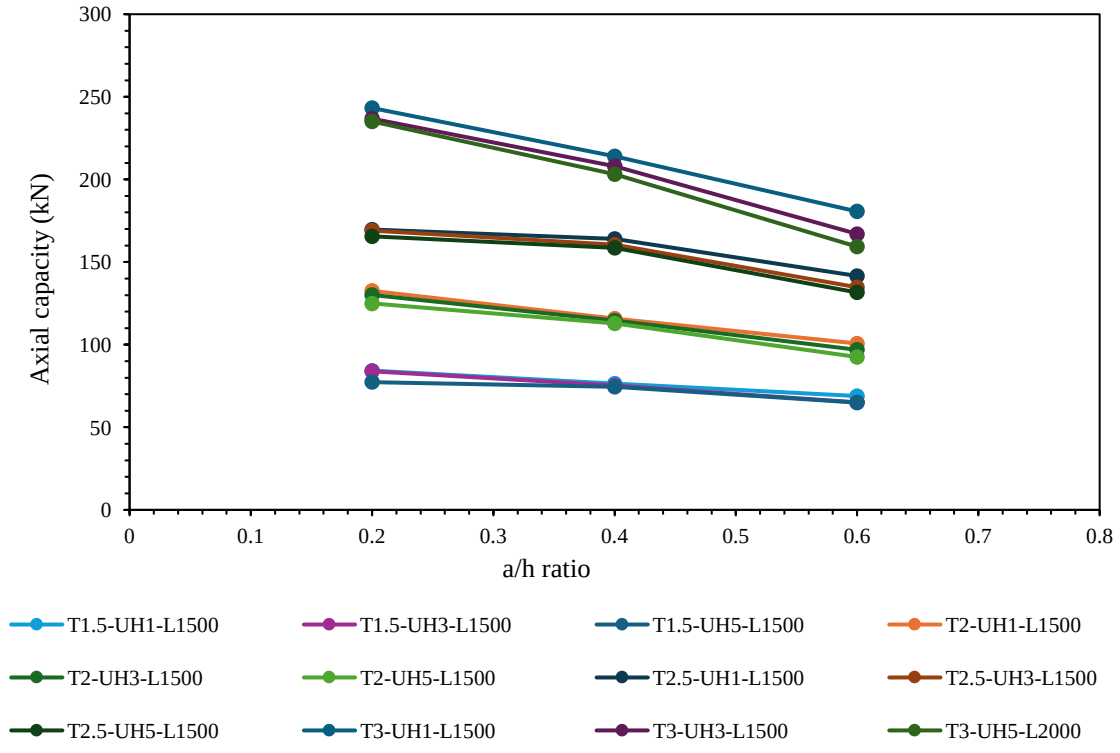

(b) Duplex

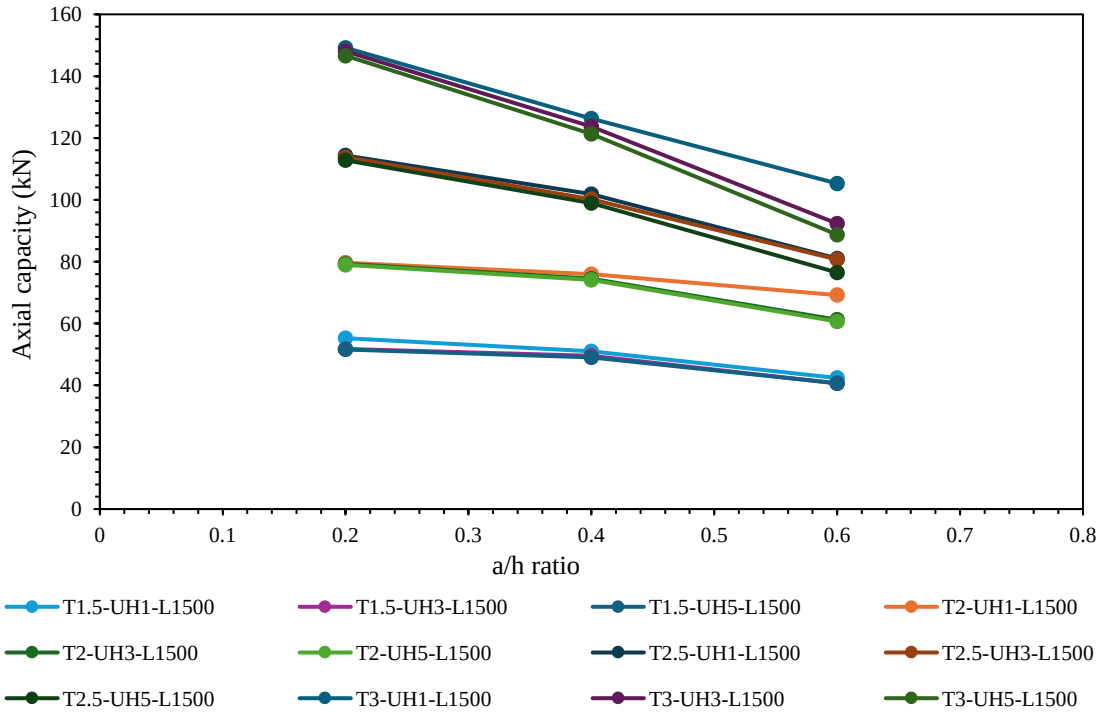

(C)Ferritic

Figure 4-4(a): Effect on a/h ratio for CFSS channel section for C200x65x15

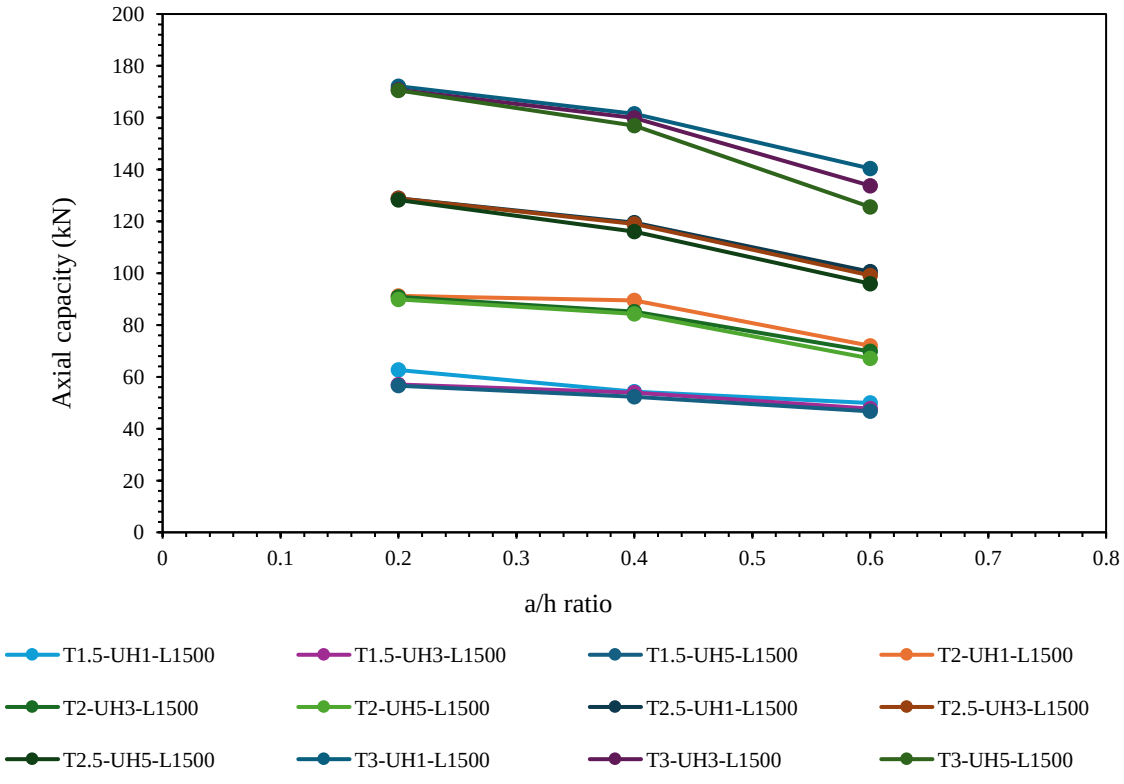

(a) Austenitic

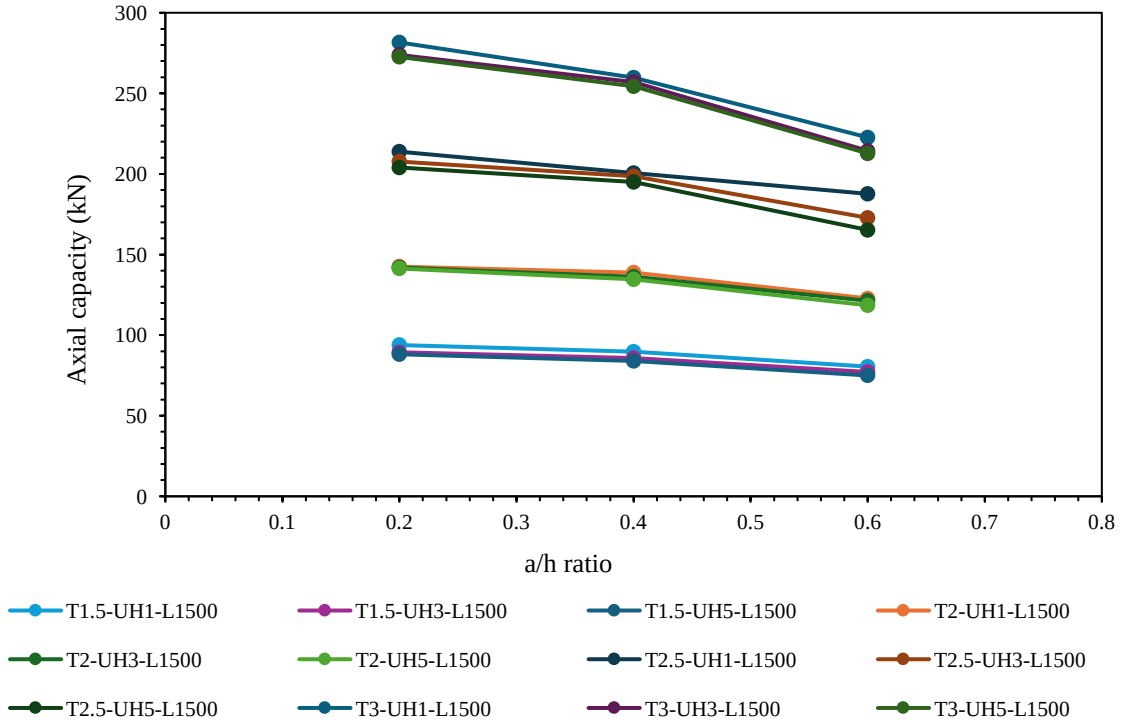

(b) Duplex

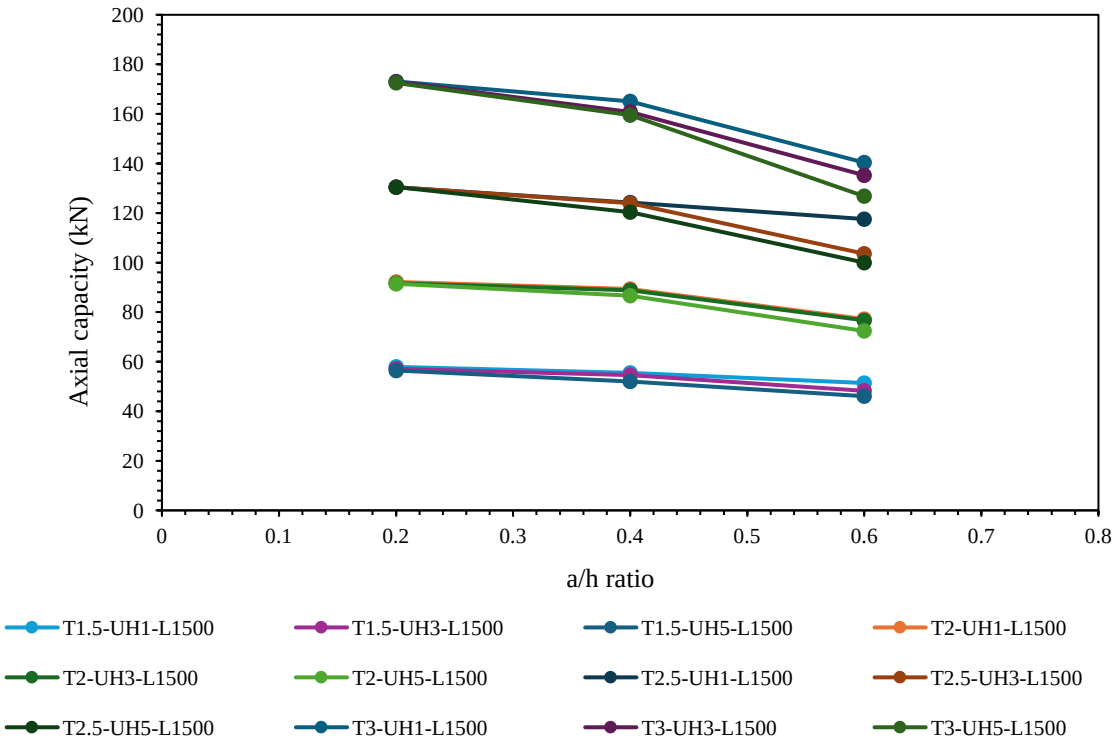

(c) Ferritic

Figure 4-4(b): Effect on a/h ratio for CFSS channel section for C300x80x20

4.3.2 Effect of different length on axial capacity for CFSS channel

As Its mentioned earlier, the overall length of the channel majorly impacts the axial capacity of CFSS channel. In Fig. 4-5(a) and 4-5(b) it shows that, the decrease in axial capacity when the length of the channel increases. Axial capacity is decreased by 5.2% when the length increased from 1000mm to 1500mm for austenitic grade. Similarly, 6.94% and 5.39% for duplex and ferritic respectively. Similarly, comparing for the lengths from 1000mm to 2000mm showed a decrease in axial capacity 13.71%, 20.32% and 14.75% for austenitic, duplex and ferritic stainless steel respectively.

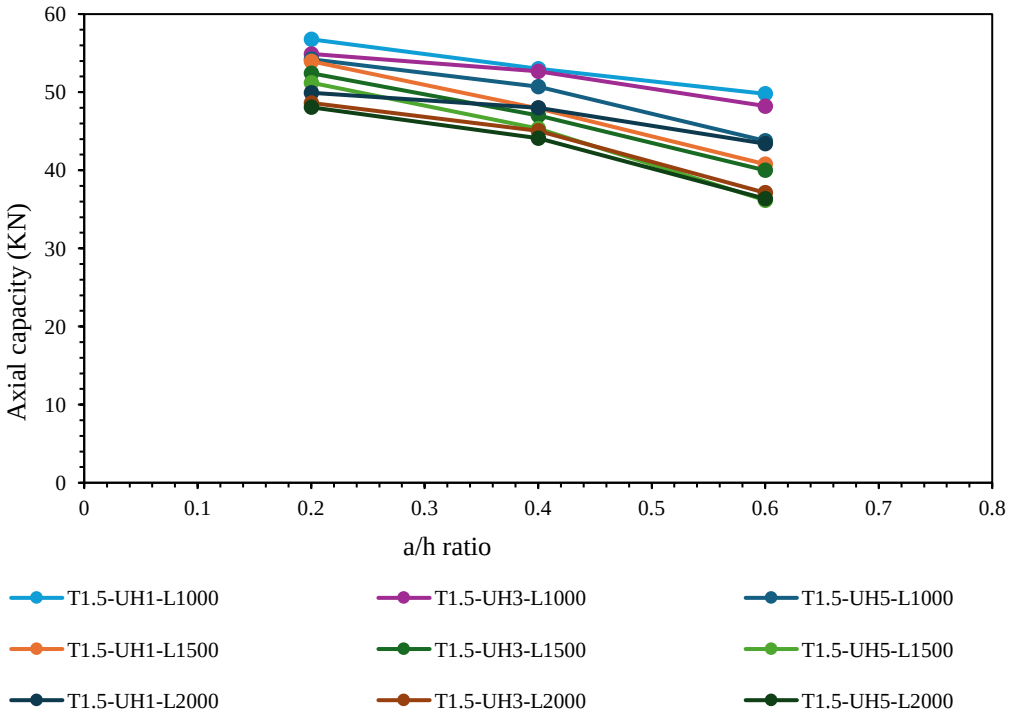

(a) Austenitic

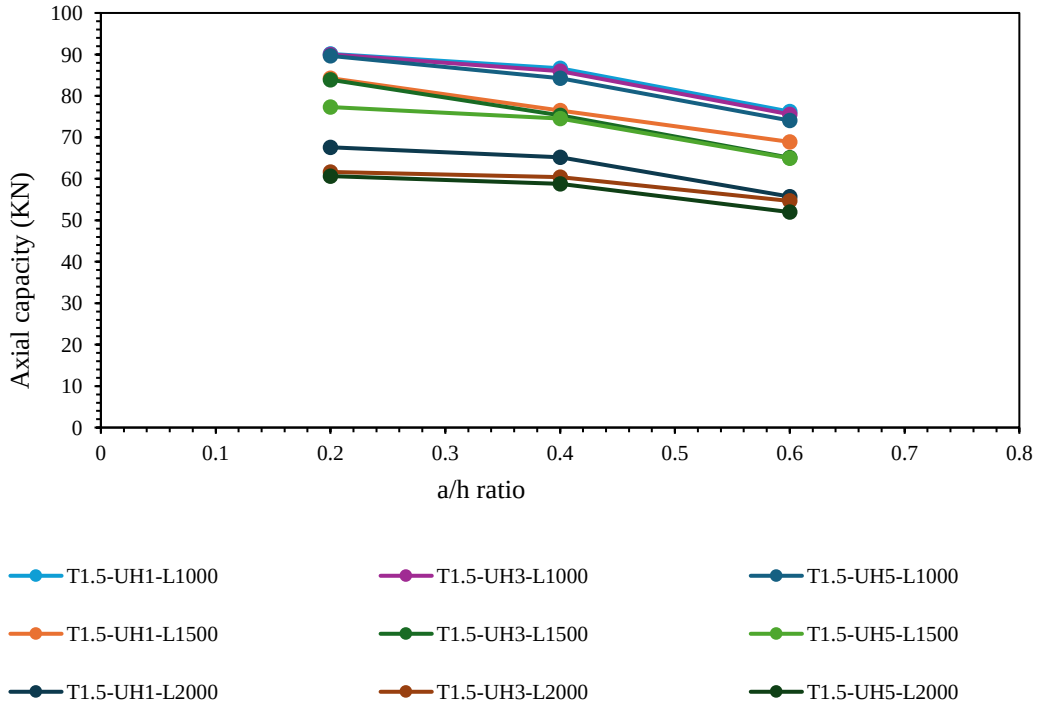

(b) Duplex

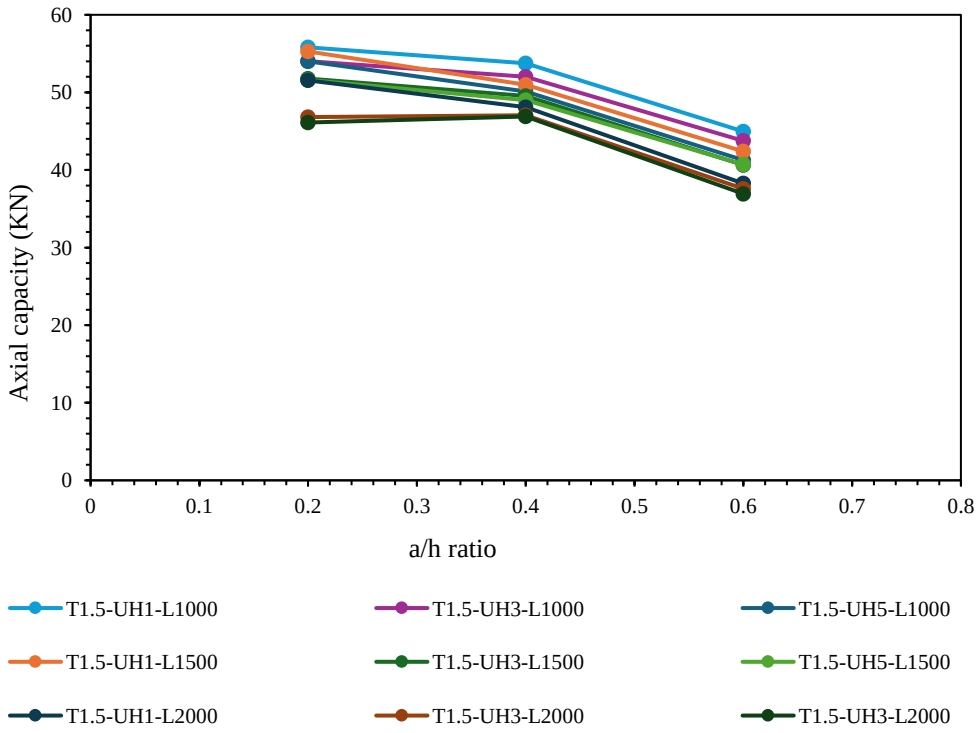

(c) Ferritic

Figure 4-5(a): Effect of different length on axial capacity of CFSS channel section for C200x65x15

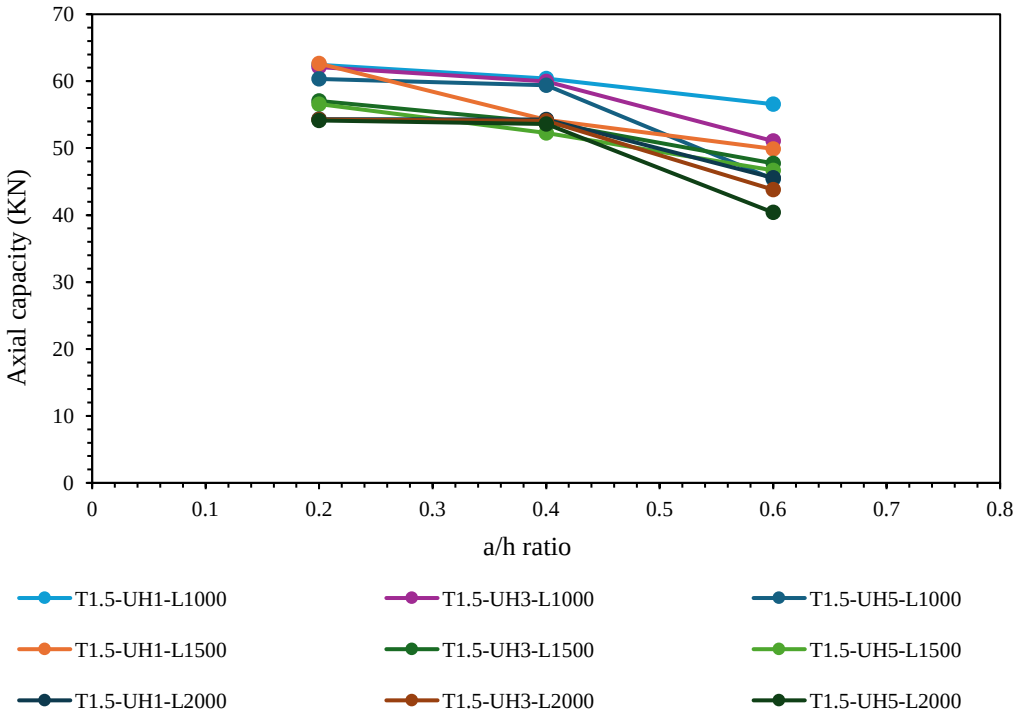

(a) Austenitic

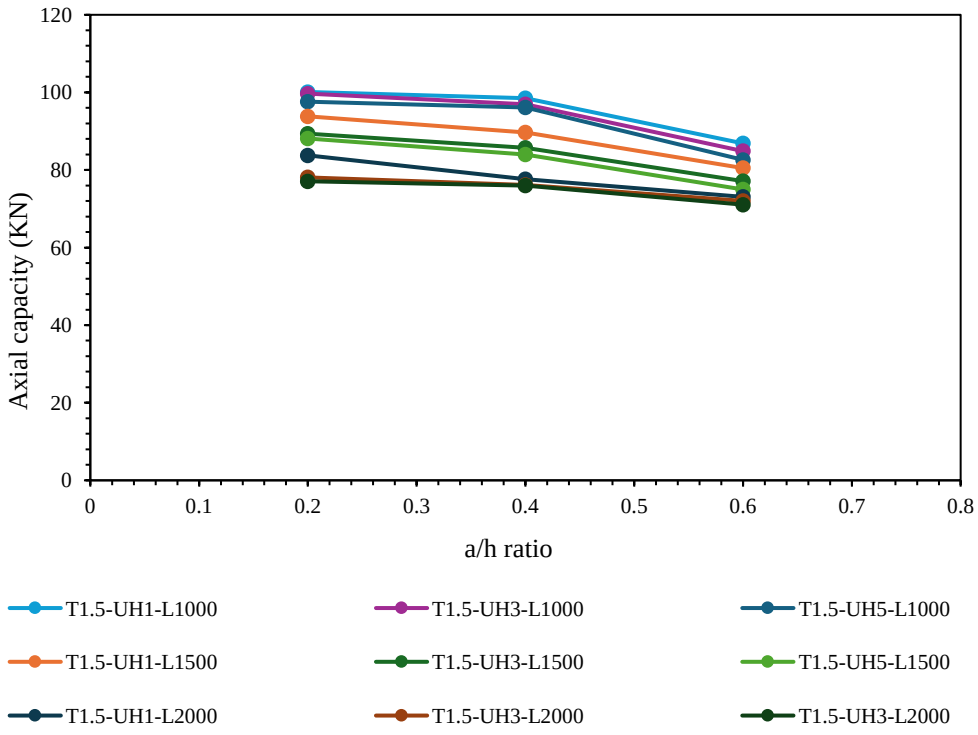

(b) Duplex

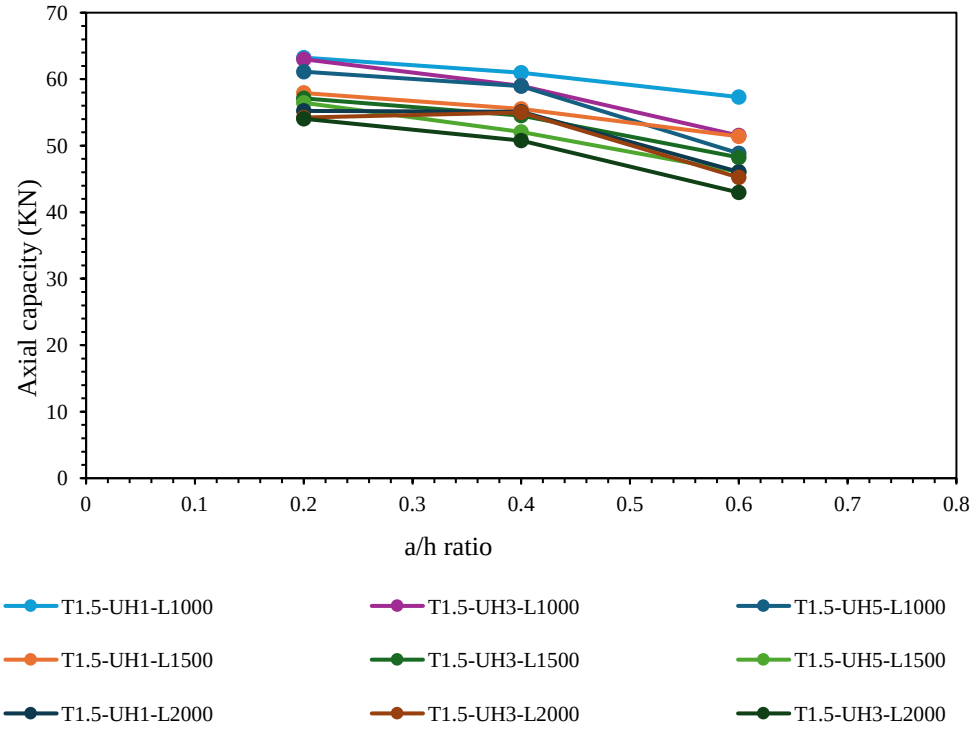

(c) Ferritic

Figure 4-5(b): Effect of different length on axial capacity of CFSS channel section for C300x80x20

4.3.3 Effect of number of holes on axial capacity for CFSS channel

The influence of the number of holes on axial capacity of CFSS channel sections with unstiffened web holes was examined. Fig. 4-6(a) and 4-6(b) shows as the number of holes increased from 1 to 3, a reduction in axial capacity was observed, with a decrease of 2.3%, 2.4% and 2.7% noted for austenitic, duplex and ferritic stainless steel, respectively. Similarly, when the number of holes increased from 1 to 5, axial capacities decreased by 7.5%, 5.95% and 7.65% respectively for same stainless steel grades.

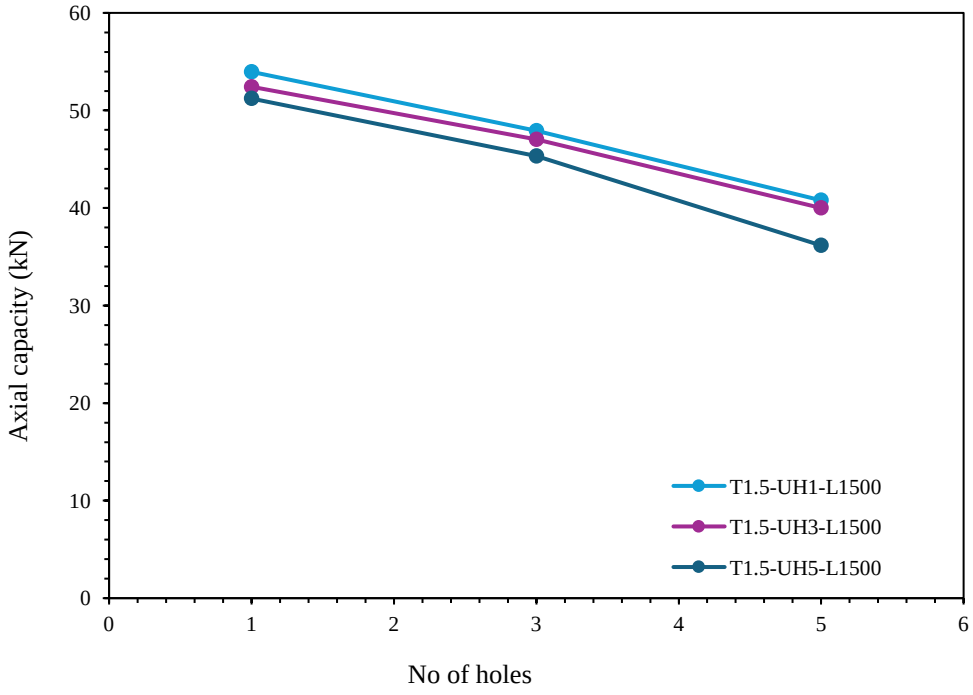

(a)Austenitic

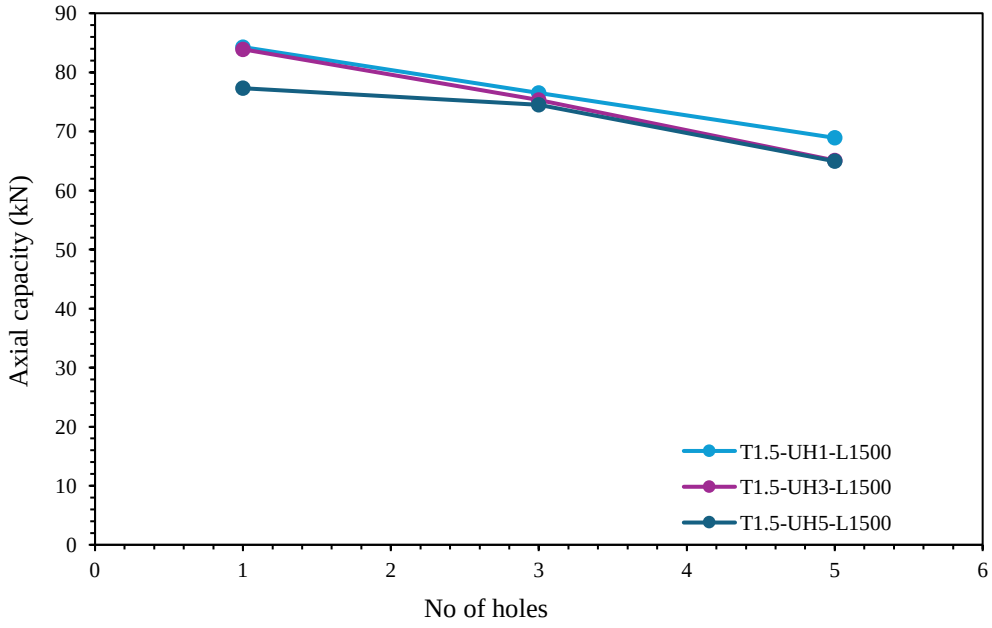

(b)Duplex

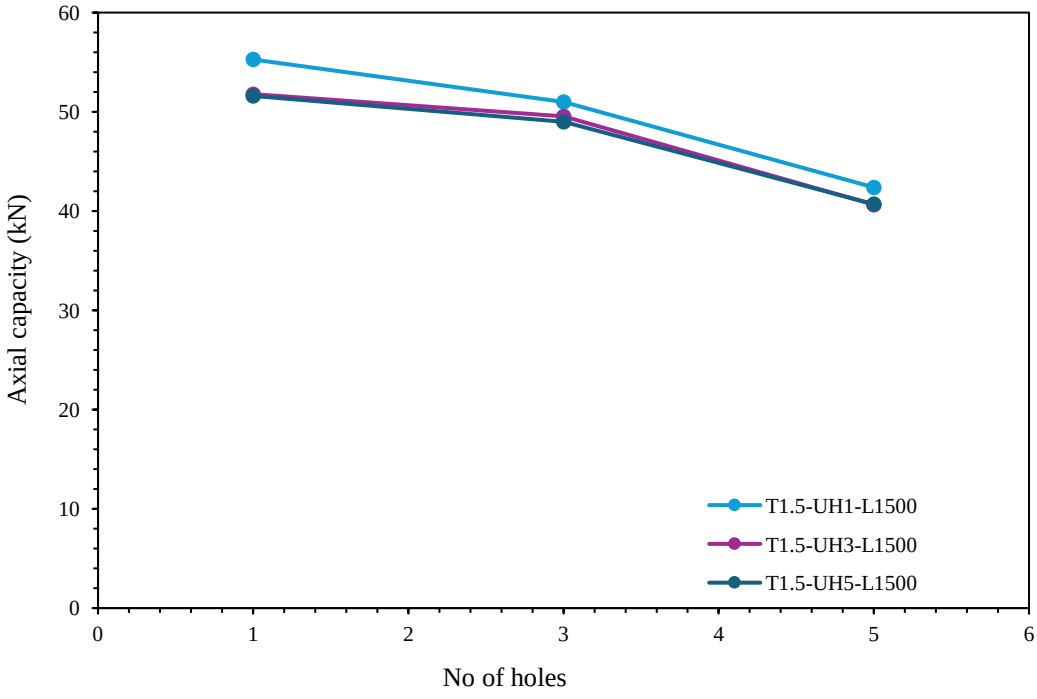

(c) Ferritic

Figure 4-6(a): Effect on number of holes for CFSS channel section C200x65x15

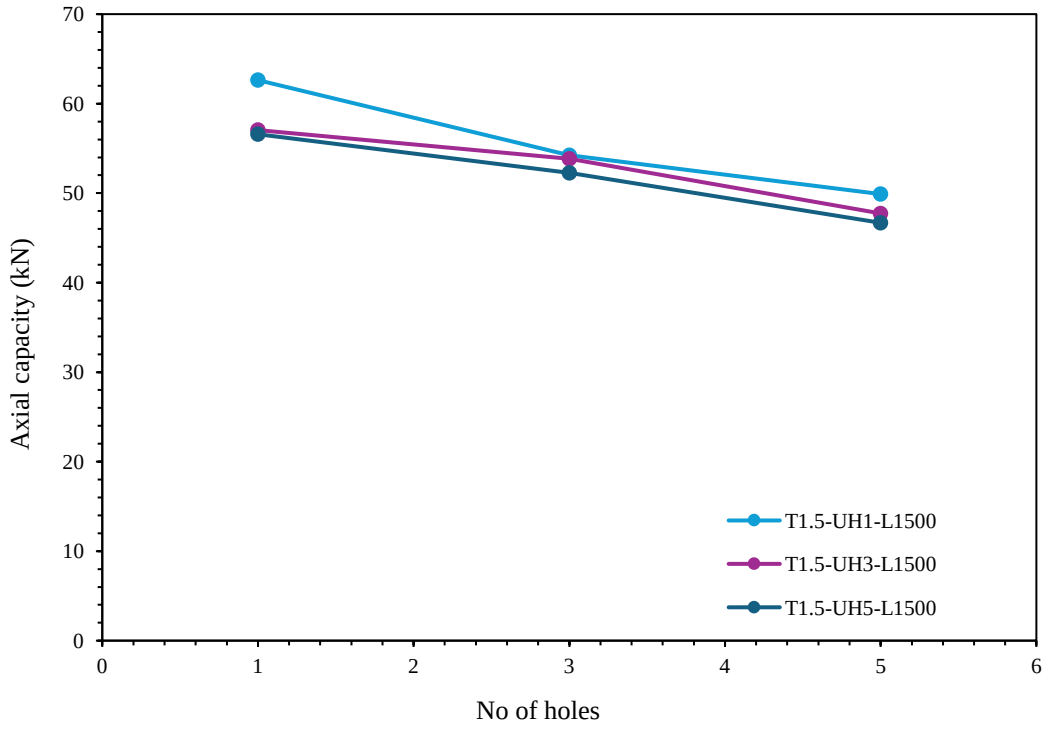

(a) Austenitic

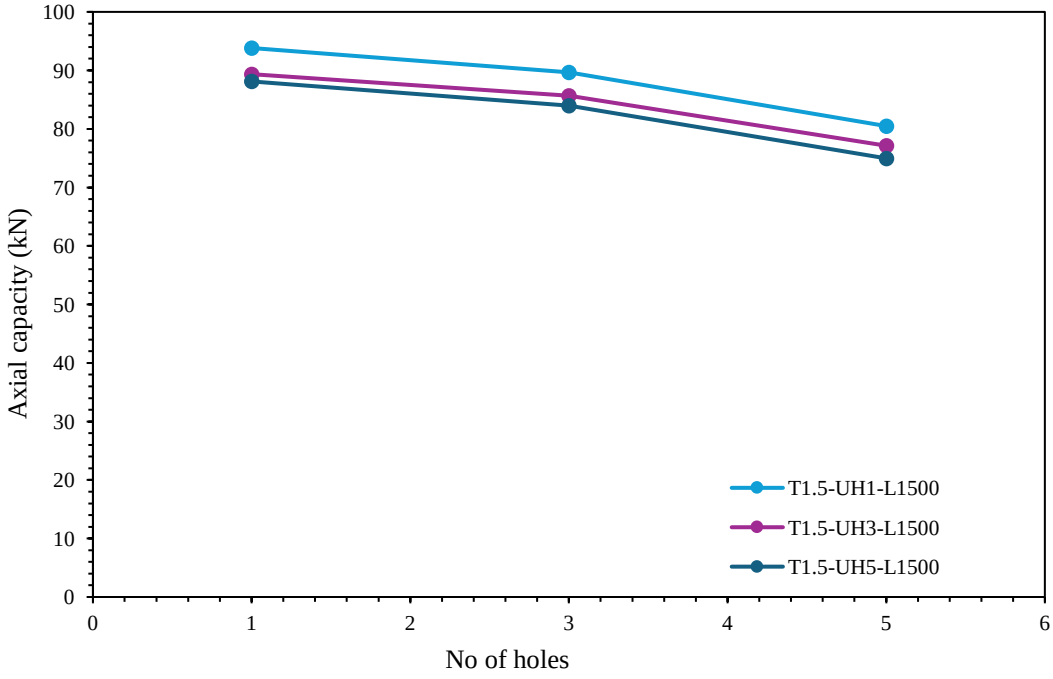

(b) Duplex

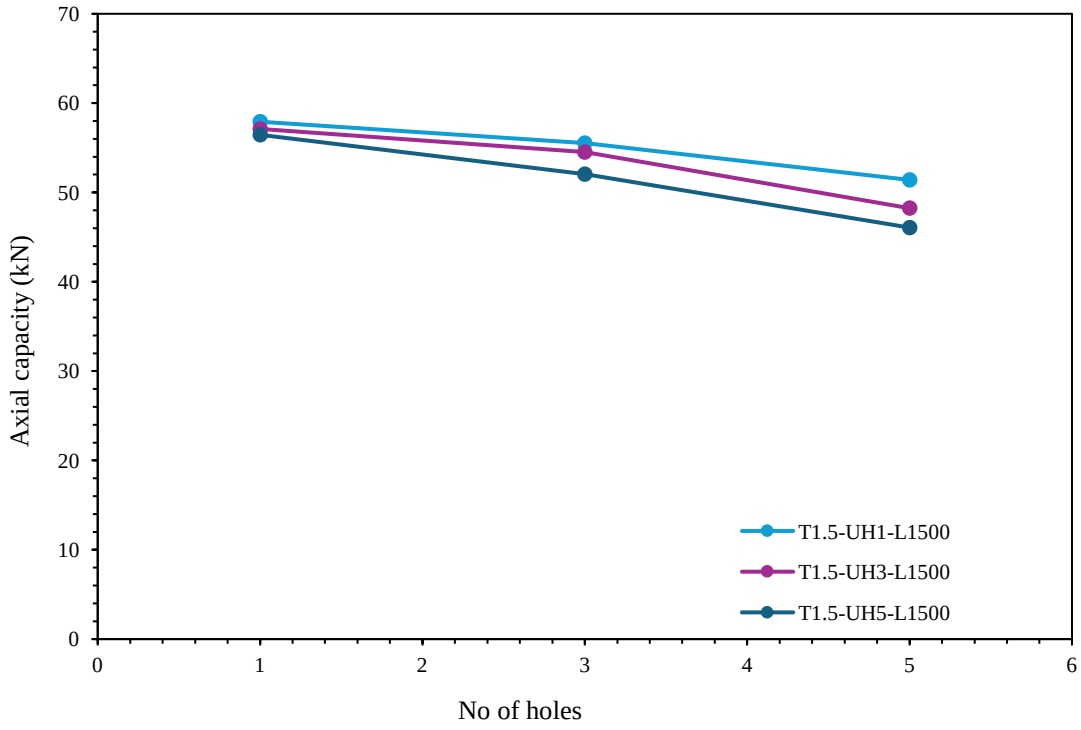

(c) Ferritic

Figure 4-6(b): Effect on number of holes for CFSS channel section C300x80x20

4.3.4 Effect of channel dimensions on Axial capacity for CFSS channel section.

Table 4 presents the axial capacity achieved for the two cross-sectional dimensions of the CFSS channel section examined in this study. It is evident that, on average, the axial capacity increased to 21.91% when transitioning from C200x65x15 to C300x80x20.

Table 4 Selected variables for parametric study

Channel section	**h**	**b**	**l**	**q**	**t**	**L**	a/h	**Material Properties**
	(mm)							
C200x65x15	200	65	15	[10&15]	[1.5-3]	1000	0.2	Ferritic stainless steel
						1500	0.4	Duplex stainless steel
C300x80x20	300	80	20			2000	0.6	Austenitic stainless steel

4.4 CFSS channel sections with Edge-stiffened web holes

4.4.1 Effect of stiffener length

In this study, the impact of stiffener length on the axial capacity for CFSS channel sections with edge-stiffened web holes was explored. It was found that, on average, there was only a marginal increase of 1.44% in axial capacity when the stiffener varied from 10mm to 15mm. Fig. 4-7(a) and 4-7(b) represents stiffener length over axial capacity with various thicknesses of channel with constant length.

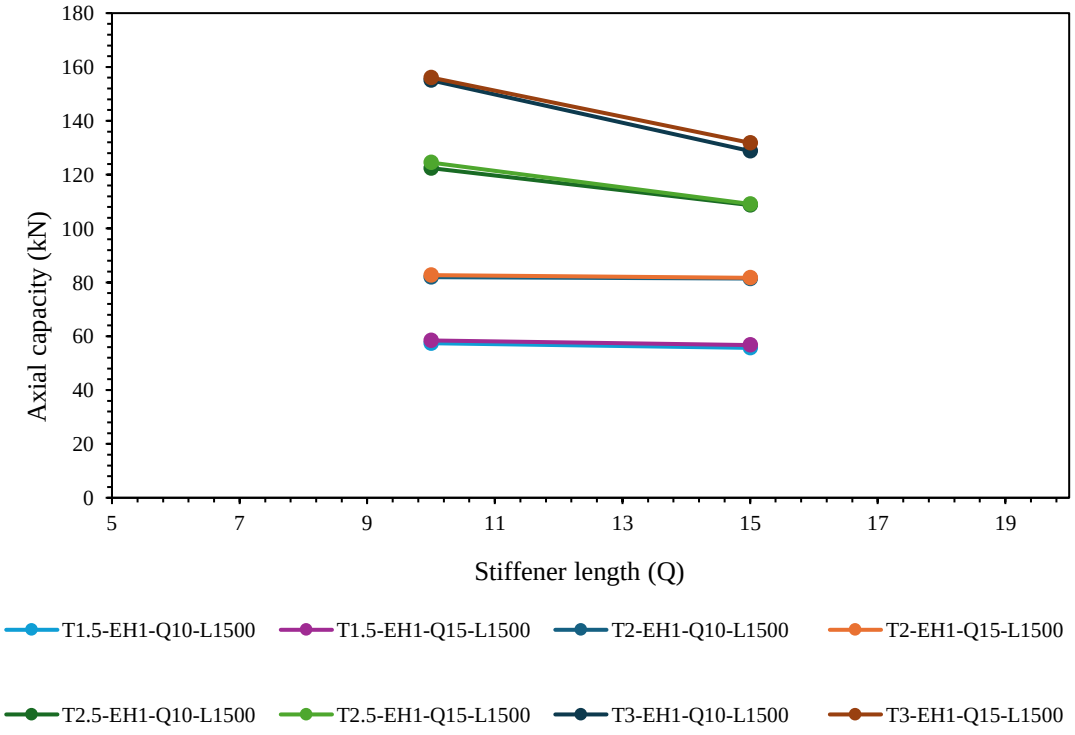

(a)Austenitic

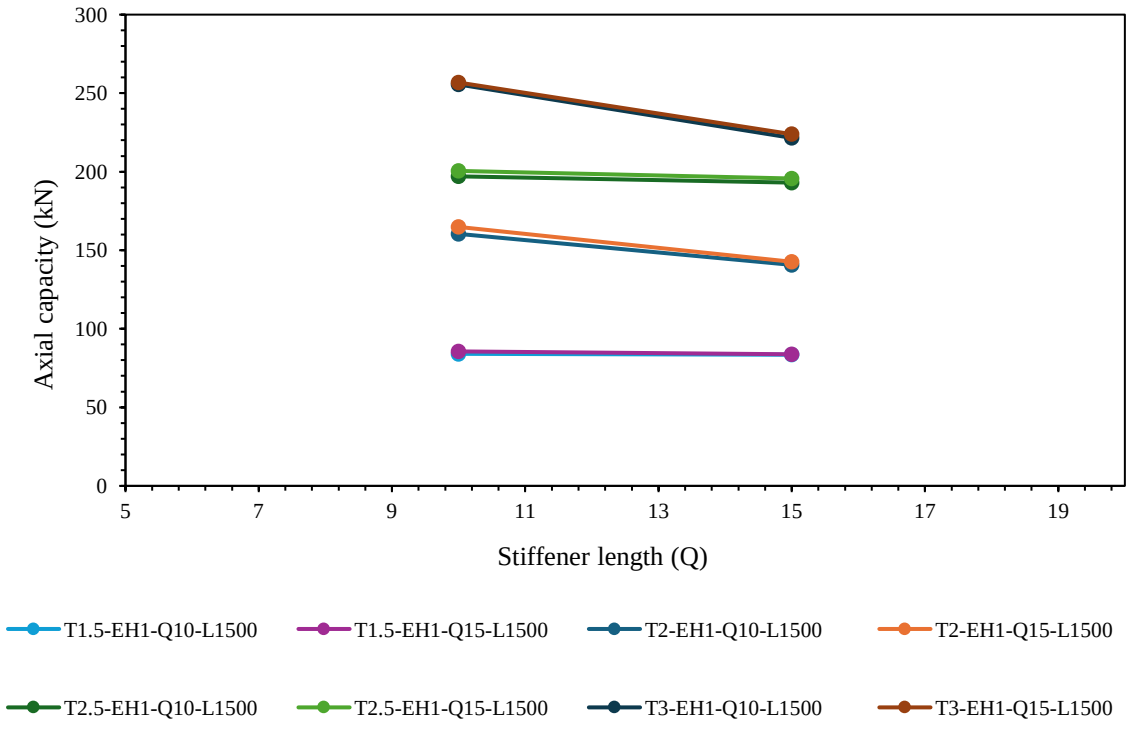

(b)Duplex

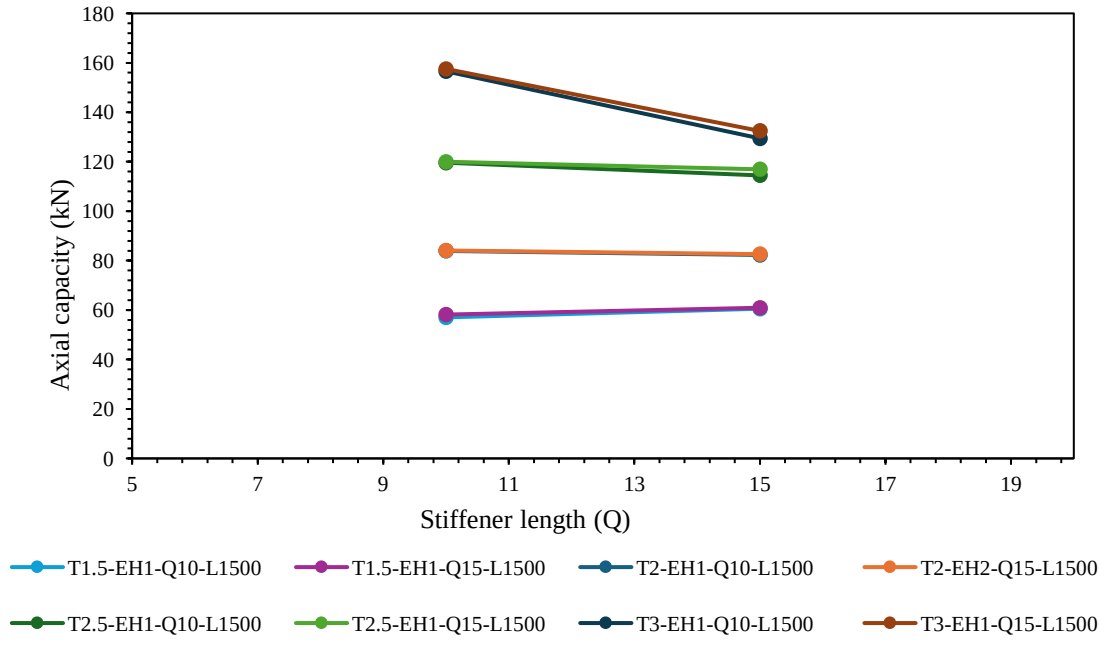

(c)Ferritic

Figure 4-7(a): Effects of stiffener length for edge-stiffened web holes for channel section C200x65x15

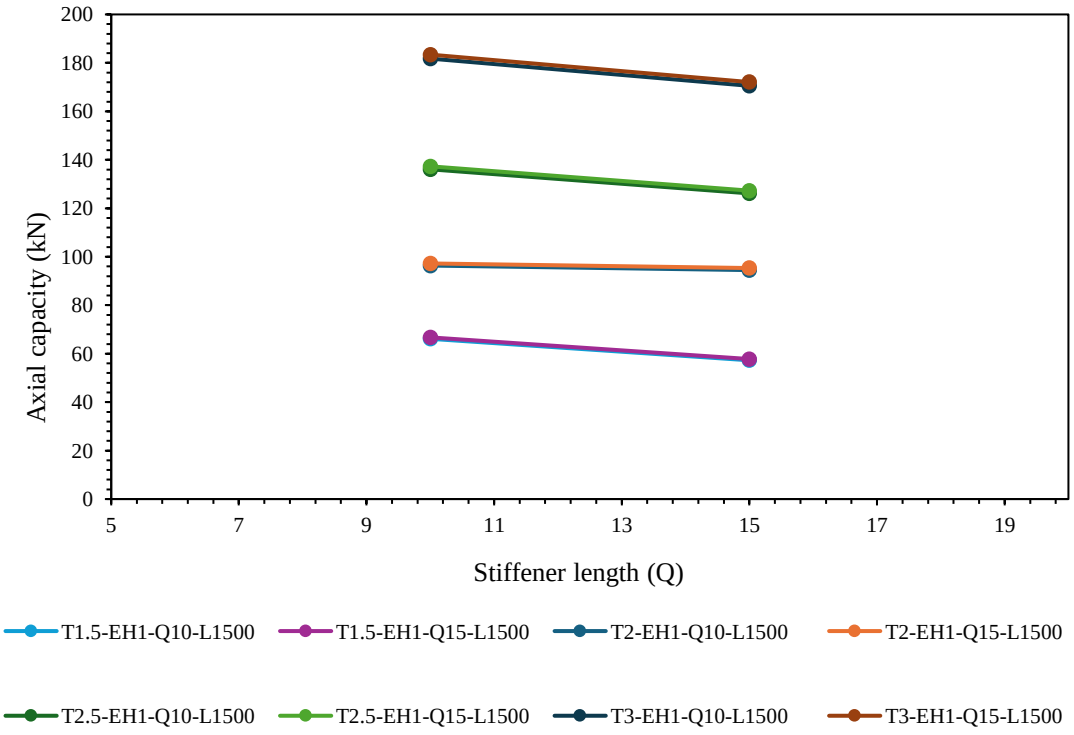

(a)Austenitic

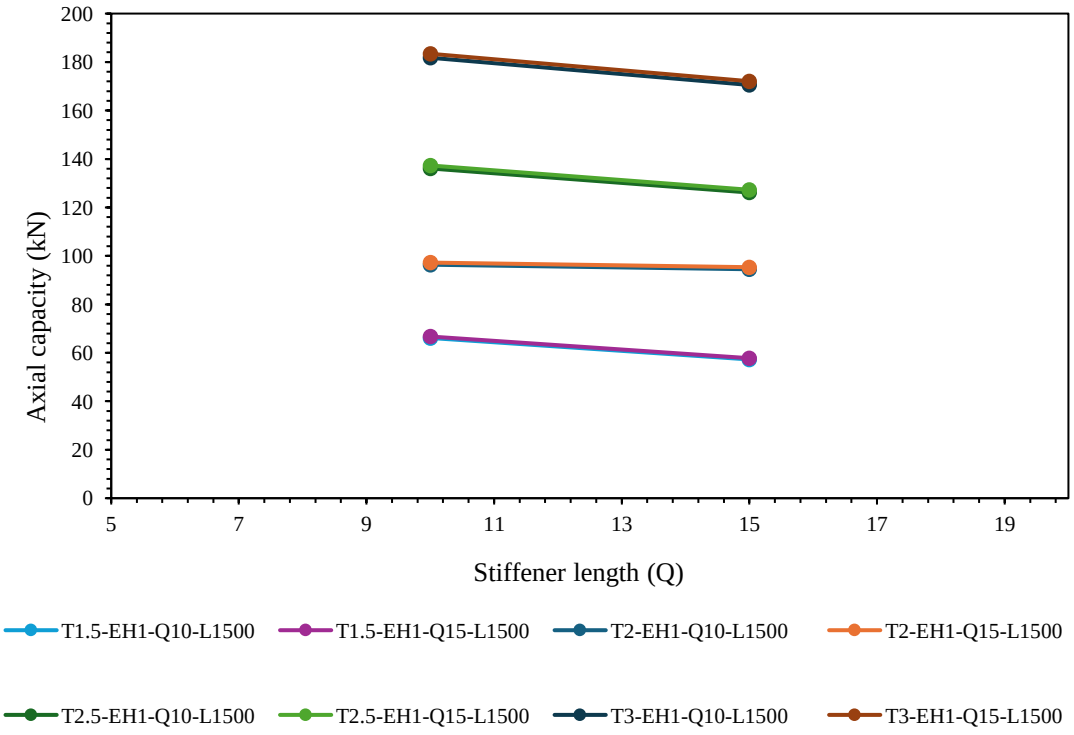

(b) Duplex

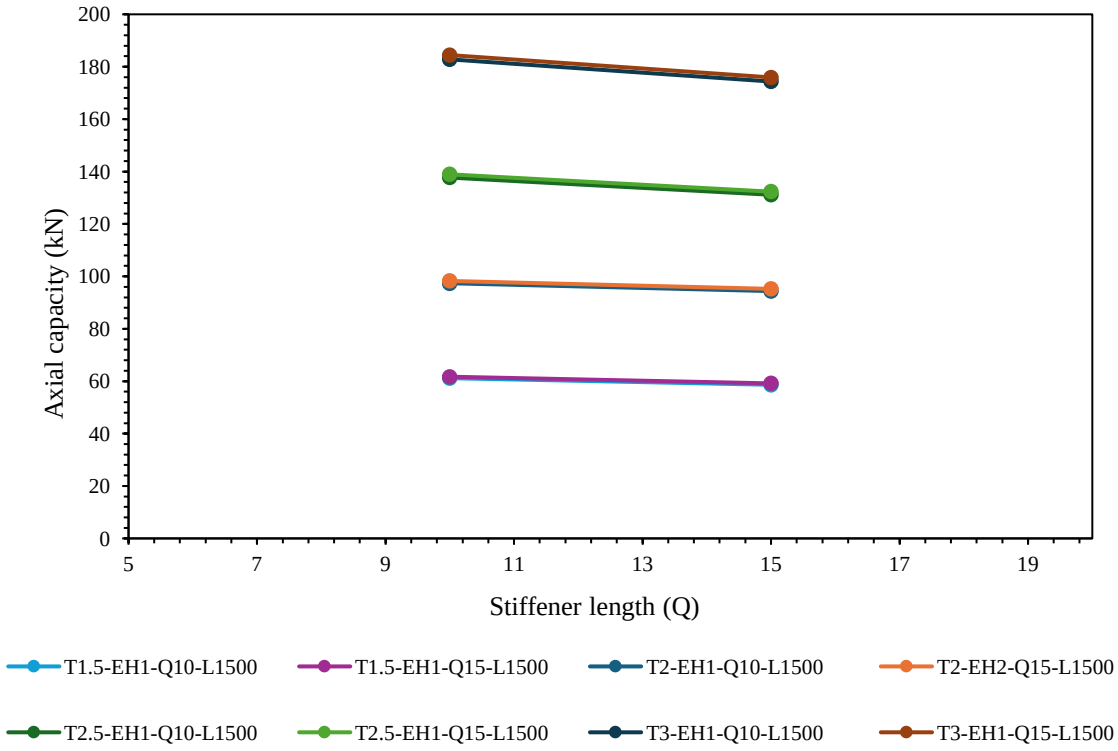

(c) Ferritic

Figure 4-7(b): Effects of stiffener length for edge-stiffened web holes for channel section C300x80x20

4.4.2 Comparison from un-stiffened to edge-stiffened web holes for austenitic, duplex and ferritic stainless steel

Table 3 shows that the axial capacity obtained from FEA for unstiffened and edge-stiffened web holes for austenitic, duplex, and ferritic stainless-steel. For edge-stiffened with 10mm stiffener length with one web hole where the a/h ratio varied from 0.2, 0.4 and 0.6, the average axial capacity increased by 7.14%. Axial capacity increased to 7.66% when compared for 3 web holes. And with 5 web holes, the axial capacity increased to 8.18%, irrespective of the grade of the stainless steel. Refer to Fig. 4-8.

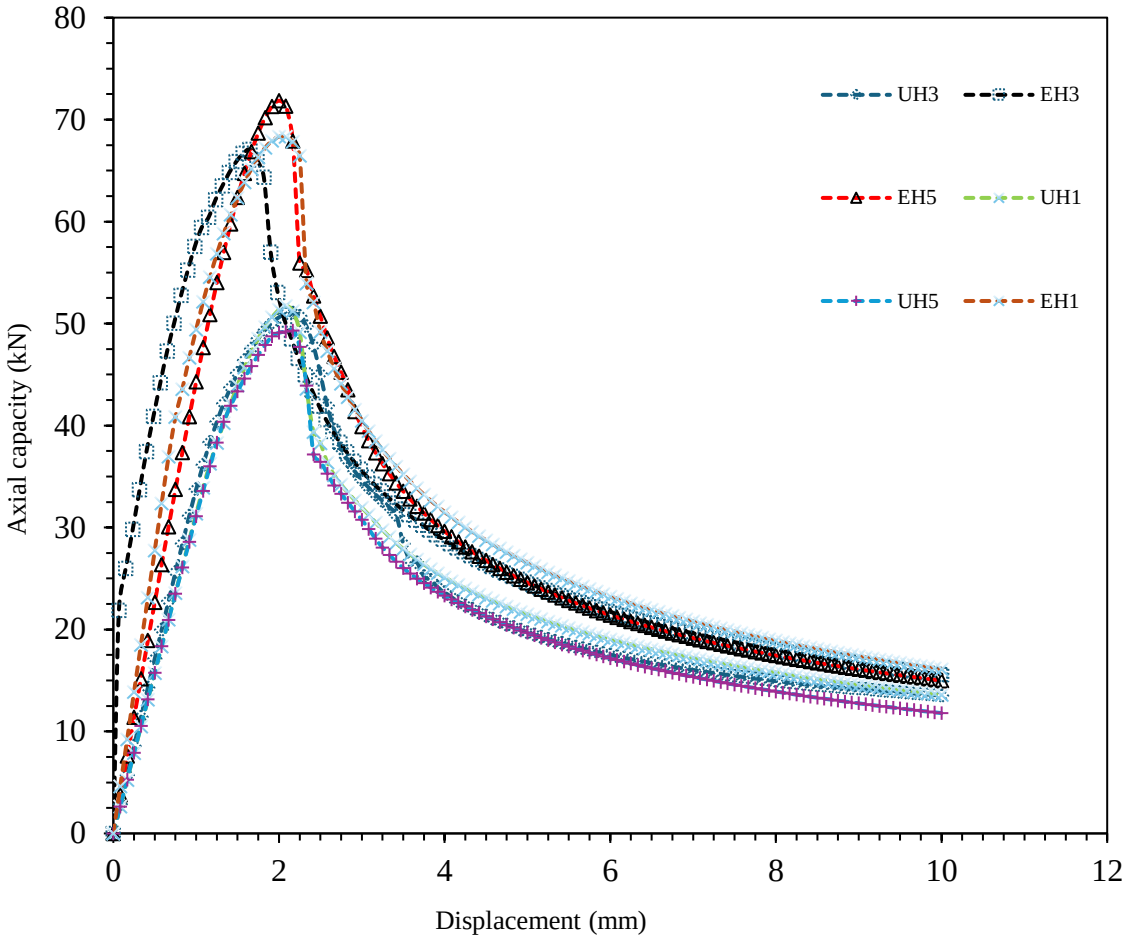

Figure 4-8: Load displacement curve comparison from unstiffened web hole to edge-stiffened web hole.

4.4.3 Effect of a/h ratio on axial capacity for CFSS section with edge stiffened web hole

In table 3 and Fig. 4-9(a) and 4-9(b) illustrate the impact of the a/h ratio on the axial capacity of the CFSS channel sections with edge-stiffened web hole. The findings from the study reveal that, for austenitic stainless steel, as the a/h ratio increased from 0.2 to 0.4, there was a decrease in axial capacity of 8.79%. Similarly, for duplex CFSS channels, the axial capacity decreased by 3%, and for ferritic CFFS channels it is decreased by 7.18%. Moreover, with an increase in a/h ratio from 0.2 to 0.6, a decrease in axial capacity was observed across all stainless steel types. Specifically, for austenitic the axial capacity decreased by 22.06%, for duplex stainless steel, it is decreased by 17.82% and for ferritic steel, it is decreased by 20.59%.

Likewise, when comparing the a/h ratio from 0.4 to 0.6, a reduction in axial capacity of 12.65%, 10.14% and 12.5% was noted for austenitic, duplex, and ferritic stainless steel respectively.

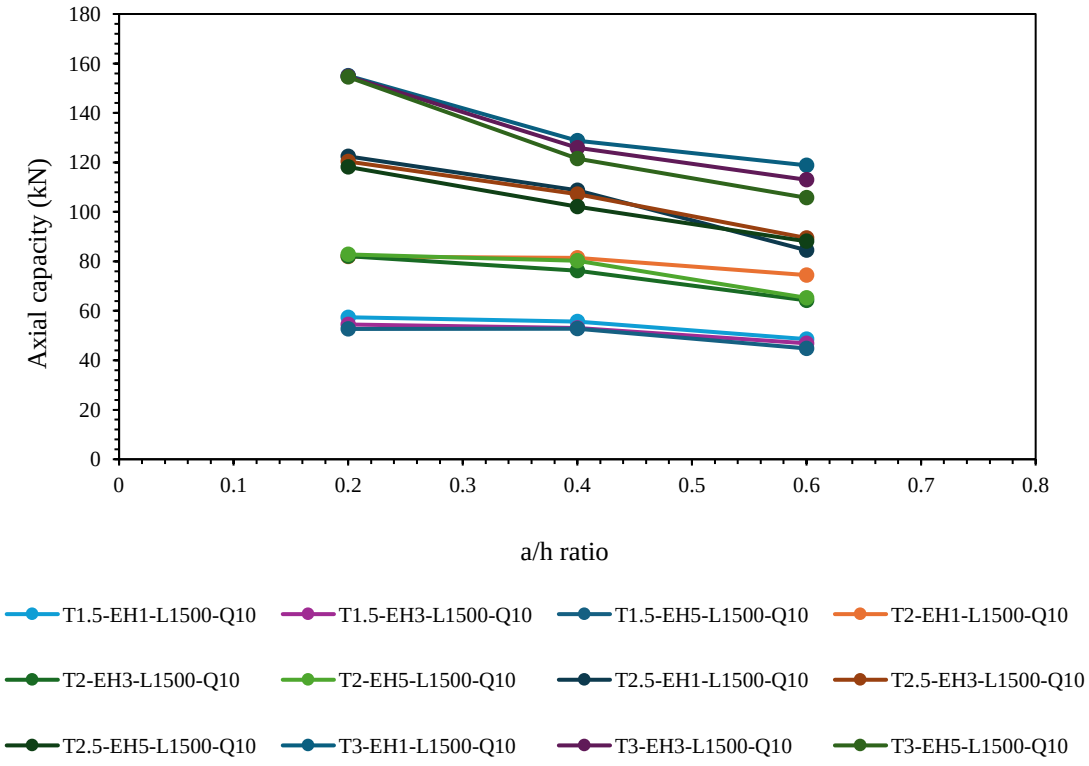

(a)Austenitic

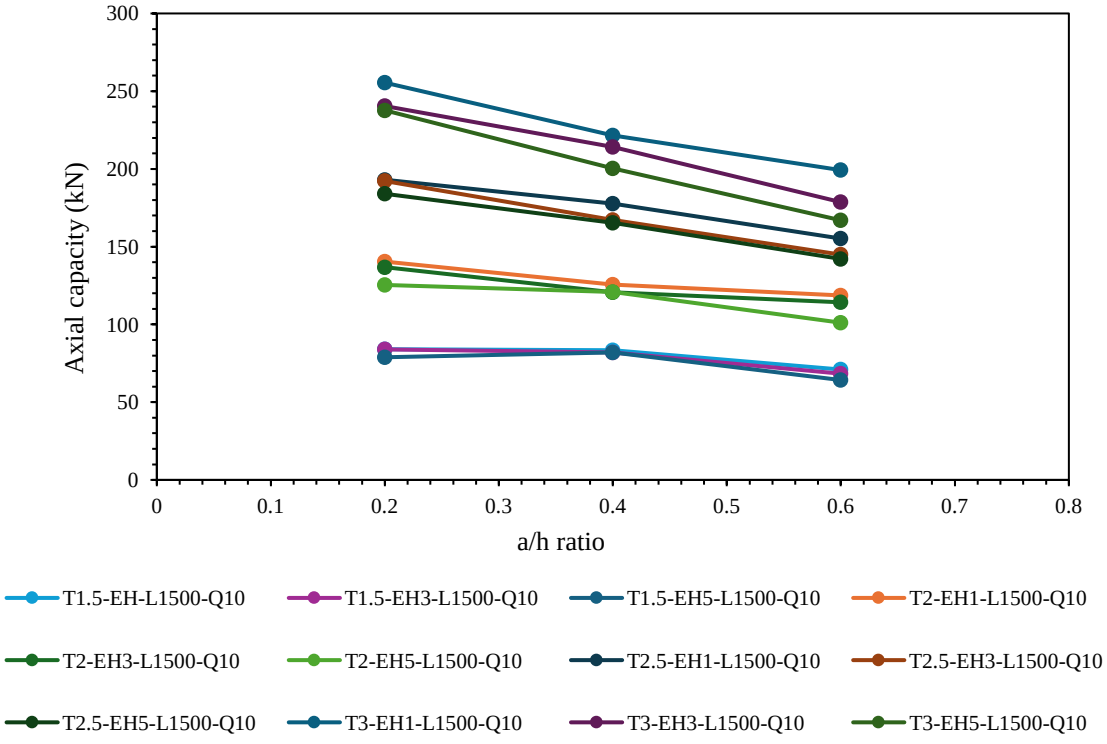

(b)Duplex

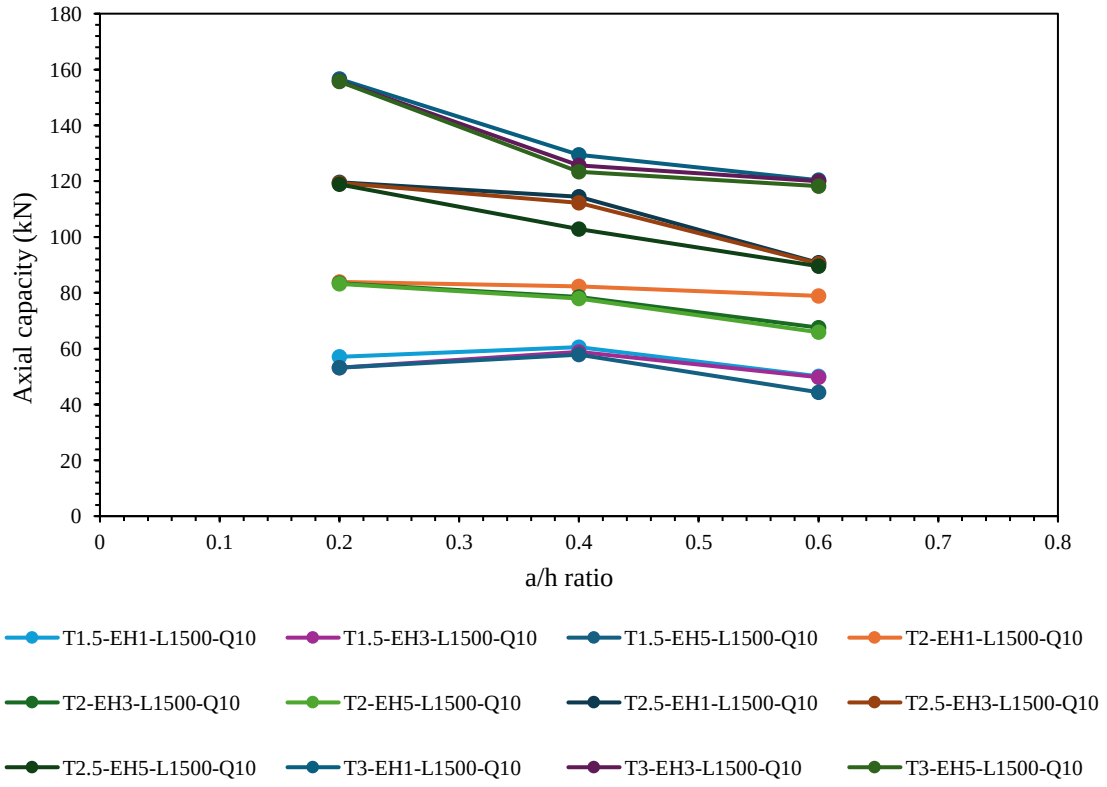

(c)Ferritic

Figure 4-9(a): Effect of a/h for edge-stiffened CFSS channel section C200-Q10-EH-T-D

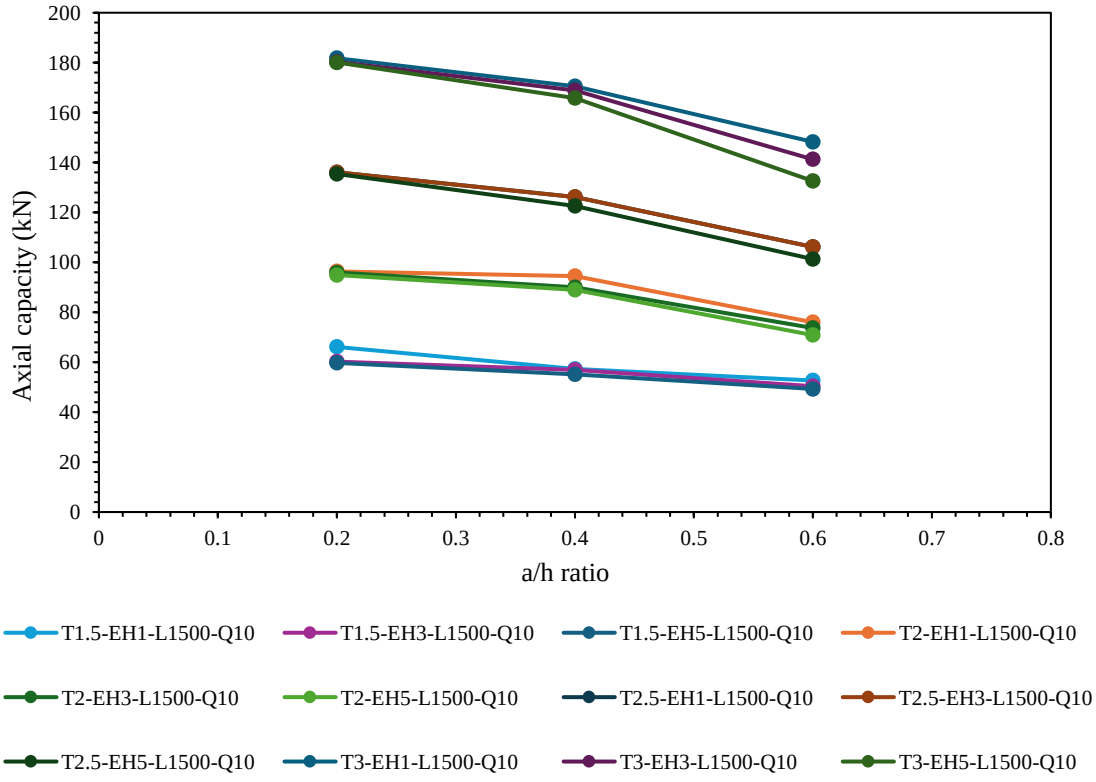

(a) Austenitic

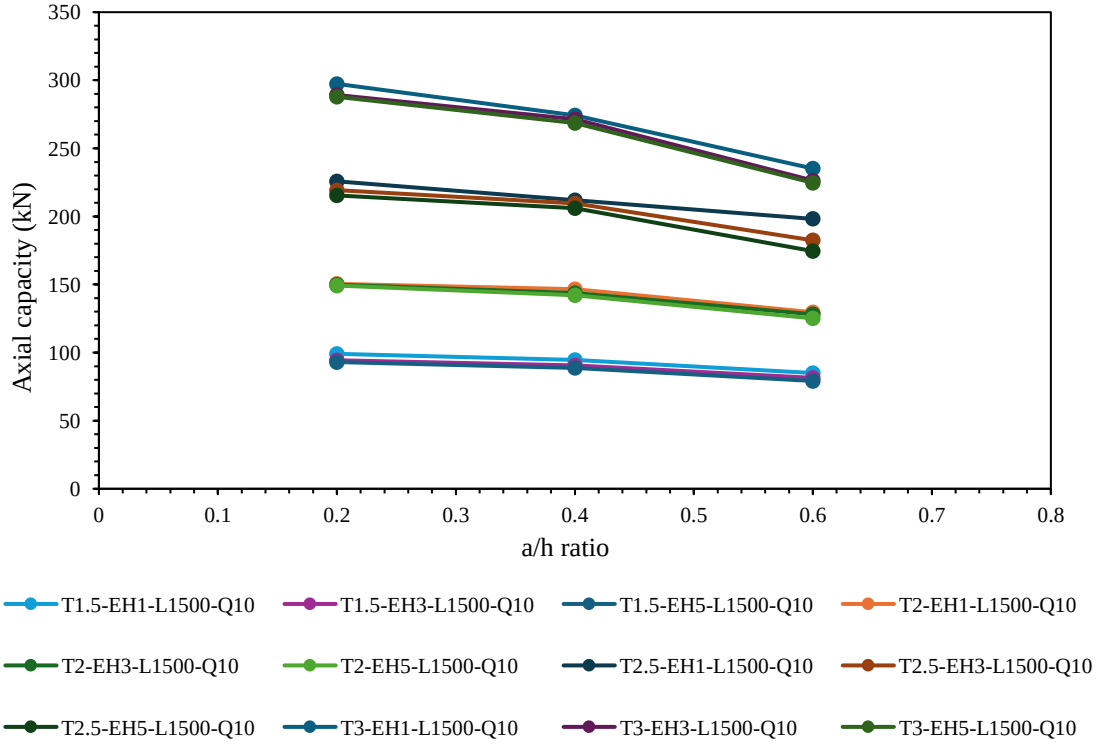

(b) Duplex

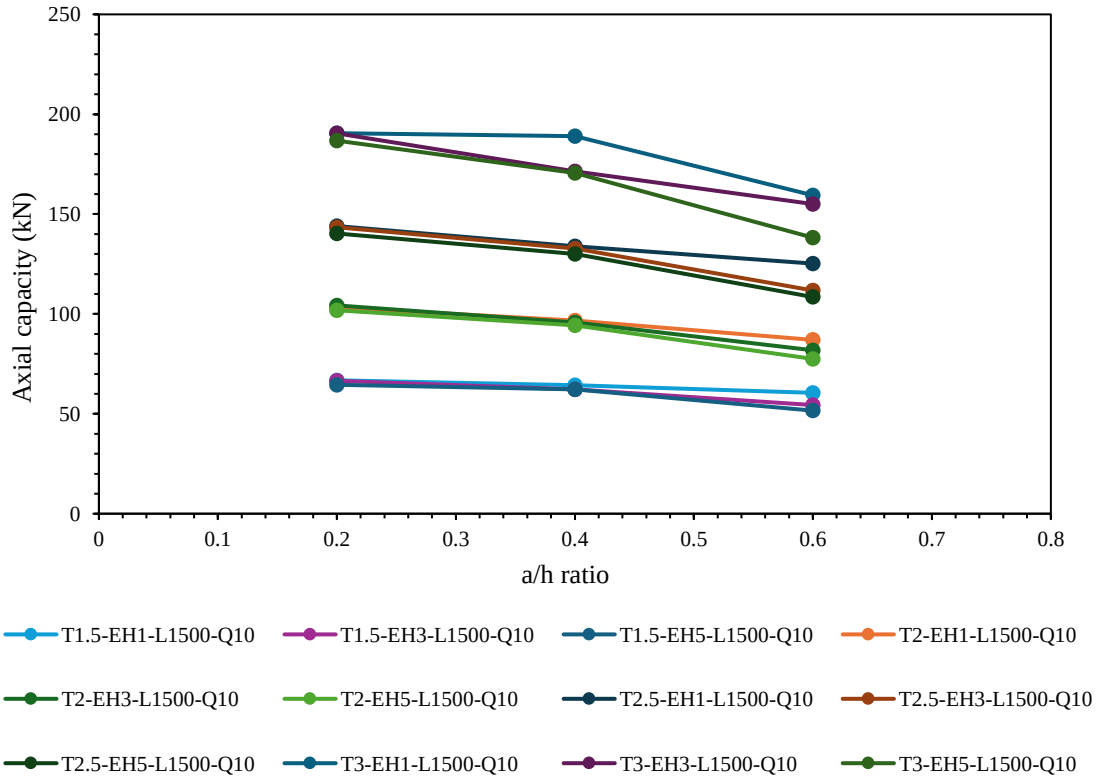

(c) Ferritic

Figure 4-9(b): Effect of a/h for edge-stiffened CFSS channel section C300-Q10-EH-T-D

4.4.4 Effect of number of holes on axial capacity for edge stiffened CFSS channel section

In table 3 and Fig. 4-10(a) and 4-10(b) illustrate how the number of holes impacts on axial capacity of CFSS channel section with edge stiffened web holes. As the number of holes increased from 1 to 3, there was a decrease in axial capacity of 2.63%, 3.54% and 2.22% for austenitic, duplex, and ferritic stainless steel, respectively. Likewise, with an increase in the number of holes from 1 to 5, the axial capacity decreased by 4.54%, 7.48% and 4.25% respectively, across the stainless-steel types.

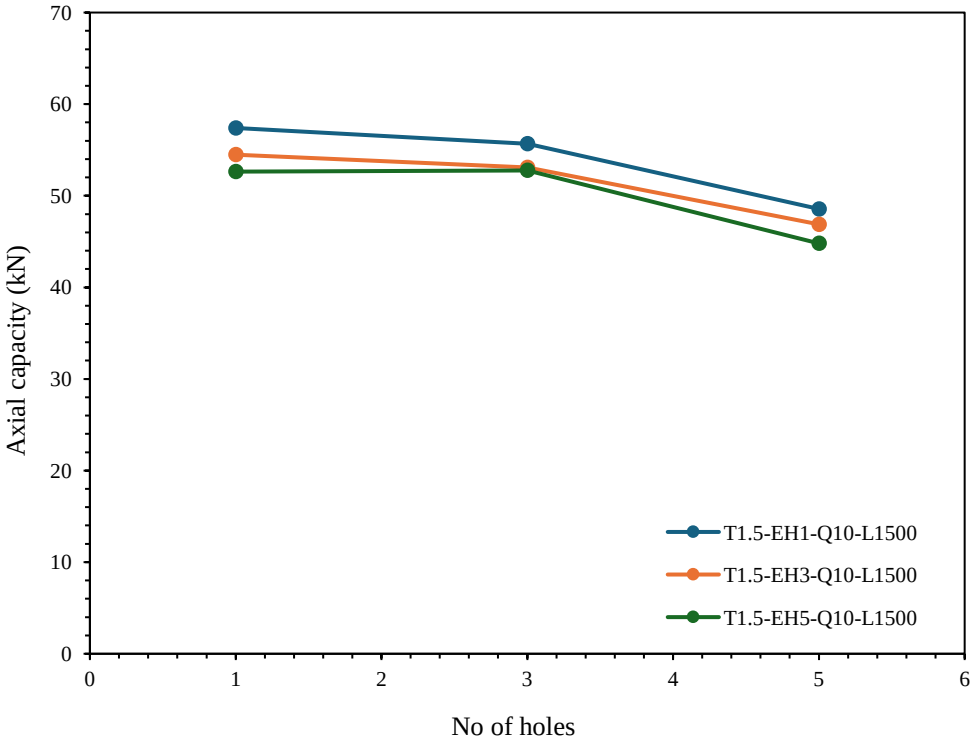

(a)Austenitic

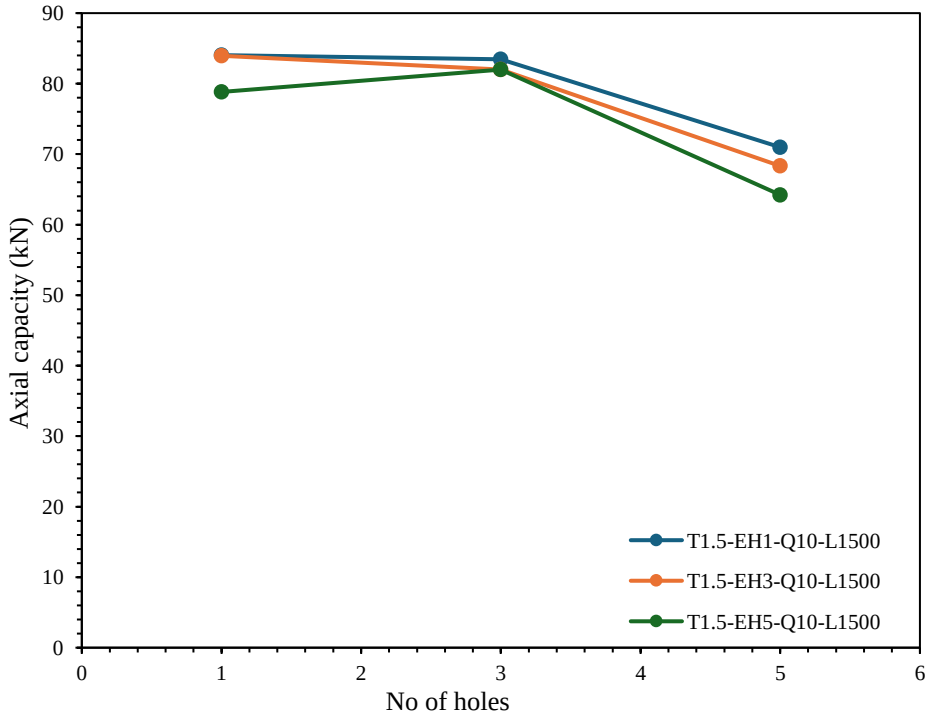

(b)Duplex

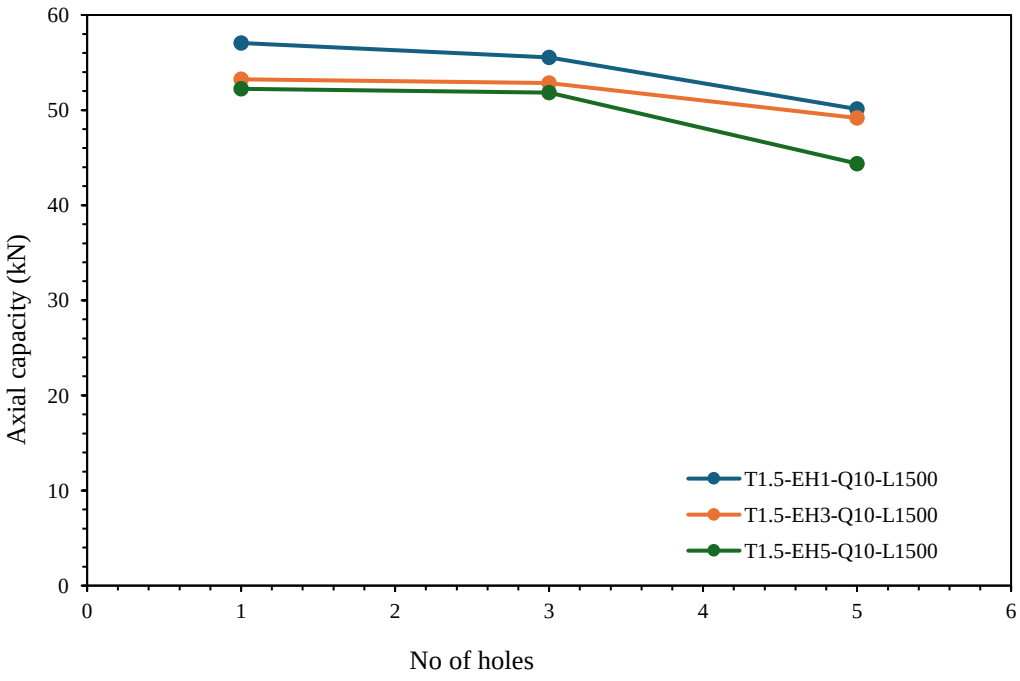

(c)Ferritic

Figure 4-10(a): Effect of number of holes for edge stiffened CFSS channel C200-T1.5-Q10-EH

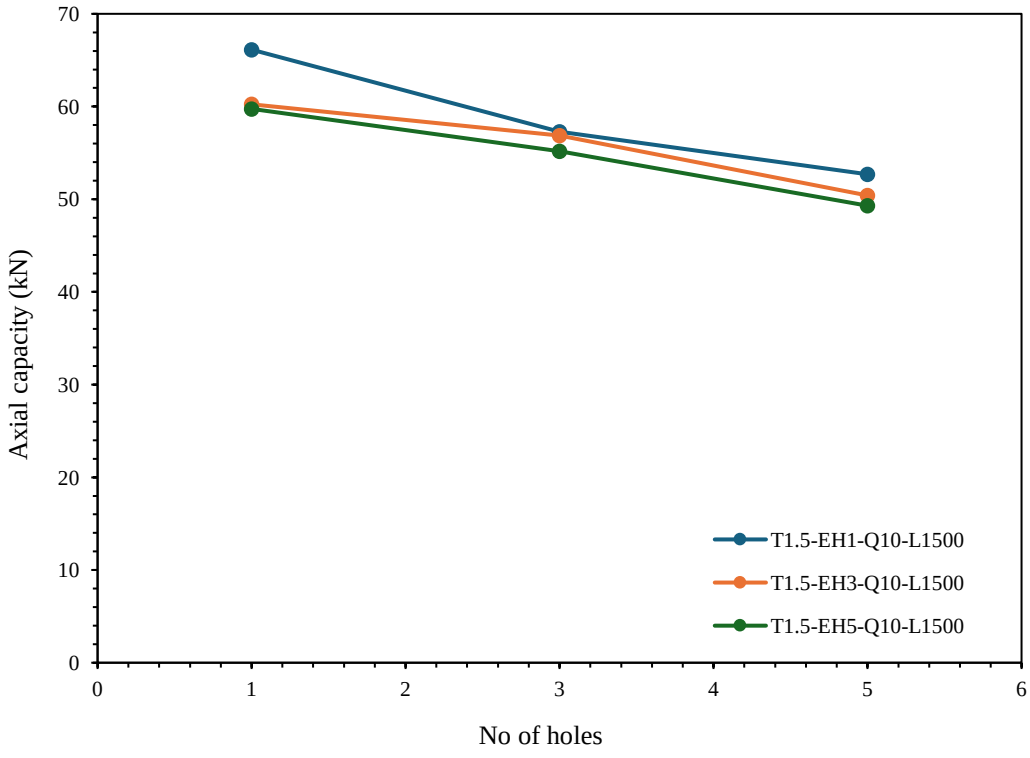

(a)Austenitic

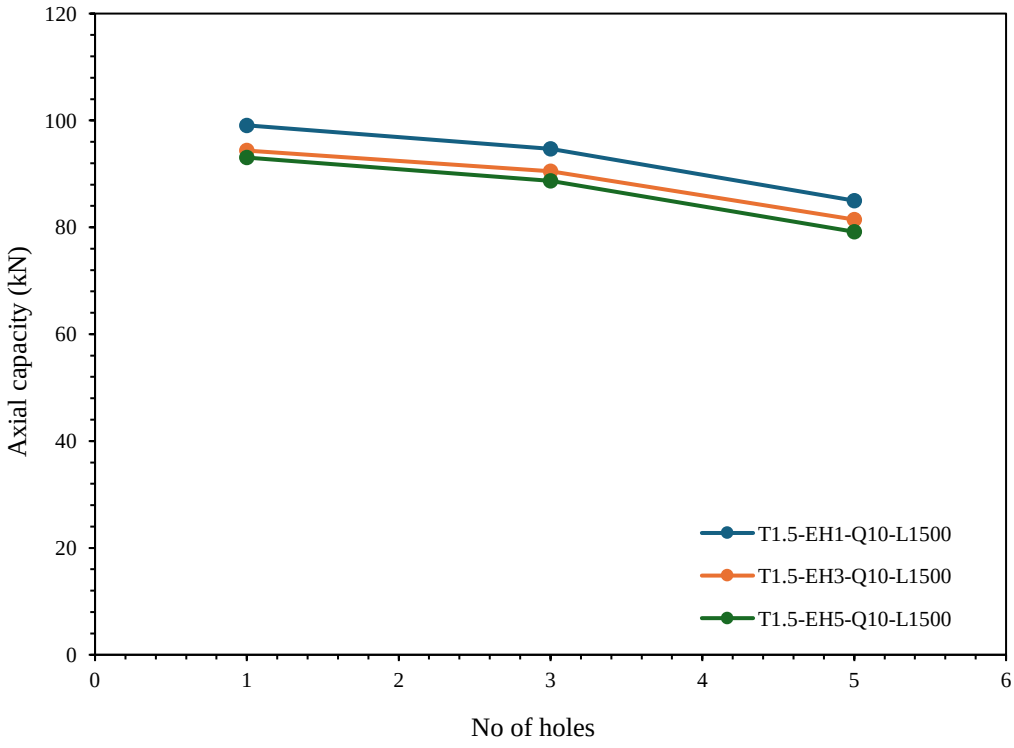

(b)Duplex

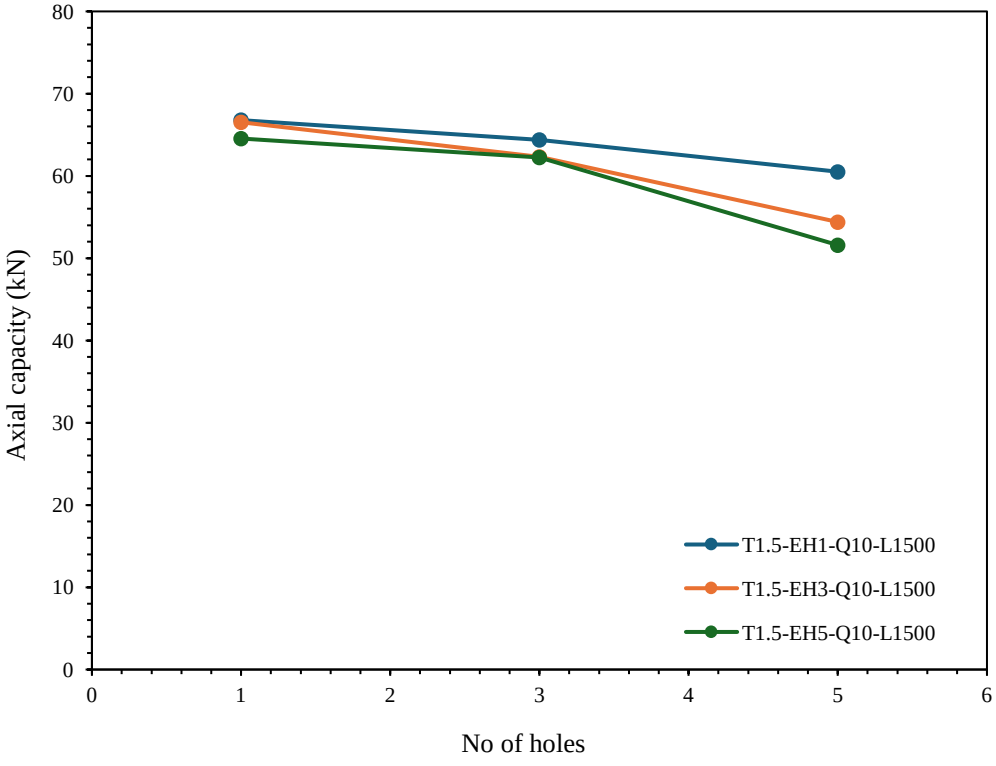

(c)Ferritic

Figure 4-10(b): Effect of number of holes for edge stiffened CFSS channel C300-T1.5-Q10-EH

CHAPTER 5. Current design guidelines

The AISI [13] and AS/NZS [14] design standards provide guidance on determining the unfactored axial capacity of the CFSS channel sections with plain webs and unstiffened web holes. Both the effective width method (EWM) and DSM approach are viable options for assessing the design capacity of these CFSS sections according to the specified standards. However, there exists a noticeable absence in design guidelines for evaluating the axial capacity of CFSS sections with edge stiffened hole, which is apparent in the current literature and standards. The subsequent sub-sections introduce relevant design equations, aiming to enhance understanding and facilitate the calculation of axial capacity for structural configurations.

5.1 EWM for CFSS channel sections with plain webs

The design standards outlined in AS/NZS [14] offer design equations for computing the nominal axial capacity (P*) of CFSS channel sections with plain webs. The axial capacity (P*) is required to satisfy the following equations:

$$P^* \leq \phi_c P_s = \phi_c A_e f_y \tag{3}$$

$$P^* \leq \phi_c P_c = A_e f_y \tag{4}$$

Where, P_s is the nominal section capacity of columns; P_c is nominal member capacity of columns; ϕ_c is the capacity reduction factor; P_n is the critical stress; A_e is the effective area and f_y is the yield stress.

The design equations to determine the critical stress P_n are given in Eqs. (5–7)

$$For\ \lambda_c < 1.5\ ; P_n = \left(0.658^{{\lambda_c}^2}\right) f_y \tag{5}$$

$$For\ \lambda_c < 1.5\ ; P_n = \left(\frac{0.877}{{\lambda_c}^2}\right) f_y \tag{6}$$

$$\lambda_c = \sqrt{\frac{f_y}{f_{oc}}} \tag{7}$$

Where, λ_c is non-dimensional slenderness; f_{oc} is the flexural–torsional buckling stresses calculated in accordance with Appendix D of AS/NZS 4600:2018 [14]

5.2 DSM for CFSS channel sections with plain webs

For CFSS channel sections with plain webs, the design capacity ($P_{AISI\&AS/NZS}$) is established by determining the minimum value among the local buckling capacity (P_{nl}), distortional buckling capacity P_{nd}, and global buckling capacity P_{ne} [13, 14].

$$P_{AISI\&AS/NZ} = \min(P_{nl}, P_{nd}, P_{ne}) \tag{8}$$

The design equations to obtain the local buckling capacity (P_{nl}) are given in Eqs. (9–11):

$$For\ \lambda_l \leq 0.776\ ;\ P_{nl} = P_{ne} \tag{9}$$

$$For\ \lambda_l > 0.776\ ;\ P_{nl} = \left[1 - 0.15\left(\frac{P_{crl}}{P_{ne}}\right)^{0.4}\right]\left(\frac{P_{crl}}{P_{ne}}\right)^{0.4} P_{ne} \tag{10}$$

$$\lambda_l = \sqrt{\frac{P_{ne}}{P_{crl}}} \tag{11}$$

The design equations to obtain the distortional buckling capacity (P_{nd}) are given in Eqs. (12–14):

$$For\ \lambda_d \leq 0.561\ ;\ P_{nd} = P_y \tag{12}$$

$$For\ \lambda_d > 0.561\ ;\ P_{nd} = \left[1 - 0.25\left(\frac{P_{crd}}{P_y}\right)^{0.6}\right]\left(\frac{P_{crd}}{P_y}\right)^{0.6} P_y \tag{13}$$

$$\lambda_d = \sqrt{\frac{P_y}{P_{crd}}} \tag{14}$$

The design equations to obtain the global buckling capacity (P_{ne}) are given in Eqs. (15–17):

$$For\ \lambda_c \leq 1.5\ ;\ P_{ne} = \left(0.658^{\lambda_c{}^2}\right) P_y \tag{15}$$

$$For\ \lambda_c > 1.5\ ;\ P_{ne} = \left(\frac{0.877}{\lambda_c{}^2}\right) P_y \tag{16}$$

$$\lambda_c = \sqrt{\frac{P_y}{P_{cre}}} \tag{17}$$

Where P_{crl}, P_{crd}, P_{cre} are the elastic local, distortional and global buckling load, respectively, which were determined by the finite strip analysis method using constrained and unconstrained finite strip method (CUFSM) software [22], as described by Moen and Schafer [23, 24].

5.3 DSM for CFSS channel sections with unstiffened web holes

The design standards outlined in AISI [13] and AS/NZS [14] for CFSS offer design equations aimed at calculating the axial capacity of CFSS channel sections featuring unstiffened web holes. These equations are derived from the design equations proposed by Moen and Schafer [23, 24].

Moen and Schafer [23, 24] proposed a "weighted average" method for assessing the global buckling capacity (P_{ne}) of CFSS channel sections featuring web holes. The classical equation used to compute the elastic global buckling load (P_{creh}) for such columns is presented in Equation 18 below:

$$P_{creh} = \frac{\pi^2 EI_{avg}}{A_g (KL)^2} \tag{18}$$

To determine the local buckling capacity (P_{nl}) of CFS sections with unstiffened web holes, the design equations are given in Eqs. (19–21):

$$For\ \lambda_l \leq 0.776\ ;\ P_{nl} = P_{ne} \leq P_{ynet} \tag{19}$$

$$For\ \lambda_l > 0.776\ ;\ P_{nl} = \left[1 - 0.15\left(\frac{P_{crlh}}{P_{ne}}\right)^{0.4}\right]\left(\frac{P_{crlh}}{P_{ne}}\right)^{0.4} P_{ne}\ \leq\ P_{ynet} \tag{20}$$

$$\lambda_l = \sqrt{\frac{P_{ne}}{P_{crlh}}} \tag{21}$$

To determine the distortional buckling capacity (P_{nd}) of CFSS sections with unstiffened web holes, the design equations are given in Eqs. (22–27):

$$For\ \lambda_d \leq\ \lambda_{d1};\ P_{nd} =\ P_{ynet} \tag{22}$$

$$For\ \lambda_{d1} < \lambda_d \leq \lambda_{d2}\ ; P_{nd} =\ P_{ynet} - \left(\frac{P_{ynet} - P_{d2}}{\lambda_{d2} - \lambda_{d2}}\right)(\lambda_d -\ \lambda_{d1}) \tag{23}$$

$$For\ \lambda_d > \lambda_{d2}\ ;\ P_{nd} = \left[1 - 0.25\ \left(\frac{P_{ynet}}{P_y}\right)^{0.6}\right]\left(\frac{P_{ynet}}{P_y}\right)^{0.6} P_y \tag{24}$$

$$\lambda_{\mathrm{d}} =\ \sqrt{\frac{P_{\mathrm{y}}}{P_{\mathrm{crdh}}}} \tag{25}$$

$$\lambda_{\mathrm{d1}} = 0.561\left(\frac{P_{\mathrm{ynet}}}{P_{\mathrm{y}}}\right) \tag{26}$$

$$\lambda_{\mathrm{d2}} = 0.561\left[14\left(\frac{P_{\mathrm{y}}}{P_{\mathrm{ynet}}}\right)^{0.4} - 13\right] \tag{27}$$

Where P_{y} and P_{ynet} are the member yield capacity of the gross section and net section, respectively. Moreover, P_{crlh}, P_{crdh}, P_{creh} are the elastic local, distortional, and global buckling load, respectively, for the CFS channel sections with unstiffened web holes.

5.4 Comparison of design strength with the FEA results

The axial capacity of CFSS channel section with plain webs, as derived from the parametric study, was compared against the axial capacities calculated using the EWM equations [13, 14]. analysing the comparison result (refer to table 5 and Fig. 5-1), the mean and coefficient of variation (COV) of P_{FEA}/ $P_{\mathrm{AISI\&AS/NZS\ (EWM)}}$ ratio are 0.93 and 0.08 respectively for austenitic stainless steel. Similarly, 0.95 and 0.06 for duplex and 0.93 and 0.08 for ferritic

stainless steel respectively. Consequently, the design strengths projected by the EWM equations [13, 14] exhibit an average conservatism of 6%

The mean values of the $P_{FEA}/ P_{AISI\&AS/NZS\ (DSM)}$ ratio are 0.93 and 0.04 for CFSS channels with plain webs. Consequently, the DSM equations of the AISI [13] and AS/NZ [14] standards are found to be conservative by 6% in determining the axial capacity of CFSS channel sections with plain webs.

The FEA findings for CFSS channel sections featuring unstiffened holes were compared with the predictive design strength derived from the DSM equations outlined in AISI [13] and AS/NZS [14] standards. Fig. 5-2 illustrates the comparison of axial capacity between CFSS channel with UH, as projected by the FE model and DSM equations [13, 14], indicating mean $P_{FEA}/ P_{AISI\&AS/NZS\ (DSM)}$ ratio values of 0.89 and 0.08 for austenitic stainless steel. Similarly, 0.92 and 0.09 for duplex and 0.90 and 0.09 for ferritic stainless steel (refer table 5). Consequently, the DSM equations of AISI [13] and AS/NZS [14] standards exhibit a slight conservatism of only 9% when estimating the axial capacity of CFSS channel sections with unstiffened holes.

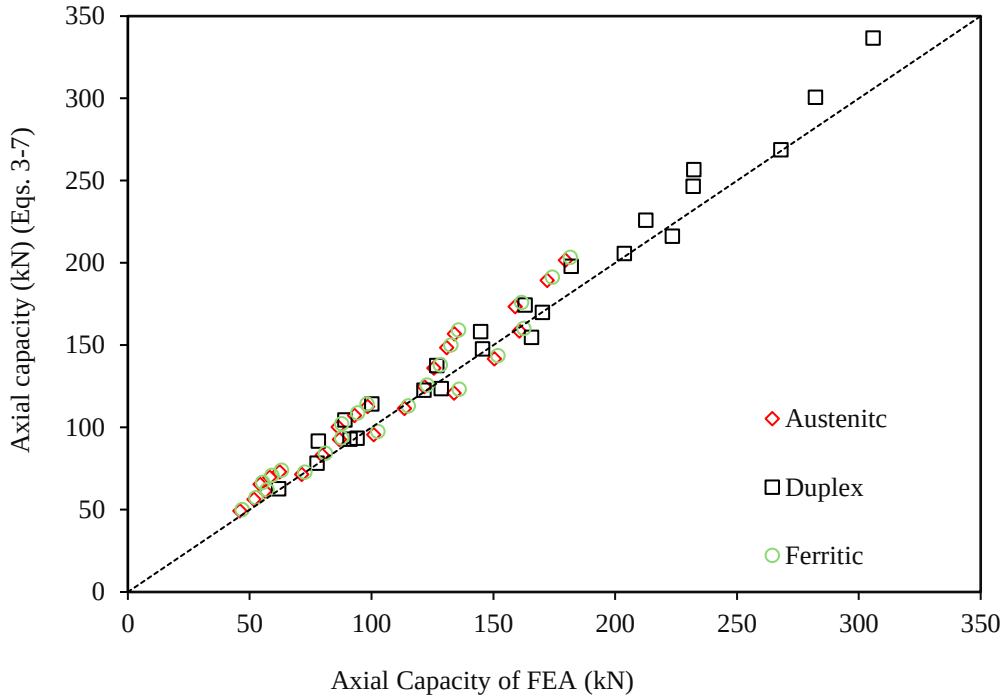

Figure 5-1: Comparing the outcomes of the EWM equations with Finite Element Analysis (FEA) results for CFSS channel sections featuring plain webs.

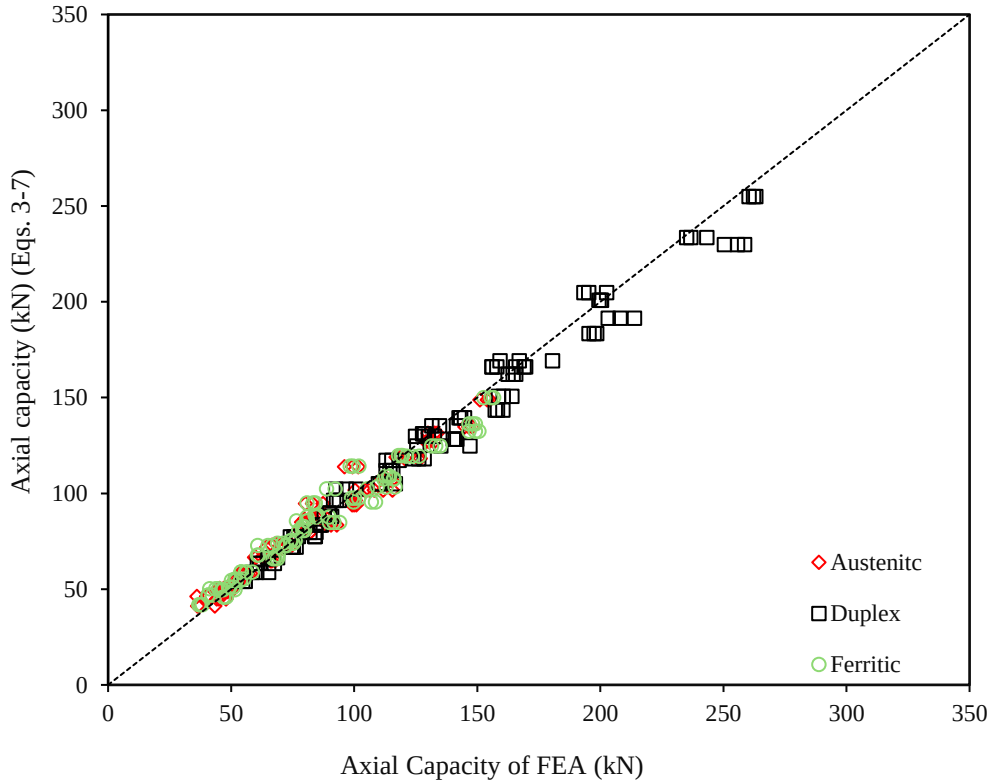

Figure 5-2: Comparing the outcomes obtained from EWM equations FEA results of CFSS channel sections with unstiffened holes.

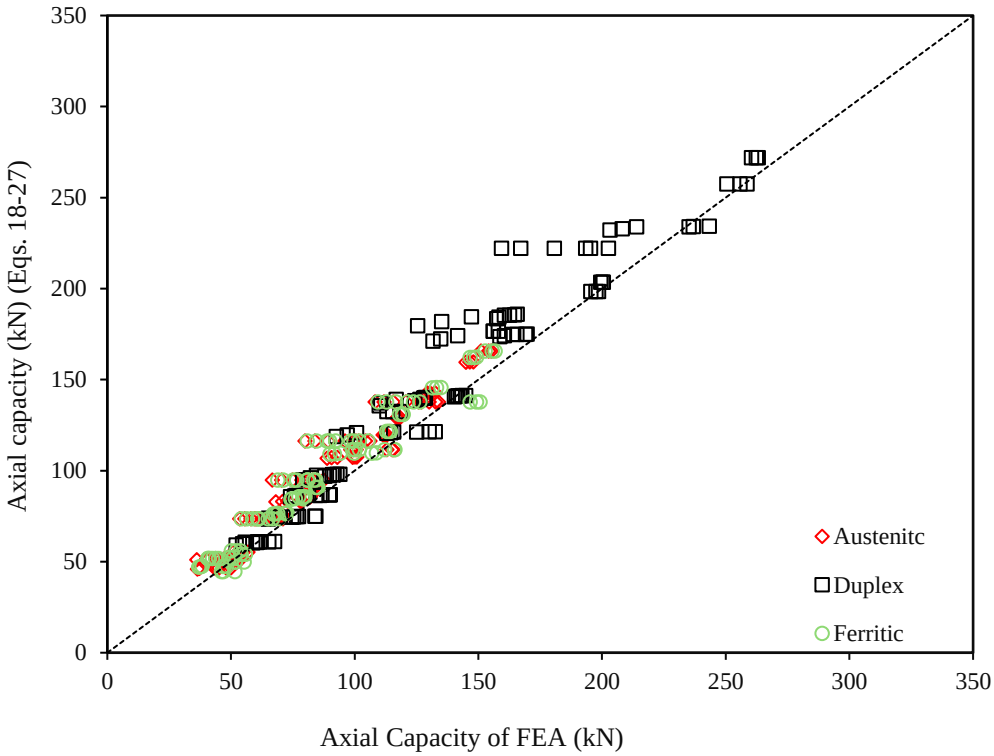

Figure 5-3: Comparing the outcomes obtained from DSM equations FEA results of CFSS channel sections with unstiffened holes.

Table 5 The comparison between FEA results and the capacities predicted by the existing design equations.

Design guidelines	Design equations	Type of section	Equations	Comparison	Mean	COV
AISI [14] & AS/NZS [15]	EWM	Plain webs	Eqs. 3-7	$P_{FEA}/P_{EWM\ [14,15]}$	0.93	0.08
AISI [14] & AS/NZS [15]	DSM	Plain webs	Eqs. 8-17	$P_{FEA}/P_{DSM\ [14,15]}$	0.93	0.04
AISI [14] & AS/NZS [15]	DSM	UH	Eqs. 18-27	$P_{FEA}/P_{DSM\ [14,15]}$	0.89	0.08

CHAPTER 6. Proposed design equations

6.1 Proposed modified EWM equations

The parametric study showed that the web depth(d_1), depth of web holes (d_w), thickness (t), width of flange (b_f) and stiffener length (q) are significant factors influencing the axial capacities of CFSS channel with edge stiffened holes. Since the FEA results align closely with EWM for unstiffened holes, there is no necessity to introduce new EWM design equations. Consequently, to enhance the accuracy of predicting the axial capacity of these channels, modifications were made to the effective width method (EWM) equations found in design standards [13, 14] for CFSS channels with plain webs. This adjustment involved incorporating a capacity reduction factor and a capacity enhancement factor, both derived from bivariate linear regression analysis. The resulting design equations, aimed at determining the axial capacity of CFSS channels with EH (Eqs. 28) are presented below.

For CFSS channel section with edge stiffened hole,

$$P_{Prop} = \left[0.875 - 0.088\left(\frac{d_w}{d_1}\right) + 11.17\left(\frac{t}{d_1}\right) + 1.88\left(\frac{q}{d_1}\right)\right] \times P_{EWM} \qquad for < 0.45\,\lambda_c < 1.41 \tag{28}$$

Figure 6-1 illustrates a comparison between Finite Element Analysis (FEA) outcomes and the projections generated by the proposed Effective Width Method (EWM) equations for CFSS channel sections featuring edge-stiffened holes. The EWM-based design equations demonstrate a commendable alignment with the FE results in assessing the axial capacity for CFSS channel sections with edge stiffeners. Table 6 provides the mean and Coefficient of Variation (COV) values for FEA in according to the proposed EWM design equations for edge-stiffened holes. The scope of the proposed design equations is confined to specific parameters: $0.45 < \lambda c < 1.41$, $0.2 \leq dw/d1 \leq 0.6$, $0.0075 \leq t/d1 \leq 0.015$, and $0.05 \leq q/d1 \leq 0.075$. The ratio $P_{FEA}/P_{prop(EWM)}$ is examined within these constraints.

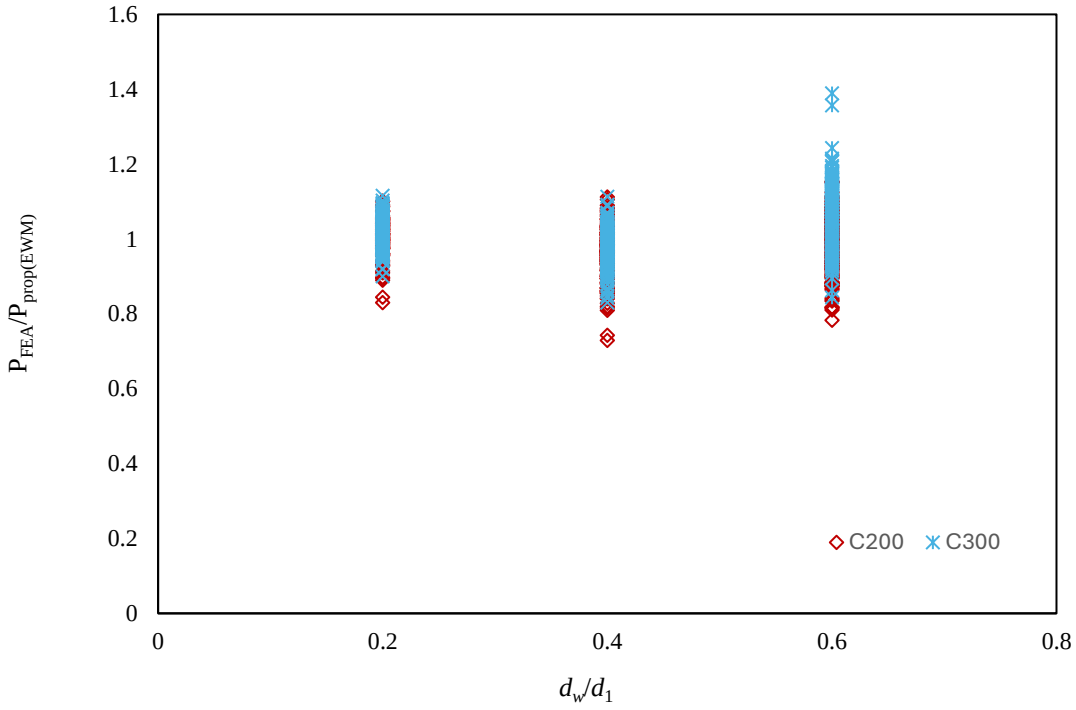

Figure 6-1: For CFSS channel sections with EH (28)

6.2 Proposed modified DSM equations

The findings from the parametric analysis of CFSS channel columns incorporating edge stiffened hole ($0.45<\lambda_c<1.41$) were subjected to local buckling or distortional buckling. However, there is no design equations available to calculate axial capacity of CFSS channel columns with edge stiffened holes. Therefore, this study proposed DSM equations [Eqs. 29-37] to estimate the nominal axial capacity (P_{prop}) of CFSS channel with edge stiffened holes. These equations were developed by leveraging the design strength of CFSS channel sections with unstiffened hole, as referred in [13, 14].

For Local buckling

$$For\ \lambda_l \leq 0.776\ ;\ P_{nl,prop} = P_{ne} \leq P_{ynet} \tag{29}$$

$$For\ \lambda_l > 0.776\ ;\ P_{nl,prop} = \left[1 - 0.17\left(\frac{P_{crlh}}{P_{ne}}\right)^{0.36}\right]\left(\frac{P_{crlh}}{P_{ne}}\right)^{0.36} P_{ne} \leq P_{ynet} \tag{30}$$

$$\lambda_l = \sqrt{\frac{P_{ne}}{P_{crlh}}} \tag{31}$$

For the assessment of the elastic local buckling load (P_{crlh}) of CFSS channel sections with unstiffened hole, as well as the member yield capacity of the net cross-section (P_{ynet}) of such sections, finite strip analysis was conducted. This analysis encompassed both gross and net sections and utilized constrained and unconstrained finite strip methods (CUFSM) software [22], following the methodology outlined by Moen and Schafer [23, 24].

For distortional buckling

$$For\ \lambda_d \leq \lambda_{d1};\ P_{nd} = P_{ynet} \tag{32}$$

$$For\ \lambda_{d1} < \lambda_d \leq \lambda_{d2}\ ; P_{nd,prop} = P_{ynet} - \left(\frac{P_{ynet} - P_{d2}}{\lambda_{d2} - \lambda_{d1}}\right)(\lambda_d - \lambda_{d1})^{0.92} \tag{33}$$

$$For\ \lambda_d > \lambda_{d2}\ ;\ P_{nd,prop} = \left[1 - 0.25\left(\frac{P_{ynet}}{P_y}\right)^{0.54}\right]\left(\frac{P_{ynet}}{P_y}\right)^{0.54} P_y \tag{34}$$

$$\lambda_{\mathrm{d}} = \sqrt{\frac{P_{\mathrm{y}}}{P_{\mathrm{crdh}}}} \tag{35}$$

$$\lambda_{\mathrm{d1}} = 0.561\left(\frac{P_{\mathrm{ynet}}}{P_{\mathrm{y}}}\right) \tag{36}$$

$$\lambda_{\mathrm{d2}} = 0.561\left[14\left(\frac{P_{\mathrm{y}}}{P_{\mathrm{ynet}}}\right)^{0.4} - 13\right] \tag{37}$$

Fig. 6-2 illustrates a comparison between the FEA results and the predictions derived from the proposed DSM equations. Notable, the proposed DSM design equations exhibit favorable correspondence with the FE results, particularly in assessing the axial capacity of CFSS channels with EH at local buckling. Table 7 presents the mean and coefficient of variation (COV) values associated with the proposed DSM equations for CFSS channels featuring EH.

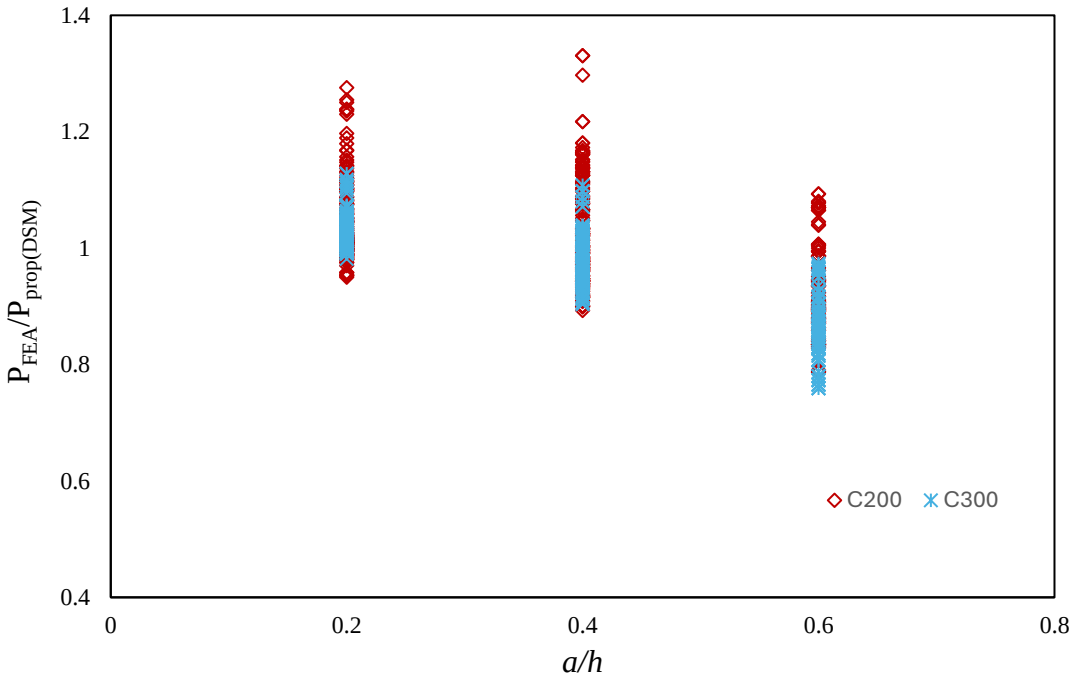

(a) For CFSS sections with EH (Eqs. 29-31)

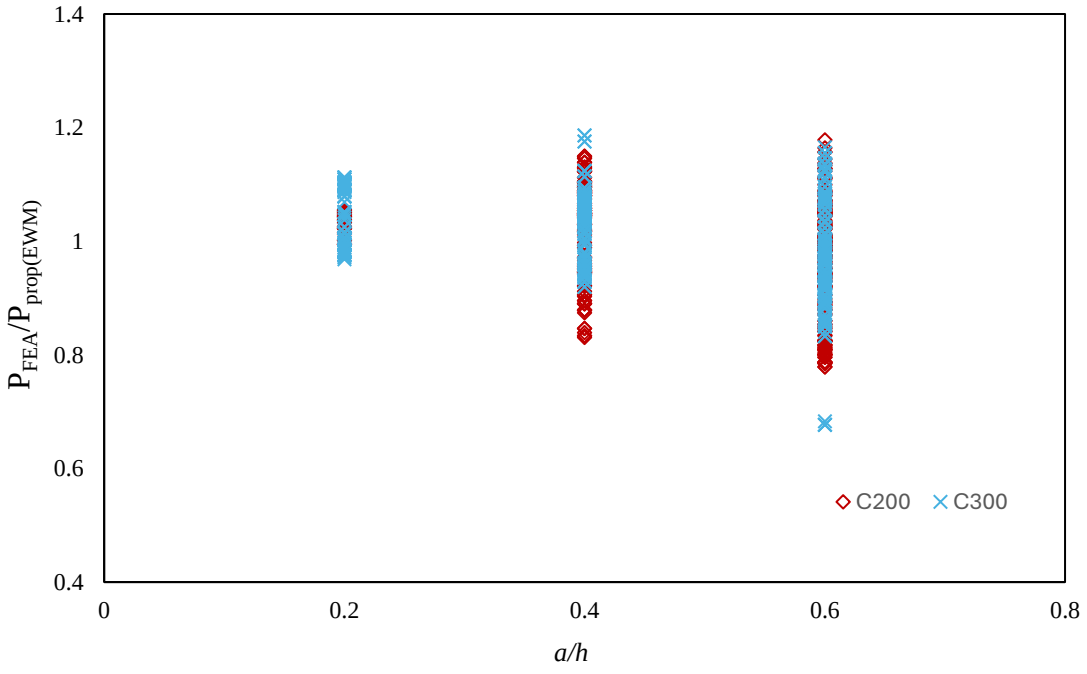

(b) For CFSS sections with EH (Eqs. 32-37)

Figure 6-2: FEA results against the projections of the suggested DSM equations for CFSS channel sections with edge stiffened holes.

6.3 Reliability analysis

A subsequent reliability analysis was carried out to evaluate the accuracy of the proposed design equation for CFSS channel sections with both UH and EH. According to AISI specifications [13], a minimum target reliability index (β) value of 2.5 is recommended for CFSS structural members. The results of the reliability analysis indicated that the reliability indices obtained from both the EWM-based proposed equations and the modified DSM equations surpassed 2.5 for CFSS channel sections with UH and EH (refer to Table 6 and 7). This suggests that the proposed equations are reliable and capable of accurately predicting the axial capacity of CFSS channel sections with both UH and EH.

$$\varphi = 1.52 M_m F_m P_m e^{-\beta \sqrt{\{V_m^2 + V_f^2 + C_p V_p^2 + V_q^2\}}} \quad (38)$$

Table 6 The reliability analysis for EWM based proposed equations for CFSS channel sections with EH

	Eq. 28
Number of data	1296
COV	0.46
Mean, P_m	1
Resistance factor, φ	0.85
Reliability index, β	2.78

Table 7 The reliability analysis for proposed DSM equations for CFSS channel sections with EH

	For intermediate columns ($0.45<\lambda_c<0.9$)	For slender columns ($0.9<\lambda_c<1.41$)
	Eqs. 29-31	Eqs. 32-37
Number of data	740	556
COV, V_P	0.079	0.089
Mean, P_m	1.00	1.00
Resistance factor, φ	0.85	0.85
Reliability index, β	2.68	2.67

CHAPTER 7. Conclusion and limitations of the current study and future study

This study investigates the axial capacity of Cold-Formed Stainless Steel (CFSS) channel sections with plain sections, unstiffened holes (UH), and edge-stiffened holes (EH) utilizing finite element analysis (FEA). The study begins by developing and validating FE models against experimental results provided by Kulatunga et al. (2014) and Chen et al. (2019), demonstrating favourable agreement in ultimate axial capacity, failure behaviour, and load displacement curves. Subsequently, a comprehensive parametric investigation involving 2016 FE models is undertaken to analyse the influence of key parameters such as the a/h ratio, overall length, thickness, and stiffener length on the axial capacity of CFSS channel sections. The outcomes of this study contribute to a deeper understanding of the structural performance of CFSS channel sections, providing valuable insights for design and engineering practices in the field of cold-formed steel structures.

(1) Based on the results of the parametric study, comprising 2016 finite element model it is evident that the ratio of a/h, overall length, thickness, and stiffener length exert a notable influence on the axial capacity of CFSS channel sections featuring EH and UH. Furthermore, it is noted that the influence of EH into CFSS channel

sections resulted in an average increase in axial capacity by 7.14%, 7.66% and 8.18% for austenitic, duplex and ferritic stainless steel respectively when compared to sections featuring UH.

(2) Upon comparison of numerical simulation results with the design strength derived from the design equations specified in the American Iron and Steel Institute (AISI 2016) and Australia/New Zealand standards (AS/NZS 2018) for CFSS channel sections with plain webs, it was noted that both the EWM and DSM equations demonstrated conservatism, with an average conservatism of 6%. Specifically concerning CFSS channel sections with unstiffened holes (UH), the DSM equations exhibited an average conservatism of 9% when predicting the axial capacity of such sections.

(3) Capacity reduction factor and enhancement factor were introduced for the EWM to establish design equations for determining the axial capacity of CFSS channel sections with both UH and EH. Furthermore, modified DSM design equations were proposed specifically for CFSS channel sections featuring EH to forecast their axial capacity. It's important to note that these proposed equations are applicable within defined ranges: $0.45<\lambda_c<1.41$, $0.2\leq d_w/d_1 \leq 0.6$, $0.0075 \leq t/d_1 \leq 0.015$ and $0.05 \leq q/d_1 \leq 0.075$

(4) Finally, a reliability analysis was conducted, affirming the reliability of both the proposed EWM and modified DSM equations.

These are the limitations of the current study:

- The research is confined to specific grades of stainless steel (austenitic, duplex, and ferritic).
- Only two cross-sectional dimensions (C200x65x15 and C300x80x20) were investigated numerically.

- Only two stiffener length (Q = 10 and 15 mm) was considered.

Therefore, the proposed reduction factor equations were limited to the considered parameters using FEA analysis. However, it is known from previous research studies that the stiffener length of channel sections will also influence the structural behaviour and axial capacity of the CFSS channel sections. Therefore, here are some of the further research recommendations.

- Conduct experimental research on the CFSS channel sections.
- Investigate different loading conditions like shear behaviour and eccentric capacity.
- Further exploration is needed to examine the parametric effects of the varied length and different hole diameter of the CFSS channel sections, cross-section dimensions and other grades of stainless steel.

Acknowledgement

The author extends sincere gratitude to the University of Waikato for generously providing computational facilities.

References

[1] Yousefi, A. M., Lim, J. B., Uzzaman, A., Lian, Y., Clifton, G. C., & Young, B. (2016). Web crippling strength of cold-formed stainless steel lipped channel-sections with web openings subjected to interior-one-flange loading condition. Steel and Composite Structures, 21(3), 629-659.

[2] Fang, Z., Roy, K., Padiyara, S., Chen, B., Raftery, G. M., & Lim, J. B. (2023, January). Web crippling design of cold-formed stainless-steel channels under interior-two-flange loading condition using deep belief network. In Structures (Vol. 47, pp. 1967-1990). Elsevier.

[3] Fang Zhiyuan, Roy Krishanu, Ma Quincy, Uzzaman Asraf, Lim James BP. Application of deep learning method in web crippling strength prediction of cold-formed stainless steel channel sections under end-two-flange loading. Struct 2021; 33:2903–42.

[4] Fang, Z., Roy, K., Ma, Q., Uzzaman, A., & Lim, J. B. (2021, October). Application of deep learning method in web crippling strength prediction of cold-formed stainless steel channel sections under end-two-flange loading. In Structures (Vol. 33, pp. 2903-2942). Elsevier.

[5] American Society of Civil Engineers (ASCE). Specification for the Design of Cold-formed Stainless Steel Structural Members. Reston, Va: SEI/ASCE 8-02; 2002.

[6] Cruise, R. B., & Gardner, L. (2008). Strength enhancements induced during cold forming of stainless steel sections. *Journal of constructional steel research*, *64*(11), 1310-1316.

[7] SCI Steel knowledge. (2010). The pavilion, regent's place: structural stainless steel case study 07. Report. https://www.teamstainless.org/resources/information-center-for-stainless-steel-in-construction/case-studies/structure/

[8] SCI Steel knowledge. (2010). Cala Galdana bridge: structural stainless steel case study 02. Report. https://www.teamstainless.org/resources/information-center-for-stainless-steel-in-construction/case-studies/structure/

[9] Howick Floor, Joist System, 2013.

[10] Roy, K., & Lim, J. B. (2019). Numerical investigation into the buckling behaviour of face-to-face built-up cold-formed stainless steel channel sections under axial compression. In Structures (Vol. 20, pp. 42-73). Elsevier.

[11] Roy, K., Lau, H. H., & Lim, J. B. (2019). Finite element modelling of back-to-back built-up cold-formed stainless-steel lipped channels under axial compression. *Steel Compos. Struct*, *33*(1), 37-66.

[12] Yousefi, A. M., Samali, B., Hajirasouliha, I., Yu, Y., & Clifton, G. C. (2022). Unified design equations for web crippling failure of cold-formed ferritic stainless steel unlipped channel-sections with web holes. Journal of Building Engineering, 45, 103685.

[13] AISI (American Iron and Steel Institute). North American specification for the design of cold-formed steel structural members. AISI S100-16 2016; Washington, DC: AISI

[14] AS/NZS (Australia/New Zealand Standard). Cold-formed steel structures. AS/NZS 4600 2018; Sydney, Australia: AS/NZS.

[15] Yousefi, A. M., Lim, J. B., & Clifton, G. C. (2019). Web crippling design of cold-formed ferritic stainless steel unlipped channels with fastened flanges under end-two-flange loading condition. Journal of constructional steel research, 152, 12-28.

[16] Eurocode 3: Design of steel structures—part 1.4 (EN 1993-1-4). General Rules—Supplementary Rules for Stainless Steels, European Committee for Standardization (CEN), Brussel (2006)

[17] Yousefi, A. M., Samali, B., & Yu, Y. (2021, October). Shear behaviour and design of cold-formed ferritic stainless-steel channels with circular web openings. In Structures (Vol. 33, pp. 4162-4175). Elsevier.

[18] Chen B, Roy K, Uzzaman A, Raftery GM, Nash D, Clifton GC, Lim JB. Effects of edge-stiffened web openings on the behaviour of cold-formed steel channel sections under compression. Thin-Walled Structures 2019; 144, 106307.

[19] ABAQUS Analysis User's Manual-Version 6.14-2, ABAQUS Inc., USA, 2018.

[20] Yousefi, A. M., Lim, J. B., Uzzaman, A., Lian, Y., Clifton, G. C., & Young, B. (2016). Web crippling strength of cold-formed stainless steel lipped channel-sections with web openings subjected to interior-one-flange loading condition. Steel and Composite Structures, 21(3), 629-659.

[21] Kulatunga, M. P., & Macdonald, M. (2013). Investigation of cold-formed steel structural members with perforations of different arrangements subjected to compression loading. Thin-Walled Structures, 67, 78-87.

[22] Committee on specifications for the design of cold-formed steel structural members. Development of CUFSM hole module and design tables for the cold-formed steel cross-sections with typical web holes in AISI D100. American Iron and Steel Institute (AISI) Specifications 2001; 226.

[23] C. D. Moen and B. W. Schafer, “Experiments on cold-formed steel columns with holes,” Thin-Walled Structures, vol. 46, no. 10, pp. 1164–1182, 2008.

[24] C. D. Moen and B. W. Schafer, “Direct strength method for design of cold-formed steel columns with holes,” Journal of Structural Engineering, ASCE, vol. 137, no. 5, pp. 559–570, 2016.

[25] Fang, Z., Roy, K., Chi, Y., Chen, B., & Lim, J. B. (2021, December). Finite element analysis and proposed design rules for cold-formed stainless-steel channels with web holes under end-one-flange loading. In Structures (Vol. 34, pp. 2876-2899). Elsevier.

[26] Walker A.C. (Ed.), Design and Analysis of Cold-Formed Sections, John Wiley & Sons (1975)

Notations

CFSS	Cold-formed stainless steel
CFS	Cold-formed steel
FE	Finite element
FEA	Finite element analysis
DSM	Direct strength method
EWM	Effective width method
AISI	American Iron and Steel Institute
AS/NZS	Australia/New Zealand Standards
EH	Edge-stiffened web holes
UH	Unstiffened web holes
σ	Engineering stress
ε	Engineering strain
E	Young's modulus of elasticity
σ_{true}	True stress
ε_{true}	True strain
d	Overall depth of the section
t	Thickness of section
a	Diameter of circular web holes
h	Depth of the flat portion of the web
L	Total length of CFSS channel sections
f_y	Yield strength of CFS section
d_w	Depth of web holes
b_w	Overall length of web holes
b_f	Width of the flange
d_1	Web depth of the section
b_l	Length of lip of the section
q	Stiffener length
λ_c	Non-dimensional column slenderness
R_q	Inner bent radius between the web and stiffener
P_s	Nominal section capacity of column
P_c	Nominal member capacity of column
ϕ_c	Capacity reduction factor
P_n	Critical stress of the section
A_e	Effective area of the section
f_{oc}	flexural–torsional buckling stresses of the section
P_{nl}	Local buckling capacity
P_{nd}	Distortional buckling capacity
P_{nd}	Global buckling capacity
P_{crl}	elastic local buckling load for section with plain webs
P_{crd}	Elastic distortional buckling load for section with plain webs
P_{cre}	Elastic global buckling load for section with plain webs
P_y	Member yield capacity of the gross section
P_{ynet}	Member yield capacity of the net section
P_{creh}	elastic local buckling load for section with web holes
P_{crdh}	Elastic distortional buckling load for section with web holes
P_{creh}	Elastic global buckling load for section with web holes
I_{avg}	Average moment of inertial for the gross and net section
A_g	Area of the gross section
P_{EXP}	Moment capacity of test

P_{FEA}	Moment capacity of parametric study
P_{Prop}	Moment capacity of the proposed equation
P_m	Mean value of the proposed equation
V_p	Coefficient of variation of the proposed equation
β	Reliability index
φ	Resistance factor
M_m	Mean of the material factor for CFS section (1.1)
V_m	COV of the material factor for CFS section (0.1)
F_m	Mean of the fabrication factor for CFS section (1.0)
V_f	COV of the fabrication factor for CFS section (0.05)
V_q	COV of the load effect for CFS section (0.21)
C_p	Correction factor